Teresa Duque da Silva Pissarro

Bachelor's degree in Biochemistry

Exploring novel copper(II) binding azole compounds as potential antifungal drugs

Master's Thesis in Biochemistry for Health

Supervisor: Doctor Luís Lima, PhD, ITQB NOVA
Co-Supervisor: Doctor Catarina Pimentel, PhD, ITQB NOVA

April 2022

Teresa Duque da Silva Pissarro

Bachelor's degree in Biochemistry

Exploring novel copper(II) binding azole compounds as potential antifungal drugs

Master's Thesis in Biochemistry for Health

Supervisor: Doctor Luís Lima, PhD, ITQB NOVA
Co-supervisor: Doctor Catarina Pimentel, PhD, ITQB NOVA

Júri:

Presidente: Doctor Pedro Manuel Marques Henriques Matias, PhD, ITQB NOVA
Arguente: Doctor Paulo Nuno Martinho, PhD, FCUL
Vogal: Doctor Ana Maria Varela Coelho, PhD, ITQB NOVA

Instituto de Tecnologia Química e Biológica António Xavier, Universidade NOVA de Lisboa

April 2022

Teresa Duque da Silva Pissarro

Degree in Biochemistry

Exploring novel copper(II) binding azole compounds as potential antifungal drugs

Master's Thesis in Biochemistry for Health

Acknowledgements

The work presented in this thesis would not have been possible without the support of several people. I would first like to thank my supervisor Luís Lima, for all his patience and insightful guidance in helping me achieve the goals of this work, and for the long hours of detailed explanations.

I want to thank the Organometallic Catalysis group and particularly the group leader Beatriz Royo for welcoming me in their lab, and also Sara Realista, Sofia Friães, and Henrique Mourão for always having a smile on their face even with the constant use of their vacuum lines. A big thank you to my masters and lab colleague Luana Ferreira, which was a big source of support and became a big friend.

To my co-supervisor Catarina Pimentel for welcoming me in the lab and for the excitement about my work and results. To Carolina Gaspar-Cordeiro and Catarina Amaral for the help with the experimental work.

I must acknowledge the support of the scientific services at ITQB, namely the CERMAX NMR facility, the Mass Spectrometry Unit (UniMS), and Cristina Leitão for the support with the HPLC.

Last, but definitely not least, to all my family and friends that supported and helped me in all the ups and downs, not only in this period of time, but my whole life. To my parents for giving me the courage to pursue what I wanted to study. To my sisters Susana, Sofia, Margarida and Marta, and cousin Patrícia for showing me that despite all I could go through in life I will have my best friends beside me. And to my close friends for listening to me and bringing me joy every day.

Abstract

Invasive fungal infections are a major cause of morbidity and mortality among hospitalized patients and immunocompromised individuals. The increasing resistance of pathogenic fungi to the limited number of antifungal classes available makes the development of new and improved antifungals a pressing issue. This work aims to synthesize new azole compounds by molecular simplification of the model antifungal drug fluconazole while incorporating chemical functions that bind copper(II), to explore a potential synergy between the azoles and the metal. The target compounds designed are based on a central amine functionalized with three functions: an azole, a dihalogenobenzyl, and a varying copper(II) binding function. The 15 target compounds synthesized are organized in three families, which differ on the azole used (triazole or imidazole) and the length of the alkyl chain separating the central amine and the azole. Differences within each family are the copper(II) binding function used and, in one case, also the dihalogenobenzyl moiety. Such structural variations are expected to allow for a structure-activity relationship study based on the results of biological activity assays performed. The conditional copper(II) binding constants for each target compound were determined by spectrophotometric titrations, the susceptibility of *Candida glabrata* to the target compounds was studied, and the ergosterol levels of cells treated with the target compounds were quantified by HPLC. The highest antifungal activities were obtained for the target compounds containing hydroxyquinoline or bromophenol functions, possibly due to the disruption of copper homeostasis or ergosterol synthesis inhibition, respectively. The structure of a tertiary amine with a triazole function appended on a propylene chain appears as the best one for developing new antifungal drugs; one of the most promising target compounds is based on that structure and contains a bromophenol function.

Keywords: Antifungal, azole, copper, *Candida*

Resumo

As infeções fúngicas invasivas são uma das principais causas de morbidade e mortalidade entre pacientes hospitalizados e indivíduos imunocomprometidos. A crescente resistência dos fungos patogénicos ao número limitado de classes de fármacos antifúngicos disponíveis torna urgente o desenvolvimento de fármacos antifúngicos novos e melhorados. Este trabalho tem como objetivo a síntese de novos compostos azólicos por simplificação molecular do fármaco antifúngico modelo fluconazol, incorporando funções químicas que coordenem cobre(II) de modo a explorar uma potencial sinergia entre os compostos azólicos e o metal. Os compostos-alvo desenhados são baseados numa amina central funcionalizada com três funções: um azol, um dihalogenobenzeno, e uma função variável para coordenação de cobre(II). Os 15 compostos-alvo sintetizados estão organizados em três famílias, que diferem no azol utilizado (triazol ou imidazol) e no comprimento da cadeia alquílica que separa a amina central e o azol. As diferenças dentro de cada família são o grupo de coordenação a cobre(II) usado e, num caso, também o grupo dihalogenobenzeno. Espera-se que tais variações permitam um estudo da relação estrutura-atividade baseado nos resultados dos ensaios biológicos realizados. Para cada composto-alvo, as constantes condicionais de ligação a cobre(II) foram determinadas por titulações espectrofotométricas, a suscetibilidade de *Candida glabrata* aos compostos-alvo foi estudada e os níveis de ergosterol nas células tratadas com os compostos-alvo foram quantificados por HPLC. As maiores atividades antifúngicas foram obtidas para compostos alvo contendo as funções hidroxiquinolina ou bromofenol, possivelmente devido à perturbação da homeostase de cobre ou à inibição da síntese de ergosterol, respetivamente. A estrutura da amina terciária com uma função triazol separada por uma cadeia propileno parece ser a melhor para o desenvolvimento de novos fármacos antifúngicos; um dos compostos mais promissores baseia-se nessa estrutura e contém uma função bromofenol.

Palavras-chave: Antifúngico, azol, cobre, *Candida*

Index

Figures Index

Tables Index

Abbreviation List

A	ABC	ATP-binding cassette
	AcOH	Acetic acid
	ADME	Absorption, distribution, metabolism, and excretion
	APT	Attached proton test
B	BOPIDY	Boron-dipyrromethene
	br	Broad
C	*C.*	*Candida*
	COSY	Correlated Spectroscopy
	CYP51	Cytochrome P450 Family 51
D	d	Doublet
	dd	Doublet of doublets
	ddd	Doublet of doublet of doublets
	DCE	1,2-dichloroethane
	DMF	Dimethylformamide
	DMSO	Dimethyl sulfoxide
	DNA	Deoxyribonucleic acid
E	EPR	Electron paramagnetic resonance
	ER	Endoplasmic reticulum
	Erg11	Lanosterol 14 α-demethylase
	ESI-HRMS	Electrospray ionization high resolution mass spectrometry
	EtOH	Ethanol
H	HMQC	Heteronuclear multiple quantum coherence
	HPLC	High performance liquid chromatography
	HSAB	Hard and soft acids and bases principle
I	ICP-AES	Inductively coupled plasma atomic emission spectroscopy
	ICU	Intensive Care Unit
	IFI	Invasive fungal infection
J	*J*	Coupling constant
L	LD_{50}	50% lethal dose
M	m	Multiplet
	MeOH	Methanol
	MFS	Major facilitator superfamily
	MIC	Minimum inhibitory concentration
	MOPS	3-(*N*-morpholino)propanesulfonic acid
N	NMR	Nuclear magnetic resonance
O	OD	Optical density
P	ppm	Parts per million
	PTFE	Polytetrafluoroethylene
Q	q	Quartet
	quint	Quintuplet
R	ROS	Reactive oxygen species
	RPMI	Roswell Park Memorial Institute
S	s	Singlet
	spp.	Several species
T	t	Triplet
	td	Triplet of doublets
	TBAB	Tetrabutylammonium bromide
	TLC	Thin Layer Chromatography
	TMS	Tetramethylsilane
U	UV	Ultraviolet

V	Vis	Visible
Y	YPD	Yeast peptone dextrose

1. Introduction

1.1 Fungal infections

The kingdom Fungi is composed of a wide variety of eukaryotic organisms, among which are yeasts and molds. At the cellular level, fungi differ from animals and plants due to the presence of chitin in the cell wall and ergosterol in the membranes. There are approximately five million different species of fungi,[1] many of which are used in biotechnology, for example as the primary source of the antibiotic penicillin.

Of the currently known fungal species, around 8000 have been proven to be pathogenic for plants and 300 for humans.[2] Most pathogenic fungi are opportunistic, meaning most hosts are equipped to deal with them under normal physiological conditions. However, in the particular case of humans, when individuals are immunocompromised, fungi may replicate and lead to infection and inflammation, either local or systemic.[3] Local infections of the skin, nails or scalp affect regularly at least 20% of the world population. Allergic fungal infections occur when the fungus reaches the respiratory tract and are common in patients with pre-existing conditions such as asthma.[4] Oral and vulvovaginal candidiasis, which are mucosal infections, affect more than 75% of the female population.[5] Invasive fungal infections (IFIs) are the most serious, often life-threatening, infections caused by fungi, killing more than one million people per year.[6]

Most IFIs are caused by *Candida*, *Aspergillus* or *Cryptococcus* spp..[7] In the hospital context, *Candida* species are the most frequent pathogens causing invasive fungal infections (invasive candidiasis). Candida bloodstream infection, also known as candidaemia, is the most common form of invasive candidiasis.[8] There are at least 15 pathogenic species of *Candida*, but the majority of invasive candidiasis are caused by *Candida albicans*, *Candida glabrata*, *Candida tropicalis*, *Candida parapsilosis* and *Candida krusei*.[9] *Candida* spp. exist in the human skin and gut microbiota in 60% of healthy people. Several risk factors contribute to the transition of these fungi from commensal to pathogenic. Among them are antimicrobial abuse, presence of a central venous catheter, recent major surgery, and prolonged stay in the Intensive Care Unit (ICU). Approximately 50% of the invasive candidiasis cases are caused by *Candida albicans,* however the increased use of antifungal drugs has been triggering a progressive shift to non-*albicans Candida* spp. that are less susceptible to antifungal drugs, such as *Candida glabrata*.[8]

The morbidity and mortality rates associated with IFIs have grown in the last decades in immunocompromised individuals, such as cancer patients and HIV-infected people. In the early 2000s when the HIV epidemic peaked, it was estimated that over one million people

were infected each year with C*ryptococcus,* 600,000 of whom died.[10] Technology advances in medicine have greatly contributed to the intensification of IFIs, since some of these advances have led to an increase in the number of immunocompromised individuals – there are more people surviving different types of cancer and more people receiving organ transplants.[1]

1.2 Antifungal drugs

As eukaryotic organisms, fungi share many biological processes with animals and plants, so it is difficult to find a therapy selective to fungi that does not compromise the host.[11] The antifungal drugs currently available to treat IFIs belong to a few classes of chemical compounds, namely polyenes, echinocandins, antimetabolites and azoles.[12] Echinocandins are unique since they inhibit the synthesis of 1,3-β-D glucans, which plays an important role in the integrity of the cell wall, and are generally fungicidal in several fungi species.[13] Polyene drugs have alternated single and double carbon-carbon bonds, and they bind to ergosterol affecting the permeability of the cell wall.[14] Antimetabolite drugs have similar structures to pyrimidine bases, inhibiting RNA and DNA synthesis. 5-flucytosine (5-FC) is the only antifungal antimetabolite, being used normally in combination with other antifungal drugs due to high development of resistance if used alone.[15] Azoles are by far the most common antifungal drugs, inhibiting the biosynthesis of ergosterol, which include imidazole and triazole drugs that are mainly used topically or orally, respectively.[16]

The main target of polyenes and azoles is ergosterol, a sterol found in fungal membranes, which has the same function as cholesterol in animal cells.[17] Ergosterol does not exist in animal cells, making it a useful target for antifungal therapies. Ergosterol is a demethylated derivative of lanosterol (**Figure 1.1**). The sterol biosynthesis of ergosterol and cholesterol are catalyzed by the same enzymes until the formation of zymosterol (the seventh reaction in a total of eleven reactions in the synthesis of ergosterol).[18] Two additional double bonds and a methyl group on carbon 24 in ergosterol, compared with cholesterol, make this compound less flexible and therefore generates a more rigid membrane.[19]

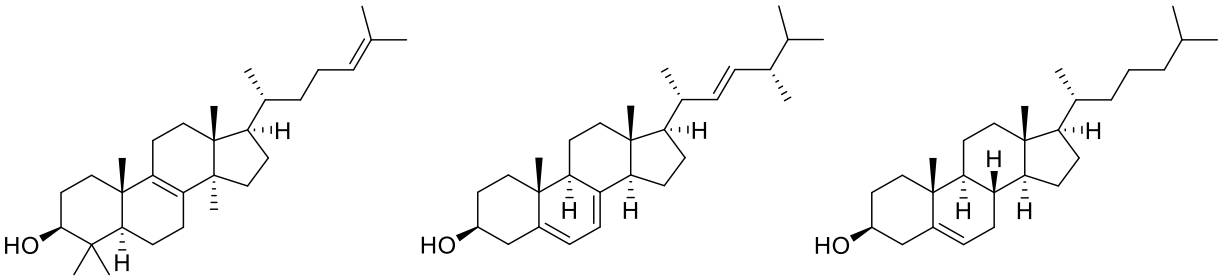

Figure 1.1 – Structures of lanosterol (left), ergosterol (middle), and cholesterol (right).

Polyenes are a group of natural drugs formed by polyhydroxylic lactone rings with 20–40 carbon atoms and 4–7 conjugated double bonds. They bind to ergosterol and originate pores that cause the disruption of the cell membrane and promote the leakage of K^+ and Na^+ ions, which are lethal to the cell.[14] Polyenes have side effects since they also bind to cholesterol, although the affinity for ergosterol is higher. Despite their toxicity, three polyenes – nystatin, natamycin and amphotericin B – are currently used as antifungal therapies.[16]

Echinocandins are a recent class of semi-synthetic antifungal drugs, which inhibit the synthesis of 1,3-β-D glucan by noncompetitive inhibition of the enzyme 1,3-β-D glucan synthetase. Glucans play an important role in the integrity of the cell wall and disruption of their synthesis leads to cell death.[13,17] There are three echinocandins available to date – caspofungin, micafungin and anidulafungin – which are fungicidal against several fungal species, including azole-resistant species.[7]

1.2.1 Azoles

Antifungal azoles are synthetic compounds and the most common antifungal drugs in clinical use. They inhibit the biosynthesis of ergosterol by competitive inhibition of the cytochrome P450-dependent enzyme, lanosterol 14α-demethylase (Erg11, encoded by gene *ERG11*), also known as CYP51A (**Figure 1.2**).[20] The cytochrome P450 (CYP450) superfamily is one of the largest families of cytochromes and is named after its absorbance peak at 450 nm due to the species bound to carbon monoxide. They range in size from 48 to 60 kDa and are heme-thiolate enzymes.[21] This family is believed to have one common ancestral about three billion years ago, and is thus found in all class of known organisms.[22] In humans the P450 family is well known for its role in drug metabolism, while in fungi it is important for the metabolism of sterols.

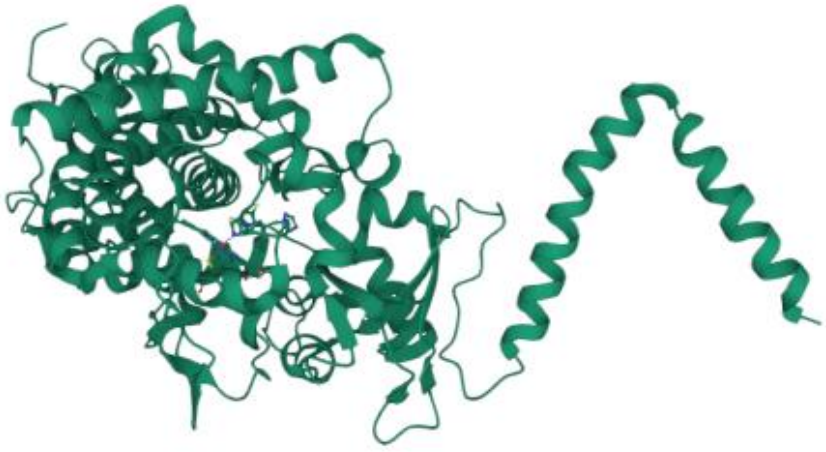

Figure 1.2 – Structure of the lanosterol 14α-demethylase (Erg11) enzyme. Plotted using Chimera.

The Erg11 enzyme catalyzes the oxidative removal of the 14α-methyl group of lanosterol in a 3-step reaction (**Figure 1.3**).[23] Azoles block this enzymatic reaction by binding to the active center of Erg11 mainly through coordination of a nitrogen atom of the azole to the iron of the heme, as illustrated for fluconazole (**Figure 1.4**). However, additional interactions of the azoles with Erg11 need to be established for an effective inhibition of the enzyme to occur. The dihalogenophenyl and other heteroatom-containing functions present in the azole drugs (e.g. hydroxyl or amine) are also involved in several weaker interactions within the active site of Erg11.[24] Other potential non-bonding interactions such as hydrogen bonds, ionic, hydrophobic and van der Waals interactions, and π effects, although individually weak may collectively have a strong influence on the drug binding strength. Consequently, both the azole and dihalogenophenyl chemical functions, among others, may be considered pharmacophores of the azole drugs.

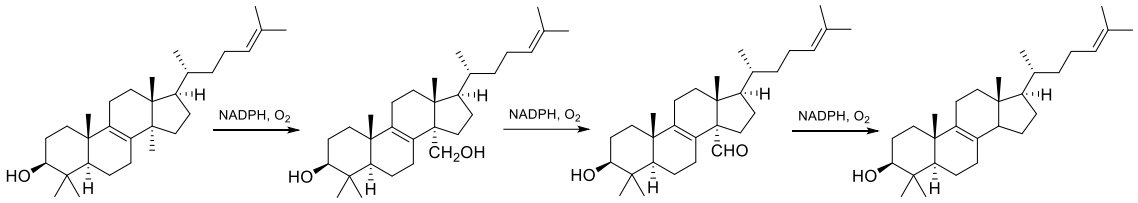

Figure 1.3 – Three-step reaction for the oxidative removal of the 14α-methyl group of lanosterol.

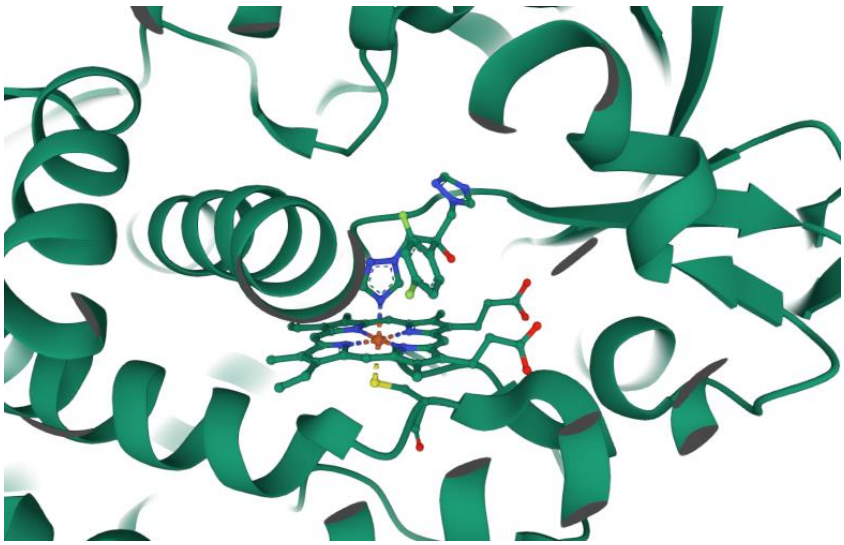

Figure 1.4 – Coordination of the *N*-4 nitrogen atom of fluconazole to the iron of the heme in Erg11. Plotted using Chimera.

As a result of the enzymatic inhibition, 14α-methylated sterols accumulate and fungal cells cannot replicate.[16] In most cases, this effect is only fungistatic and does not kill fungi. However, in some cases the cell membrane can be disrupted leading to fungal death (fungicidal). Azoles are also used in the prophylaxis of systemic fungal infections.[25]

The first azoles to appear on the market were mainly imidazole derivatives such as clotrimazole, miconazole, and ketoconazole, but due to their side effects and interaction with other drugs they are now only used to treat superficial infections. Imidazoles have been largely replaced by triazoles such as fluconazole, itraconazole, voriconazole, and posaconazole (**Figure 1.5**),[16] which have a broader antifungal spectrum, higher potency, and lower toxicity to humans.[25]

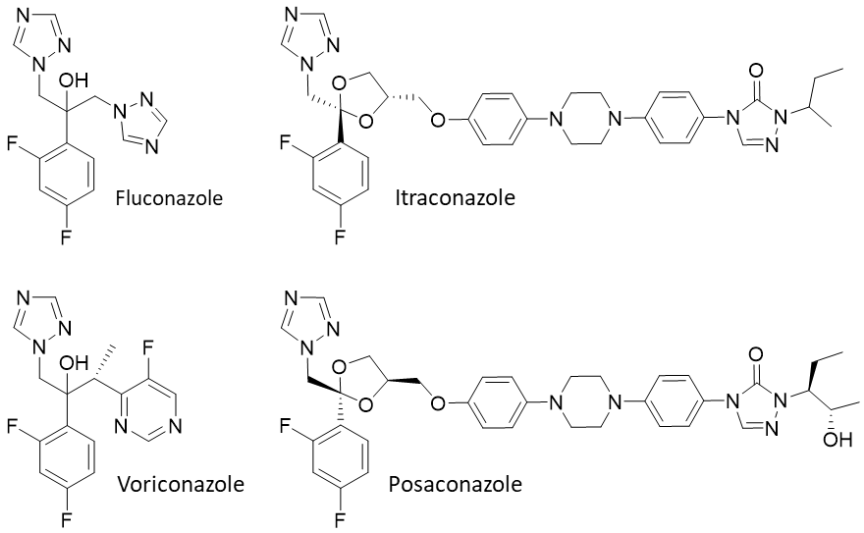

Figure 1.5 – Structures of selected antifungal triazoles: fluconazole, itraconazole, voriconazole, and posaconazole.

Fluconazole is the most used azole in the treatment of IFIs. It is composed of a difluorophenyl function, two 1,2,4-triazoles, and a hydroxyl, all appended on a quaternary carbon atom. It is active against some yeast species like *Candida* and *Cryptococcus* but not against molds like *Aspergillus*. It can be administrated orally or intravenously, since it is water soluble and has a good pharmacokinetic profile (with a long half-life) that allows once-daily dosing.[20]

1.3 Azole resistance

The widespread use of azoles has prompted the emergence of azole resistance, which poses a serious health threat as it diminishes the already limited treatment options. There are many reports of azole-resistant *Candida* spp., mainly because azoles are fungistatic and not fungicidal.[16] The prolonged exposure to azoles, for example in the context of prophylactic measures, is known to foster resistance. Moreover, it is possible that the use of azoles in agriculture also promotes the emergence of resistant fungal species in humans through ingestion of infected crops.[26]

The length of the side chains in azole drugs may have an impact on azole resistance. Small molecules display fewer weak interactions within the active site of Erg11 and thus promote resistance acquisition by fungi. This was shown in studies where mutations in the active site led to resistance to fluconazole and voriconazole (short chain azoles) but not to posaconazole and itraconazole (long chain azoles).[27] The mutations typically lead to a lower susceptibility to fluconazole, and therefore to a higher minimum inhibitory concentration (MIC) of the drug. Flowers et al. showed that even single-nucleotide changes can significantly alter the MIC of fluconazole, although for itraconazole and voriconazole the change in MIC is not as significant.[28] The authors suggested that new antifungal azole compounds should have a long chain to increase the interactions within the active site of the enzyme.

There are three major mechanisms of azole-resistance acquisition in fungi: 1) mutations in the region of the *ERG11* gene encoding the Erg11 active site, which decrease the affinity of the azole to the active site of the enzyme (**Figure 1.6.A**);[26] 2) overexpression of Erg11, which overcomes the inhibition of the enzyme (**Figure 1.6.B**);[29] and 3) increase in azole efflux by ATP-binding cassette (ABC) and major facilitator superfamily (MFS) transporters, leading to less accumulation of azoles in cells, which in turn prevents Erg11 inhibition (**Figure 1.6.C**).[30]

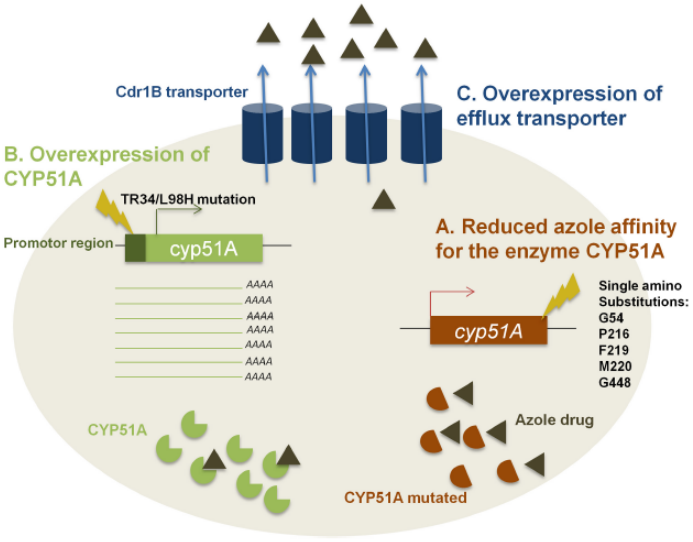

Figure 1.6 – Three major mechanisms of azole-resistance acquisition in fungi. Taken from Berger et al.[26]

1.4 Copper

Copper is an essential trace element with potential toxic properties that stem from its ability to generate reactive oxidative species (ROS) and also to displace metals, such as iron and zinc, from biomolecules. As such, organisms have intrinsic homeostatic mechanisms to

simultaneously ensure adequate copper uptake and distribution to fulfill physiological needs and avoid the toxic effects of the metal.

During infection, the host activates an intrinsic process called nutritional immunity, aimed at depriving the invading microorganism of essential nutrients such as iron or calcium to limit its proliferation.[31] However, in the case of copper, the opposite occurs and the host macrophages, after engulfing the microorganism, accumulate this metal in phagolysosomes where the toxic properties of copper are used as an antimicrobial.[32]

Copper has been used as a fungicidal pesticide since the 17th century and is still used for this purpose, for example in the form of copper sulfate on the Bordeaux mixture used as a preventive treatment for vines, potatoes, and tomatoes.[33]

1.4.1 Copper coordination chemistry

The hard and soft acids and bases (HSAB) principle may be used in order to predict which ligands will be best suited for each metal cation. This principle generalizes that hard bases will preferably bind to hard acids, and soft bases bind to soft acids, with metals seen as Lewis acids (will accept an electron pair) and ligands seen as Lewis bases (capable of donating an electron pair). The formation of a coordinate (or dative) covalent bond between a metal and a ligand can be seen as an acid-base Lewis reaction. The categorization as hard or soft is essentially based on the polarizability of the species, i.e. on the ability of the electron cloud of a species to deform. The more polarizable species are classified as soft (electronic cloud easily deformable) and the less polarizable ones are classified as hard. Still, polarizability is not the only relevant factor that determines interaction, with frequent exceptions existing to the HSAB principle.[34,35]

Copper is a first-row transition metal with a $3d^{10}$ $4s^{1}$ electronic configuration. It has two major oxidation states, copper(I) and copper(II), but free copper is mostly found as copper(II) since the other form is not very stable in aqueous media.[36] Copper(I) has a d^{10} configuration and is diamagnetic, being considered a soft acid that prefers soft donors such as thioethers, phosphines, nitriles, isonitriles, iodide, cyanide, and thiolates. Its complexes have most frequently a tetrahedral coordination geometry. Copper(II) has a d^{9} configuration, thus being paramagnetic. It has a borderline softness that favors binding to amines, imines, and bidentate ligands. In aqueous solution it displays coordination numbers ranging from four to six depending on the denticity and structure of the ligands, and is a very adaptable cation regarding its coordination properties. The 4-coordinated complexes usually have a square planar or tetrahedral geometry, while the 5-coordinated complexes often have a square-

pyramidal geometry or a trigonal bipyramidal one. The 6-coordinated complexes frequently have distorted octahedral geometries due to the Jahn-Teller effect, in which there is an axial elongation of the weak bonds with the two apical donor atoms.[37,38]

A ligand containing two or more donor atoms is said to be polydentate. A bidentate ligand such as ethylenediamine can form a chelate complex, since the two donor atoms are linked by a small chain. Such complex will have a higher stability due to the chelate effect, which refers to the enhanced stability of a metal complex that contains chelate rings when compared to a similar complex having no chelate rings.[39] The thermodynamic stability of a complex increases as the number of chelate rings formed with the ligands increases (**Figure 1.7**).[40] The principles of thermodynamics say that a reaction is spontaneous when the enthalpy variation is negative and the entropy variation is positive. The chelate effect can be explained by an increasing entropy due to the increased number of ligand species in solution from the release of monodentate ligands upon complex formation.[41] The size of the preferential chelate ring depends on the size of the cation. Small metal cations such as copper(II) prefer 5- and 6-membered rings, and the stability of the complex decreases significantly as the chelate ring increases beyond 6. For larger metal cations the stability of the complex decreases when shifting from 5-membered to 6-membered chelate rings, since these metals accept more donor atoms and thus prefer smaller chelate ring sizes.[39]

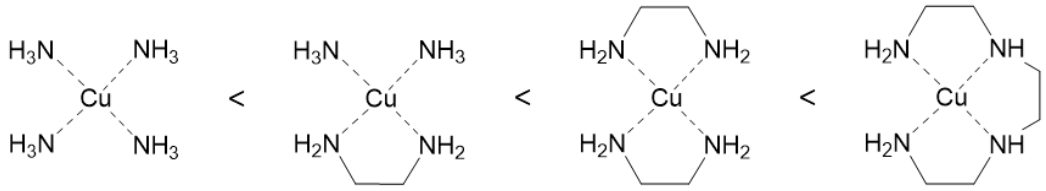

Figure 1.7 – Representation of the increase in stability of copper(II) complexes by consecutive increase of chelate rings based on the same donor atoms.

Compounds that interact with metals, such as chelators, shuttles, and ionophores can all be used in therapeutic applications (**Figure 1.8**). Chelation therapy has been used to reduce the toxic levels of certain metals (e.g. lead, mercury or iron) by exploring the ability of chelators to form complexes via multiple coordination bonds. Metal shuttles do not alter the intracellular free metal concentration, but instead deliver the metal to a specific target while chelated. Metal ionophores are similar to metal chelators, because they also coordinate the metal via multiple bonds, but are usually associated with an increase in the intracellular free metal concentration since they facilitate the transport of the metal into the lipid bilayer by formation of a lipophilic metal complex.[42,43] Copper ionophores have been studied as anticancer and antimicrobial agents, but also as carriers in copper deficiency diseases.

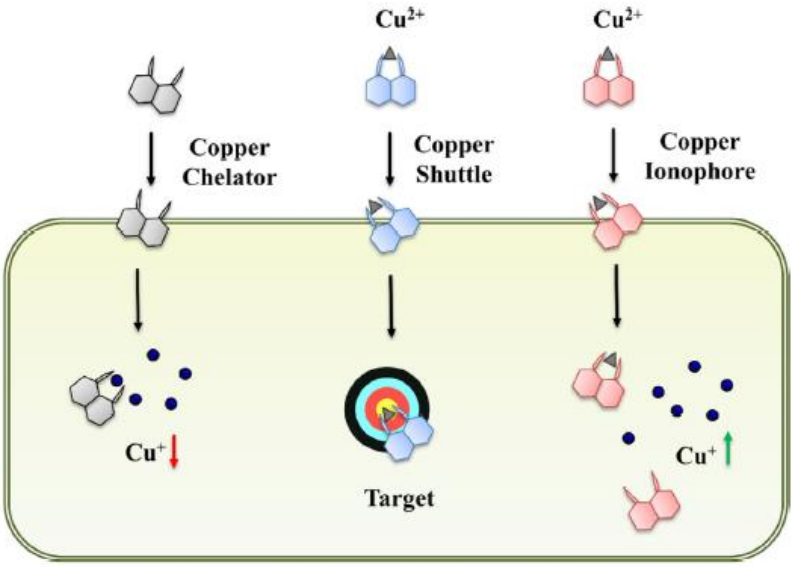

Figure 1.8 – Different ways of affecting copper homeostasis. Taken from Oliveri et al.[42]

1.4.2 Copper toxicity

One of the well-known toxicity routes of copper comes mainly from the redox properties of copper(II), which catalyses the formation of ROS. In the presence of superoxide anions, copper(II) can be reduced to copper(I), which can catalyse the decomposition of hydrogen peroxide to form hydroxyl radicals (**Figure 1.9.A**). The latter are very active and can react with biomolecules such as lipids, DNA, and proteins to cause oxidative stress and therefore cell death.[42,44] However, ROS formation cannot be the only toxicity mechanism of copper since high levels are still toxic to anaerobic bacteria and yeast cells, environments where ROS are unable to form.[43] The majority of ROS-independent toxicity mechanisms come from the binding and/or displacement of other metal ions or cofactors, like iron or zinc, since copper(II) displays the maximum stability for divalent first-row transition metal complexes, as predicted by the Irving-Williams series.[45] An example of this is the displacement of iron from iron-sulfur (Fe-S) clusters, which serve as co-factors of many proteins such as electron transfer proteins (**Figure 1.9.B**). The displacement of iron atoms from these centers alters the conformation of the enzyme, thus inactivating it and leading to a non-functional enzyme.[46] The displacement of zinc by copper in Zn-fingers, which are the largest class of DNA-binding proteins, can also affect cell function and structural integrity (**Figure 1.9.C**).[47,48]

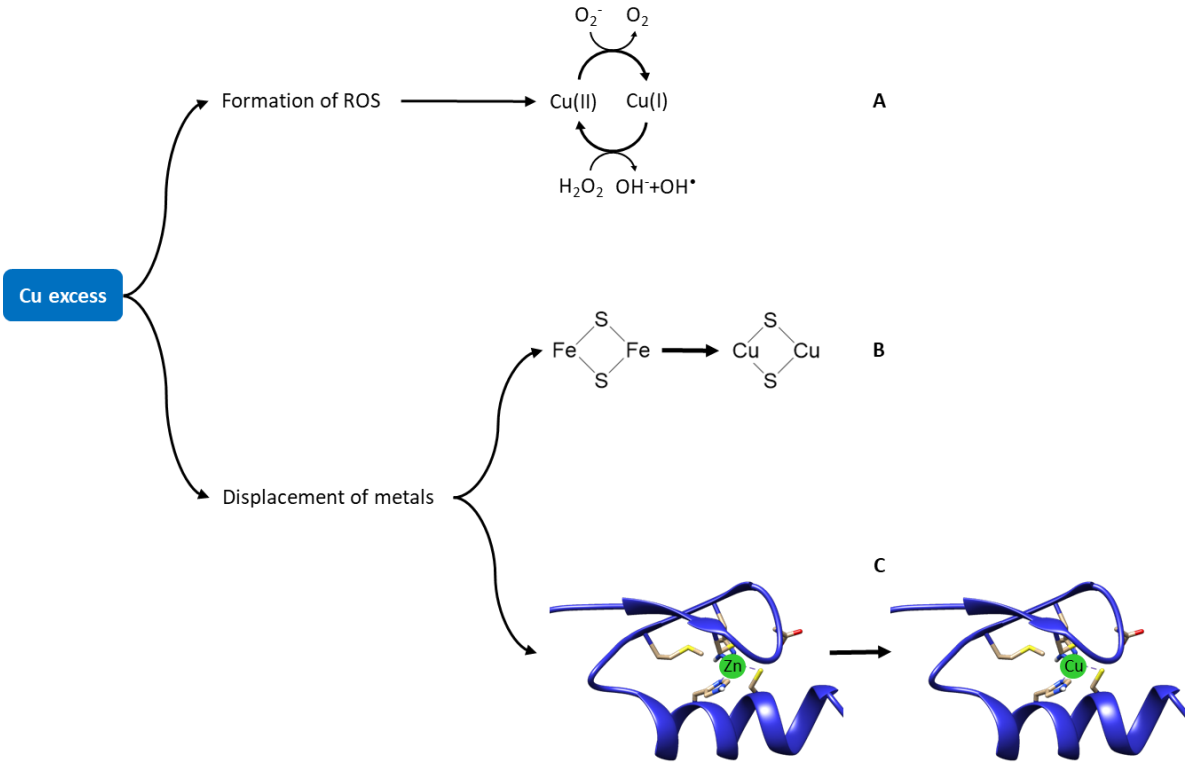

Figure 1.9 – Toxic effects caused by copper excess. Part C adapted from Tidow et al. using Chimera.[49]

1.4.3 Copper(II) synergy with azoles

Some azole drugs like fluconazole have shown a synergistic effect with copper(II) in recent years. In a 2015 study by Zabek et al., the antifungal properties of a hypothetical copper(II) complex of fluconazole were tested.[50] Such complex showed a better antifungal activity than fluconazole alone, even in non-*albicans* species that tend to have a lower susceptibility to antifungal drugs. Despite not disclosing the activity mechanism of the complex, the authors concluded that there was no formation of ROS, and that copper(II) cations did not influence fungal cell growth.

Some *Candida* spp. treated with fluconazole recover their growth by 50% when compared to the untreated control at 48h. This phenomenon is called trailing growth and indicates that fungi have adaptative mechanisms that lead to azole tolerance. This is an important phenomenon since persistence and recurrence of infection is due to tolerance of fungi to antifungal drugs. A 2019 study by Hunsaker et al. concluded that when cells are treated with fluconazole and copper, growth levels do not increase at 48h.[51] This effect also appears with addition of small levels of copper(II) to the medium. Contrarily to the hypothesis of Zabek et al., this study did not evidence the formation of a stable complex between copper(II) and fluconazole as tested by UV-vis spectrophotometry, but it showed that the activity of commercial antifungal drugs can be increased, even for resistant species of fungi.

Interfering with fungal copper homeostasis, for example by using copper(II) ionophores or shuttles, is an attractive strategy to induce cell death. In the synthesis of new antifungal drugs, some chelating groups for copper(II) should be considered in order to enhance the copper delivery, which might be useful in resensitizing resistant cells to existing drugs. Some well-known chelators for copper(II) are pyrithione, diethyldithiocarbamate, and 8-hydroxyquinoline (**Figure 1.10**).[52] Pyrithione binds divalent and trivalent metal cations and has been recognized as an antimicrobial copper ionophore; diethyldithiocarbamate has negatively charged sulfur atoms, being able to bind metal cations, and is known for its anticancer properties and formation of ROS; 8-hydroxyquinoline is capable of binding divalent and trivalent metal cations through chelation and its derivatives have shown antineurodegenerative, anticancer, antimicrobial, and other biological properties.[53] Since such small chelating molecules may have useful properties, designing new compounds incorporating copper-binding functions like these might be an idea worth exploring. A 2020 study by Hunsaker et al. reported the synthesis of compounds based on fluconazole and containing donor functions for copper replacing one of the 1,2,4-triazole functions.[54] The rationale of the study was to introduce metal-binding groups to enhance the activity of azoles against fungi and possibly promote a fungicidal rather than fungistatic activity. However, none of the synthesized fluconazole derivatives proved to be fungicidal, although two of them promoted a lower trailing growth when compared to fluconazole, and one induced alteration in the intracellular levels of copper.

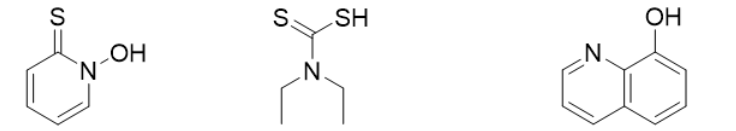

Pyrithione Diethyldithiocarbamate 8-hydroxyquinoline

Figure 1.10 – Structure of some well-known chelators for copper(II).

Gaspar-Cordeiro et al. have shown that copper ionophores or shuttles are effective against *Candida glabrata* and *Candida albicans*.[55] They reported an organic compound with an 1-(4-aminobenzyl)-1,2,4-triazole scaffold with an appended 8-hydroxyquinoline function capable of forming a complex with copper(II) (**Figure 1.11**). Such complex displayed a MIC_{50} of 31.3–62.5 µM for both species of *Candida*, being more effective than fluconazole against *Candida glabrata*. The intracellular ergosterol levels were measured after treatment with the complex to clarify if the activity resulted from inhibition of Erg11. While ergosterol levels remained unchanged after treatment with the complex, intracellular copper levels were increased, as measured by inductively coupled plasma atomic emission spectroscopy (ICP-

AES). Treatment with the copper(II) complex showed a 20% increase of copper accumulation in comparison with cells treated with $CuCl_2$, suggesting that the complex acts as a copper(II) ionophore or shuttle.

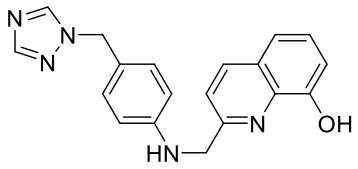

Figure 1.11 – Structure of a triazole compound developed by Gaspar-Cordeiro et al.[55]

Recently, Gaspar-Cordeiro et al. reported that the synergistic effect between copper(II) and fluconazole in *Candida glabrata* results from the accumulation of higher amounts of fluconazole inside cells, which strongly impacts sterol metabolism.[56] It was also demonstrated that co-treatment with copper(II) and fluconazole affects zinc homeostasis, and it was suggested that the displacement of zinc by copper in Zn-fingers motifs of transcription factors, could explain the observed decrease in fungal growth.

1.5 Development of new azole drugs

The increase in the number of people affected by IFIs, along with the growing resistance of fungi to current antifungals and the limited number of existing antifungals, underlines the pressing need to develop more effective antifungals.[8,14] In this regard, fluconazole may be seen not only as a model compound, but also as a solid base for the development of novel compounds with higher antifungal activity, and ideally also improved therapeutic profile.

Several authors have synthesized new fluconazole analogs, either by appending additional groups to the hydroxyl function or by changing the last step of the synthesis – the addition of the second triazole – with the addition of different groups. In the former case, there are examples of carboxylic acid and phosphate ester derivatives of fluconazole,[57] in which these compounds become prodrugs with higher lipophilicity such that their skin absorption is higher. In the latter case, the goal was to synthesize compounds that would improve the activity of fluconazole or have activity against fluconazole-resistant species like *Candida krusei*, by adding functions that could enhance the activity of the drug. In fact, some new azole compounds synthesized by the last method are already approved as drugs, such as voriconazole and albaconazole (**Figure 1.12**).

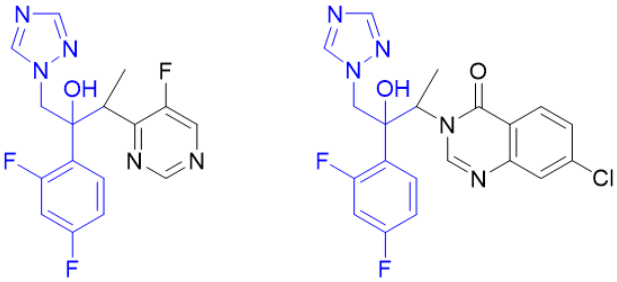

Figure 1.12 – Structures of recent azole antifungals derived from fluconazole: voriconazole and albaconazole. The conserved fluconazole structure on the azoles is represented in blue.

Sadeghpour et al. replaced the 1*H*-1,2,4-triazole with a 3-nitro-1,2,4-triazole or a 2-(piperazin-1-yl)ethanol moiety and realized that the compounds were more active against yeasts than against filamentous fungi, just like fluconazole, suggesting they have a similar activity mechanism to the model drug.[58] Hashemi et al.[59] and Lebouvier et al.[60] also synthesized new azoles with the dichlorophenyl pharmacophore, using 4-amino-3-mercapto-1,2,4-triazole and several azaheterocycles in place of one 1,2,4-triazole function. Both research groups also found lower MIC values when using the dichlorophenyl pharmacophore compared to the difluorophenyl one, which translates into higher antifungal activity.

Since cytochrome P450 enzymes exist in all classes of organisms, one factor to consider in azoles is the interaction of this class of drugs with similar enzymes in the human body such as CYP51. Warrilow et al. synthesized compound VT-1161 (**Figure 1.13**), once again by replacing one triazole function.[61] It was tested for interactions with *C. albicans* recombinant Erg11, human CYP51, and other human CYPs that play key roles on drug metabolism such as CYP2C9, CYP2C19 and CYP3A4. They concluded that VT-1161 has a high binding affinity for Erg11, but does not affect significantly the human CYP51 or the human CYPs involved in drug metabolism. They also concluded that VT-1161 has a lower MIC than voriconazole, a known Erg11 inhibitor, meaning that VT-1161 increases the amount of methylated sterols, thus decreasing the concentration of ergosterol. This compound is currently at phase III clinical trials named as oteseconazole.[12]

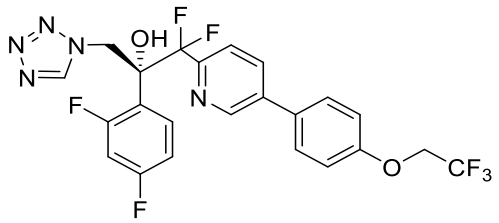

Figure 1.13 – Structure of VT-1161, also named oteseconazole.

Another application recently sought with fluconazole derivatives is their fluorescent tracking in fungal cells. In 2017, Benhamou et al. synthesized two novel azoles with the pharmacophore part of fluconazole appended with two different fluorescent dyes, and both had antifungal activity against several *Candida* species.[62] Ergosterol biosynthesis takes place mainly in the endoplasmic reticulum (ER), where most of the enzymes of this biosynthesis (such as Erg11) are located, but both probes located in the mitochondria instead of the ER, which leads to a decreased efficacy of these antifungal probes. In 2018, the same group synthesized similar structures but with ER-directing molecular groups.[63,64] Unlike the previous probes, these new ones were detected in the nuclear envelope and cortical structure of the ER (**Figure 1.14**). The accumulation of these probes in the ER explains their higher antifungal activity in comparison with the previous probes.

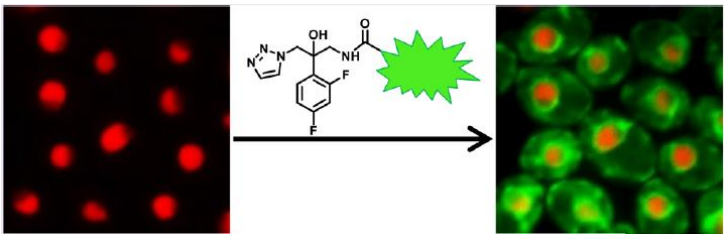

Figure 1.14 – Representation of the ER as seen by fluorescent tracking. Taken from Benhamou et al.[64]

The interaction of antifungal azoles with different metal cations is a recent focus of research, and some authors have shown that metal complexes with already existing drugs have higher activities than the drugs alone.[65] Zhang et al. showed that fluconazole forms a complex with silver(I) that increases the activity of fluconazole.[66] Martinez et al.[67] and Kljun et al.[68] synthesized ruthenium complexes with imidazole drugs including clotrimazole and miconazole, improving their antifungal activities. Gagini et al. used clotrimazole and ketoconazole to form complexes with copper, gold, and silver that enhanced the activity of the drugs.[69] Instead of using available drugs, several authors have synthesized new azole ligands capable of forming complexes with different metal ions that have higher antifungal activities than the ligands alone.[70–73] Sumrra et al. synthesized a compound (**Figure 1.15.A**) able to form complexes with different divalent metal ions such as iron(II), cobalt(II), nickel(II), copper(II), and zinc(II) in a 1:2 (M:L) stoichiometry, which have higher antifungal activity than the ligand itself.[74] Li et al. showed that the zinc(II) and copper(II) complexes of a compound based on a tetraazacyclododecane appended with two benzimidazole functions (**Figure 1.15.B**) have better antimicrobial activity than the ligand alone.[75] Aly et al.[76] and Li et al.[77] synthesized compounds able to form complexes with copper(II), **Figure 1.15.C** and **Figure 1.15.D,** respectively. Both compounds displayed enhanced antifungal activity upon complexation with

copper(II). The properties of the metals, along with the biological activity of the organic compounds of all these compounds, are expected to increase the antifungal activity of the compound, and possibly prevent emergence of resistance.

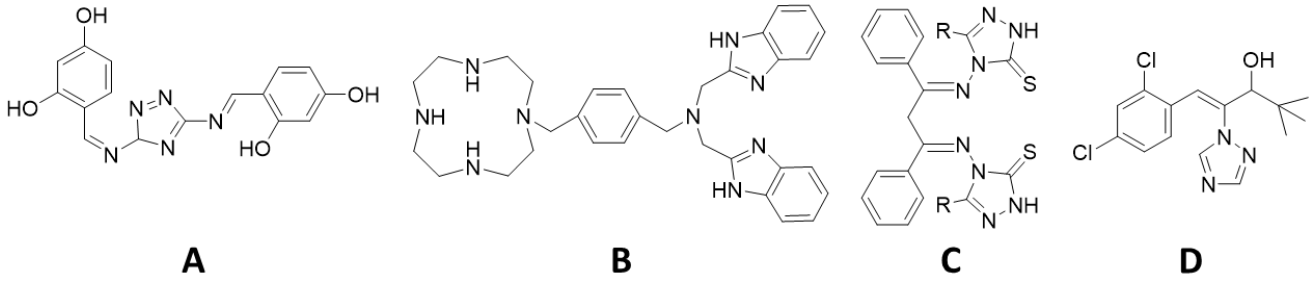

Figure 1.15 – Structures of some azole ligands developed for the complexation of divalent metal ions.

1.6 Drug pharmacokinetics and toxicity

There are three phases in the action of a drug: pharmaceutic, pharmacokinetic, and pharmacodynamic. The pharmacokinetic phase is the journey of the drug since the moment it is administered until it reaches its target or is excreted,[78] commonly known for four main aspects: absorption, distribution, metabolization, and excretion (ADME) (**Figure 1.16**).[79] When a drug is orally administrated most of the absorption takes place in the upper intestine, but to be absorbed the drug cannot be too lipophilic or lipophobic. If the drug is too lipophobic, thus having many polar groups or atoms, it will not pass the cell membranes of the intestine to the blood, but if it is too lipophilic, not having enough polar groups or atoms, the drug will be poorly soluble in the gut and blood and it will dissolve in fat globules, leading to poor absorption. It is necessary that the drug has the right equilibrium in lipophilicity to pass the intestine and target cell membranes, so it is important to study the pharmacokinetics of a drug to improve its formulation for the maximization of oral bioavailability.[80]

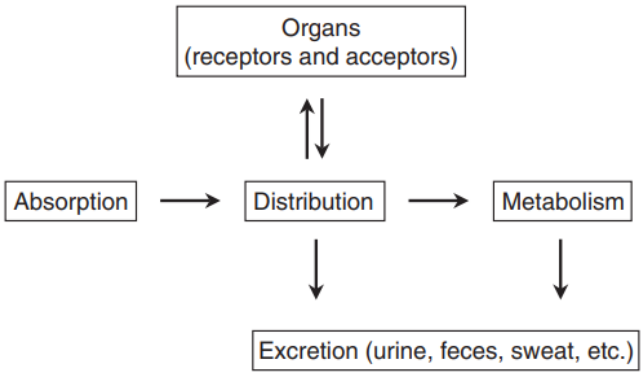

Figure 1.16 – Pharmacokinetics (ADME) in the human body. Taken from Tillement et al.[79]

Along with pharmacokinetic studies, toxicity studies are essential to prevent that drugs display severe side effects on humans. Given that every substance can be toxic when in excess, toxicity is measured by the median lethal dose (LD_{50}), which is the dose of a substance that is necessary to kill half of the population tested. The lower the LD_{50}, the more a substance is toxic. Among some of the toxicity studies performed on a potential drug are acute toxicity testing to determine the LD_{50}, skin sensitization tests, mutagenicity testing, carcinogenicity testing, embryotoxicity studies, and neurotoxicity testing.[81] Side effects from a drug can be related to lack of specificity of the drug itself, since drugs have specific targets, such as enzymes, proteins, receptors. If a drug is not specific for the target, it could interact with other biomolecules and cause unspecific interactions, leading to non-desired effects. Toxicity tests are a crucial part of the research of a new drug, not only before marketing authorisation but also after the drug is released for public use, and some causal or rare side effects not found in the initial research can be found years after marketing authorization, from client feedback or randomized studies.[82]

Pharmacokinetics and toxicity were the major causes for the investigation that led to the development of fluconazole. The best azole at that time – ketoconazole – was metabolically unstable, being a target of metabolic degradation, and so could not be administered orally as desired.[83] For all imidazole antifungals, a major part of the dose absorbed is lost by first-pass metabolism in the liver. A series of compounds related to ketoconazole were synthesized and in one of them, the imidazole was replaced by a 1,2,4-triazole. The compound had better activity *in vivo*, theoretically because the triazole is less lipophilic than the imidazole and therefore less susceptible to metabolic degradation. The authors focused on tertiary alcohols due to higher activity in animal models, and so duplicated the 1,2,4-triazole function, synthesizing the compound known as UK-47265. Although this compound had a good pharmacokinetic evaluation, it was hepatotoxic and teratogenic.[84] The authors then replaced the dichlorophenyl function by others such as 2,4-difluorophenyl, thus obtaining fluconazole that is not hepatotoxic nor teratogenic (**Figure 1.17**). Some studies previously mentioned have substituted difluorophenyl for dichlorophenyl in order to obtain antifungal drugs with higher activities,[58–60] but in light of the fact that chlorine substituents can increase toxicity of the drug, such substitution needs to be carefully considered.

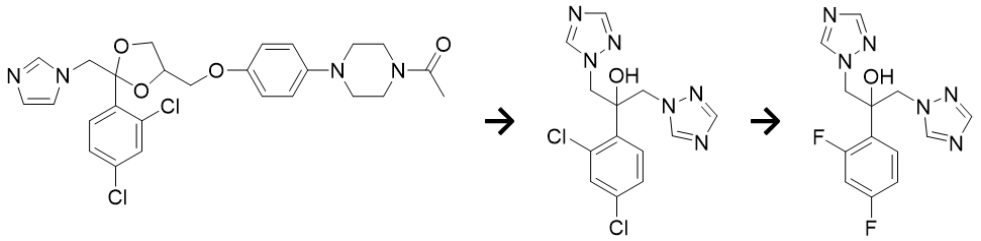

Figure 1.17 – Structural comparison of ketoconazole (left), UK-47265 (middle), and fluconazole (right).

1.7 Thesis aim

The main objective of this work is to synthesize new azole compounds containing the main pharmacophore functions present in the model drug fluconazole – the azole and the dihalogenophenyl functions – while adding functions capable of coordinating copper(II) to promote a variable interaction of the compounds with copper(II) and explore a potential synergy between the azoles and the metal, in search of a higher antifungal activity.

The proposed azole compounds are based on a central tertiary amine purposely substituted with three functional groups: a dihalogenophenyl function, an azole function, and a variable copper(II)-binding function. In this design, the target azole compounds contain at least two good donor atoms for copper(II) adequately separated for achieving metal chelation, the central tertiary amine and at least one atom from the copper(II)-binding function, thus being polydentate ligands. The structural variations proposed are expected to allow for structure-activity relationship studies based on the biological activity results to be obtained, so as to find lead compound structures for potential drug development.

The interaction of target azoles with copper(II) will be studied by UV spectrophotometry. The goal is to characterize the binding ability of the azoles towards copper(II), in order to correlate that with their biological activity when in presence of this metal cation. Since it is not currently known how strong of a copper(II) binding is beneficial for the antifungal activity increase in azoles, it would be interesting to rank the azoles in a copper(II)-binding ligand series.

The activity of the target azoles will be tested in *Candida glabrata* in order to evaluate the antifungal efficacy of the compounds alone and of their copper(II) complexes, and to compare the different compounds with each other and with fluconazole. Compounds displaying relevant antifungal activity will then be tested for their Erg11 inhibition ability, through determination of the ergosterol levels in fungal cells treated with the selected compounds.

2. Materials and methods

2.1 Synthesis

Reagents were obtained from commercial sources and used as received. Organic solvents of analytical grade were dried by distillation using established procedures.[85] All intermediate compounds were synthesized, except 1-(3-aminopropyl)imidazole (**8**) that was obtained from commercial sources. All reactions were carried out under an inert nitrogen atmosphere. The reactions were followed by thin-layer chromatography (TLC) in silica MACHEREY-NAGEL ALUGRAM Xtra SIL G/UV_{254}. The TLC spots were detected by UV radiation or by staining with iodine. All synthesized compounds were characterized by Nuclear Magnetic Resonance (NMR) spectroscopy, and all target compounds were characterized additionally by Electrospray Ionization High Resolution Mass Spectrometry (ESI-HRMS). NMR spectra of ^{1}H, ^{13}C, ^{19}F, APT, and 2D NMR correlations (COSY and HMQC) were acquired on a Bruker Avance II+ 400 MHz spectrometer in $CDCl_3$ solutions at 25 ^{o}C, at the CERMAX NMR facility. Chemical shifts (δ) are given in ppm relative to the tetramethylsilane (TMS) signal as reference. NMR assignments are based on ^{1}H integration and multiplicity as well as 2D correlation spectra. All NMR spectra were plotted and analyzed using the Mnova software from Mestrelab Research. The ESI-HRMS spectra were obtained by the Mass Spectrometry Unit (UniMS) of ITQB/iBET, from samples dissolved in MeOH or H_2O and acquired in positive mode using a Thermo Scientific Q Exactive™ Focus Hybrid Quadrupole-Orbitrap™ spectrometer.

2.1.1 Synthesis of intermediate compounds

8-hydroxy-2-quinolinecarboxaldehyde (1)

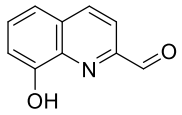

Selenium dioxide (1.447 g, 13 mmol) was dissolved in 25 mL of dioxane and 3 mL of water and heated to 95 ^{o}C. A solution of 8-hydroxy-2-methylquinoline (1.592 g, 10 mmol) in 25 mL of dioxane was added dropwise for 15 minutes, and the brown solution heated at 95 ^{o}C for 1 day. The black solids were filtered off from the mixture and the solution was evaporated to dryness. The crude compound was purified by silica column chromatography (60 Å, 70–230 mesh, 3.8 x 12.6 cm) using Hexane/EtOAc (80:20) as eluent (R_f = 0.3). The combined pure fractions were evaporated and dried under vacuum to yield pure **1** as a yellow solid (994 mg, 57%). This procedure was adapted from Tallec et al.[86]

^{1}H NMR ($CDCl_3$, 400 MHz, ppm): δ_H = 10.15 (s, 1H, C$H_{aldehyde}$), 8.26 (d, $^{3}J_{HH}$ = 8.5 Hz, 1H, C$H_{quinoline}$), 8.08 (br s, 1H, O$H_{quinoline}$), 7.99 (d, $^{3}J_{HH}$ = 8.5 Hz, 1H, C$H_{quinoline}$), 7.56 (t, $^{3}J_{HH}$ = 8.0 Hz,

1H, C$H_{quinoline}$), 7.36 (dd, $^3J_{HH}$ = 8.3 Hz, $^4J_{HH}$ = 0.9 Hz, 1H, C$H_{quinoline}$), 7.21 (dd, $^3J_{HH}$ = 7.7 Hz, $^4J_{HH}$ = 1.0 Hz, 1H, C$H_{quinoline}$).

^{13}C NMR ($CDCl_3$, 100 MHz, ppm): δ_C = 192.72 (1C, CH$_{aldehdyde}$), 153.01 (1C, $C_{q\ quinoline}$), 150.18 (1C, $C_{q\ quinoline}$), 137.83 (1C, $C_{q\ quinoline}$), 137.50 (1C, CH$_{quinoline}$), 130.95 (1C, CH$_{quinoline}$), 130.45 (1C, $C_{q\ quinoline}$), 118.07 (1C, CH$_{quinoline}$), 118.00 (1C, CH$_{quinoline}$), 111.22 (1C, CH$_{quinoline}$).

N-(2-Bromoethyl)phthalimide (2)

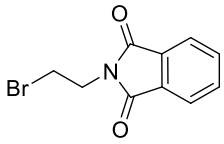

To a solution of 1,2-dibromoethane (3.45 mL, 40 mmol) in 6 mL of dry DMF was added tetrabutylammonium bromide (TBAB, 0.205 g, 0.6 mmol), potassium carbonate (2.802 g, 20 mmol), and phthalimide (1.471 g, 10 mmol). The stirred mixture was heated to 40 ^{o}C for 20h. The solids were filtered from the mixture and the solution was evaporated to dryness. The residue was taken in 50 mL of H_2O and the aqueous mixture was extracted with 4 x 15 mL of ethyl acetate. The combined organic layers were dried with anhydrous Na_2SO_4, filtered, evaporated, and dried under vacuum to yield pure **2** as a white solid (2.338 g, 92%). This procedure was adapted from Krchová et al.[87]

^{1}H NMR ($CDCl_3$, 400 MHz, ppm): δ_H = 7.84–7.79 (m, 2H, C$H_{phtalimide}$), 7.71–7.65 (m, 2H, C$H_{phtalimide}$), 4.05 (t, $^3J_{HH}$ = 6.7 Hz, 2H, C$H_{2\ ethyl}$), 3.55 (t, $^3J_{HH}$ = 6.7 Hz, 2H, C$H_{2\ ethyl}$).

^{13}C NMR ($CDCl_3$, 100 MHz, ppm): δ_C = 134.22 (2C, CH$_{phtalimide}$), 131.83 (2C, O=$C_{q\ phtalimide}$), 123.53 (2C, CH$_{phtalimide}$), 99.98 (2C, $C_{q\ phtalimide}$), 39.30 (1C, CH$_{2\ ethyl}$), 28.14 (1C, CH$_{2\ ethyl}$).

N-(2-(1,2,4-triazol-1-yl)ethyl)phthalimide (3)

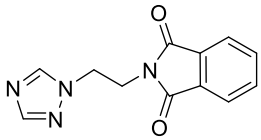

To a solution of 1,2,4-triazole (1.381 g, 20 mmol) in 60 mL of dry acetonitrile was added sodium *tert*-butoxide (1.920 g, 20 mmol), and the mixture was stirred for 1h. Then **2** (5.082 g, 20 mmol) and another 20 mL of dry acetonitrile were added to the milky white suspension, and the stirred mixture was heated to reflux over 2 days, during which time it became yellow with white solids. The solids were filtered out and the solution was evaporated to dryness. The residue was taken in 200 mL of $CHCl_3$ and 100 mL of H_2O were added. The mixture was extracted, and the separated aqueous phase was further extracted with 2 x 150 mL of $CHCl_3$. The combined organic layers were dried with anhydrous Na_2SO_4, filtered, evaporated, and

dried under vacuum. The product was purified by precipitation with approximately 20 mL of ethanol, filtered, and dried under vacuum to yield pure **3** as a white solid (2.641 g, 55%).

^{1}H NMR ($CDCl_3$, 400 MHz, ppm): δ_H = 8.51 (s, 1H, C$H_{triazole}$), 7.93 (s, 1H, C$H_{triazole}$), 7.79–7.74 (m, 2H, C$H_{phtalimide}$), 7.69–7.65 (m, 2H, C$H_{phtalimide}$), 4.53 (t, $^{3}J_{HH}$ = 5.9 Hz, 2H, C$H_{2\ ethyl}$), 4.12 (t, $^{3}J_{HH}$ = 5.9 Hz, 2H, C$H_{2\ ethyl}$).

^{13}C NMR ($CDCl_3$, 100 MHz, ppm): δ_C = 167.69 (2C, O=$C_{q\ phtalimide}$), 149.68 (1C, CH$_{triazole}$), 142.90 (1C, CH$_{triazole}$), 134.37 (2C, CH$_{phtalimide}$), 131.61 (2C, $C_{q\ phtalimide}$), 123.64 (2C, CH$_{phtalimide}$), 48.08 (1C, CH$_{2\ ethyl}$), 37.52 (1C, CH$_{2\ ethyl}$).

1-(2-aminoethyl)-1,2,4-triazole (4)

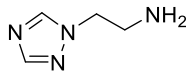

To a solution of **3** (404 mg, 1.67 mmol) in 30 mL of absolute ethanol and 10 mL of $CHCl_3$ was added hydrazine monohydrate (810 µL, 16.7 mmol), and the colorless solution was stirred at room temperature for 17 h. After that the solution was heated to 50 ^{o}C for 1 day, during which time white solids were formed. To the hot mixture were added 20 mL of $CHCl_3$ and the mixture was cooled. The mixture was filtered, and the solids washed with $CHCl_3$. The combined solution was evaporated, then co-evaporated with 2 x 5 mL of EtOH to remove the excess hydrazine, and the residue was dried under vacuum to yield pure **4** as a yellow oil (179 mg, 96%).

^{1}H NMR ($CDCl_3$, 400 MHz, ppm): δ_H = 8.20 (s, 1H, C$H_{triazole}$), 7.87 (s, 1H, C$H_{triazole}$), 4.20 (t, $^{3}J_{HH}$ = 5.7 Hz, 2H, C$H_{2\ ethyl}$), 3.09 (t, $^{3}J_{HH}$ = 5.7 Hz, 2H, C$H_{2\ ethyl}$).

^{13}C NMR ($CDCl_3$, 100 MHz, ppm): δ_C = 152.21 (1C, CH$_{triazole}$), 143.56 (1C, CH$_{triazole}$), 52.71 (1C, CH$_{2\ ethyl}$), 41.43 (1C, CH$_{2\ ethyl}$).

N-(3-Bromopropyl)phthalimide (5)

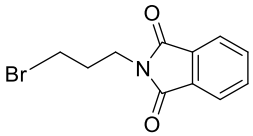

To a solution of 1,3-dibromopropane (16 mL, 160 mmol) in 34 mL of dry DMF was added tetrabutylammonium bromide (TBAB, 0.205 g, 0.6 mmol), potassium carbonate (11.072 g, 80 mmol), and phthalimide (5.884 g, 40 mmol). The mixture was stirred at room temperature for 3 days and then heated to 40 ^{o}C for 1 day, during which time it became yellow with white solids. The solids were filtered from the mixture and the solution was evaporated to dryness. The residue was taken in 150 mL of H_2O and extracted with 4 x 25 mL of ethyl acetate. The

combined organic layers were dried with anhydrous Na_2SO_4, filtered, and evaporated to dryness, producing 9.9 g of an impure compound as a white solid. 4 grams of this crude compound were purified by silica column chromatography (60 Å, 230–400 mesh, 3.8 x 7 cm) using $CHCl_3$ as eluent (R_f = 0.3). The combined pure fractions were evaporated and dried under vacuum to yield pure **5** as a white solid (3.295 g, 77%). This procedure was adapted from Krchová et al.[87]

^{1}H NMR ($CDCl_3$, 400 MHz, ppm): δ_H = 7.91–7.84 (m, 2H, C$H_{phtalimide}$), 7.78–7.71 (m, 2H, C$H_{phtalimide}$), 3.86 (t, $^3J_{HH}$ = 6.8 Hz, 2H, C$H_{2\ propyl}$), 3.44 (t, $^3J_{HH}$ = 6.7 Hz, 2H, C$H_{2\ propyl}$), 2.28 (quint, $^3J_{HH}$ = 6.8 Hz, 2H, CH_2–CH_2–$CH_{2\ propyl}$).

^{13}C NMR ($CDCl_3$, 100 MHz, ppm): δ_C = 168.24 (2C, O=$C_{q\ phtalimide}$), 134.06 (2C, $CH_{phtalimide}$), 132.00 (2C, $C_{q\ phtalimide}$), 123.33 (2C, $CH_{phtalimide}$), 36.73 (1C, $CH_{2\ propyl}$), 31.64 (1C, $CH_{2\ propyl}$), 29.79 (1C, CH_2–CH_2–$CH_{2\ propyl}$).

2-(3-(1H-1,2,4-triazol-1-yl)propyl)phthalimide (6)

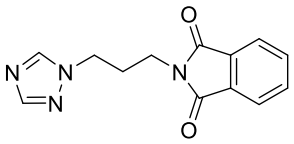

To a solution of 1,2,4-triazole (346 mg, 5 mmol) in 40 mL of dry acetonitrile was added sodium *tert*-butoxide (442 mg, 5 mmol), and the mixture was stirred for 1h. Then **5** (1.478 g, 5.5 mmol) was added to the milky white suspension in 15 mL of dry acetonitrile, dropwise for 10 minutes. The stirred mixture was heated to reflux over 2 days, during which time it became yellow with white solid. The solids were filtered out and the solution was evaporated to dryness. The residue was taken in 100 mL of $CHCl_3$ and 50 mL of H_2O were added. The mixture was extracted, and the separated aqueous phase was further extracted with 2 x 50 mL of $CHCl_3$. The combined organic layers were dried with anhydrous Na_2SO_4, filtered, evaporated, and dried under vacuum. The resulting yellow solid was washed with 20 mL of ethanol and the supernatant was filtered and evaporated to dryness. The crude compound was purified by silica column chromatography (60 Å, 230–400 mesh, 2.3 x 18 cm) using $CHCl_3$/MeOH (98:2) as eluent (R_f = 0.3). The combined pure fractions were evaporated and dried under vacuum to yield pure **6** as a yellow solid (518 mg, 40%).

^{1}H NMR ($CDCl_3$, 400 MHz, ppm): δ_H = 8.17 (s, 1H, C$H_{triazole}$), 7.85 (s, 1H, C$H_{triazole}$), 7.80–7.77 (m, 2H, C$H_{phtalimide}$), 7.69–7.66 (m, 2H, C$H_{phtalimide}$), 4.16 (t, $^3J_{HH}$ = 6.7 Hz, 2H, C$H_{2\ propyl}$), 3.66 (t, $^3J_{HH}$ = 6.2 Hz, 2H, C$H_{2\ propyl}$), 2.24 (quint, $^3J_{HH}$ = 6.7 Hz, 2H, CH_2–CH_2–$CH_{2\ propyl}$).

^{13}C NMR ($CDCl_3$, 100 MHz, ppm): δ_C = 168.37 (2C, O=$C_{q\ phtalimide}$), 152.18 (1C, $CH_{triazole}$), 143.60 (1C, $CH_{triazole}$), 134.21 (2C, $CH_{phthalimide}$), 131.87 (2C, $C_{q\ phthalimide}$), 123.40 (2C, $CH_{phthalimide}$), 47.10 (1C, $CH_{2\ propyl}$), 34.89 (1C, $CH_{2\ propyl}$), 28.97 (1C, CH_2–CH_2–$CH_{2\ propyl}$).

1-(3-aminopropyl)-1,2,4-triazole (7)

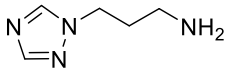

To a solution of **6** (2.800 g, 11 mmol) in 150 mL of absolute ethanol and 30 mL of $CHCl_3$ was added monohydrated hydrazine (5.3 mL, 110 mmol), and the colorless solution was stirred at room temperature for 2 days, during which time white solids were formed. To the hot mixture were added 50 mL of $CHCl_3$, the mixture was let to cool, filtered, and the solids washed with $CHCl_3$. The combined solution was evaporated, then co-evaporated with EtOH to remove the excess hydrazine, and the residue was dried under vacuum to yield pure **7** as a yellow oil (1.255 g, 91%).

^{1}H NMR ($CDCl_3$, 400 MHz, ppm): δ_H = 8.03 (s, 1H, $CH_{triazole}$), 7.87 (s, 1H, $CH_{triazole}$), 4.23 (t, $^3J_{HH}$ = 6.8 Hz, 2H, $CH_{2\ propyl}$), 2.64 (t, $^3J_{HH}$ = 6.7 Hz, 2H, $CH_{2\ propyl}$), 1.93 (quint, $^3J_{HH}$ = 6.7 Hz, 2H, CH_2–CH_2–$CH_{2\ propyl}$).

^{13}C NMR ($CDCl_3$, 100 MHz, ppm): δ_C = 151.85 (1C, $CH_{triazole}$), 143.05 (1C, $CH_{triazole}$), 46.90 (1C, $CH_{2\ propyl}$), 38.52 (1C, $CH_{2\ propyl}$), 32.96 (1C, CH_2–CH_2–$CH_{2\ propyl}$).

(E)-N-(3-(1H-imidazol-1-yl)propyl)-1-(2,4-dichlorophenyl)methanimine (9)

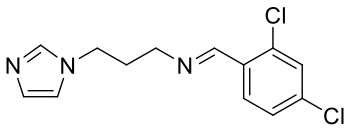

To a solution of **8** (597 µL, 5 mmol) in 50 mL of dry toluene was added 2,4-dichlorobenzaldehyde (875 mg, 5 mmol). Some 4 Å molecular sieves and 5 drops of AcOH were added to the colorless solution, and the stirred mixture was heated to reflux over 1 day, during which time it turned yellow. The solids were filtered out, and the solution was evaporated and dried under vacuum to yield pure **9** as a yellow oil (1.408 g, 99%).

^{1}H NMR ($CDCl_3$, 400 MHz, ppm): δ_H = 8.53 (s, 1H, CH_{imine}), 7.87 (d, $^3J_{HH}$ = 8.5 Hz, 1H, $CH_{benzene}$), 7.42 (s, 1H, $CH_{imidazole}$), 7.29 (d, $^4J_{HH}$ = 2.0 Hz, 1H, $CH_{benzene}$), 7.18 (dd, $^3J_{HH}$ = 8.5, 1.7 Hz, 1H, $CH_{benzene}$), 6.98 (s, 1H, $CH_{imidazole}$), 6.86 (s, 1H, $CH_{imidazole}$), 3.99 (t, $^3J_{HH}$ = 6.9 Hz, 2H, $CH_{2\ propyl}$), 3.51 (t, $^3J_{HH}$ = 7.0 Hz, 2H, $CH_{2\ propyl}$), 2.08 (quint, $^3J_{HH}$ = 6.7 Hz, 2H, CH_2–CH_2–$CH_{2\ propyl}$).

^{13}C NMR ($CDCl_3$, 100 MHz, ppm): δ_C = 157.52 (1C, CH_{imine}), 137.14 (1C, $CH_{imidazole}$), 137.05 (1C, $C_{q\ benzene}$), 135.55 (1C, $C_{q\ benzene}$), 131.46 (1C, $C_{q\ benzene}$), 129.53 (1C, $CH_{benzene}$), 129.43 (1C, $CH_{imidazole}$),

129.13 (1C, *C*H$_{benzene}$), 127.50 (1C, *C*H$_{benzene}$), 118.82 (1C, *C*H$_{imidazole}$), 57.67 (1C, *C*H$_{2\ propyl}$), 44.54 (1C, *C*H$_{2\ propyl}$), 31.89 (1C, CH$_2$–*C*H$_2$–CH$_{2\ propyl}$).

N-(2,4-dichlorobenzyl)-3-(1H-imidazol-1-yl)propan-1-amine (10)

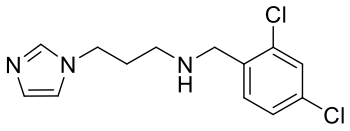

The oil of **9** (1.408 g, 4.99 mmol) was dissolved in 50 mL of dry MeOH and sodium borohydride ($NaBH_4$, 379 mg, 10 mmol) was added slowly. The yellow solution was stirred at room temperature for 6 h and then heated to reflux for 20 h, during which time it became colorless. The solution was filtered and evaporated to dryness. The residue was taken in 30 mL of $CHCl_3$ and 20 mL of H_2O were added with the pH adjusted to 9 by addition of KOH. The mixture was extracted, and the separated aqueous phase was further extracted with 2 x 30 mL of $CHCl_3$. The combined organic layers were dried with anhydrous Na_2SO_4, filtered, evaporated, and dried under vacuum to yield pure **10** as a yellow oil (1.417 g, 100%).

^{1}H NMR ($CDCl_3$, 400 MHz, ppm): δ_H = 7.39 (s, 1H, C*H*$_{imidazole}$), 7.30 (d, $^4J_{HH}$ = 1.9 Hz, 1H, C*H*$_{benzene}$), 7.21 (d, $^3J_{HH}$ = 8.1 Hz, 1H, C*H*$_{benzene}$), 7.14 (dd, $^3J_{HH}$ = 8.2, $^4J_{HH}$ = 1.9 Hz, 1H, C*H*$_{benzene}$), 6.97 (s, 1H, C*H*$_{imidazole}$), 6.82 (s, 1H, C*H*$_{imidazole}$), 3.98 (t, $^3J_{HH}$ = 6.9 Hz, 2H, C*H*$_{2\ propyl}$), 3.73 (s, 2H, NH–C*H*$_2$), 2.51 (t, $^3J_{HH}$ = 6.6 Hz, 2H, C*H*$_{2\ propyl}$), 1.86 (quint, $^3J_{HH}$ = 6.7 Hz, 2H, CH$_2$–C*H*$_2$–CH$_{2\ propyl}$).

^{13}C NMR ($CDCl_3$, 100 MHz, ppm): δ_C = 137.18 (1C, *C*H$_{imidazole}$), 136.04 (1C, *C*$_{q\ benzene}$), 134.31 (1C, *C*$_{q\ benzene}$), 133.42 (1C, *C*$_{q\ benzene}$), 130.87 (1C, *C*H$_{benzene}$), 129.40 (1C, *C*H$_{benzene}$), 129.35 (1C, *C*H$_{imidazole}$), 127.10 (1C, *C*H$_{benzene}$), 118.82 (1C, *C*H$_{imidazole}$), 50.66 (1C, N–*C*H$_2$), 45.44 (1C, *C*H$_{2\ propyl}$), 44.53 (1C, *C*H$_{2\ propyl}$), 31.22 (1C, CH$_2$–*C*H$_2$–CH$_{2\ propyl}$).

(E)-N-(3-(1H-imidazol-1-yl)propyl)-1-(2,4-difluorophenyl)methanimine (11)

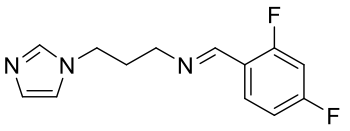

To a solution of **8** (597 µL, 5 mmol) in 20 mL of dry toluene was added 2,4-difluorobenzaldehyde (547 µL, 5 mmol). Some 4 Å molecular sieves and 5 drops of AcOH were added to the colorless solution, and the stirred mixture was heated to reflux overnight, during which time it turned yellow. The solids were filtered out, and the solution was evaporated and dried under vacuum to yield pure **11** as an orange oil (1.177 g, 94%).

^{1}H NMR ($CDCl_3$, 400 MHz, ppm): δ_H = 8.42 (s, 1H, C*H*$_{imine}$), 7.90 (td, $^4J_{HF}$ = 8.5, $^3J_{HH}$ = 6.7 Hz, 1H, C*H*$_{benzene}$), 7.44 (s, 1H, C*H*$_{imidazole}$), 7.00 (s, 1H, C*H*$_{imidazole}$), 6.91–6.82 (m, 2H), 6.76 (ddd, $^3J_{HF}$ =

10.9, $^{3}J_{HH}$ = 8.8, $^{4}J_{HH}$ = 2.4 Hz, 1H, C*H*$_{benzene}$), 4.02 (t, $^{3}J_{HH}$ = 7.0 Hz, 2H, C*H*$_{2\ propyl}$), 3.51 (t, $^{3}J_{HH}$ = 6.9 Hz, 2H, C*H*$_{2\ propyl}$), 2.10 (quint, $^{3}J_{HH}$ = 6.7 Hz, 2H, CH_2–C*H*$_2$–$CH_{2\ propyl}$).

^{13}C NMR ($CDCl_3$, 100 MHz, ppm): δ_C = 164.76 (dd, $^{1}J_{CF}$ = 218.5 Hz, $^{3}J_{CF}$ = 12.3 Hz, 1C, *C*$_{q\ benzene}$), 162.23 (dd, $^{1}J_{CF}$ = 220.0 Hz, $^{3}J_{CF}$ = 12.2 Hz, 1C, *C*$_{q\ benzene}$), 154.23 (1C, *C*H$_{imine}$), 137.17 (1C, *C*H$_{imidazole}$), 129.43 (1C, *C*H$_{imidazole}$), 129.03 (dd, $^{3}J_{CF}$ = 9.8 Hz, $^{3}J_{CF}$ = 4.1 Hz, 1C, *C*H$_{benzene}$), 120.08 (dd, $^{2}J_{CF}$ = 9.3 Hz, $^{4}J_{CF}$ = 3.2 Hz, 1C, *C*$_{q\ benzene}$), 118.82 (1C, *C*H$_{imidazole}$), 112.10 (dd, $^{2}J_{CF}$ = 21.6 Hz, $^{4}J_{CF}$ = 2.9 Hz, 1C, *C*H$_{benzene}$), 104.03 (t, $^{1}J_{CF}$ = 25.3 Hz, 1C, *C*H$_{benzene}$), 57.82 (1C, *C*H$_{2\ propyl}$), 44.63 (1C, *C*H$_{2\ propyl}$), 31.99 (1C, CH_2–*C*H_2–$CH_{2\ propyl}$).

^{19}F NMR ($CDCl_3$, 376 MHz, ppm): δ_F = −105.41 (m, 1F), −117.76 (m, 1F).

N-(2,4-difluorobenzyl)-3-(1H-imidazol-1-yl)propan-1-amine (12)

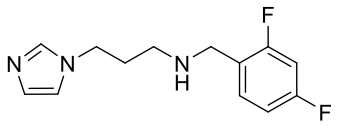

The oil of **11** (1.177 g, 5 mmol) was dissolved in 40 mL of dry MeOH and sodium borohydride ($NaBH_4$, 380 mg, 10 mmol) was added slowly. The yellow solution was stirred at room temperature for 1 h, then heated to reflux for 1 day, during which time it became colorless. The solution was filtered and evaporated to dryness. The residue was taken in 30 mL of $CHCl_3$ and 20 mL of H_2O were added, with the pH adjusted to 10 by addition of KOH. The mixture was extracted, and the separated aqueous phase was further extracted with 2 x 30 mL of $CHCl_3$. The combined organic layers were dried with anhydrous Na_2SO_4, filtered, evaporated, and dried under vacuum to yield pure **12** as a yellow oil (1.157 g, 98%).

^{1}H NMR ($CDCl_3$, 400 MHz, ppm): δ_H = 7.38 (s, 1H, C*H*$_{imidazole}$), 7.19 (td, $^{4}J_{HF}$ = 8.4, $^{3}J_{HH}$ = 6.6 Hz, 1H, C*H*$_{benzene}$), 6.97 (s, 1H, C*H*$_{imidazole}$), 6.82 (s, 1H, C*H*$_{imidazole}$), 6.80–6.68 (m, 2H), 3.97 (t, $^{3}J_{HH}$ = 6.9 Hz, 2H, C*H*$_{2\ propyl}$), 3.69 (s, 2H, NH–C*H*$_2$), 2.51 (t, $^{3}J_{HH}$ = 6.7 Hz, 2H, C*H*$_{2\ propyl}$), 1.85 (p, $^{3}J_{HH}$ = 6.8 Hz, 2H, CH_2–C*H*$_2$–$CH_{2\ propyl}$).

^{13}C NMR ($CDCl_3$, 100 MHz, ppm): δ_C = 161.17 (dd, $^{1}J_{CF}$ = 247.8, $^{3}J_{CF}$ = 12.0 Hz, 1C, *C*$_{q\ benzene}$), 160.14 (dd, $^{1}J_{CF}$ = 248.2, $^{3}J_{CF}$ = 12.1 Hz, 1C, *C*$_{q\ benzene}$), 136.19 (1C, *C*H$_{imidazole}$), 130.05 (dd, $^{3}J_{CF}$ = 8.9, $^{3}J_{CF}$ = 6.8 Hz, 1C, *C*H$_{benzene}$), 128.40 (1C, *C*H$_{imidazole}$), 121.93 (dd, $^{2}J_{CF}$ = 15.4, $^{4}J_{CF}$ = 3.1 Hz, 1C, *C*$_{q\ benzene}$), 117.81 (1C, *C*H$_{imidazole}$), 110.10 (dd, $^{2}J_{CF}$ = 20.9, $^{4}J_{CF}$ = 3.1 Hz, 1C, *C*H$_{benzene}$), 102.78 (t, $^{2}J_{CF}$ = 25.6 Hz, 1C, *C*H$_{benzene}$), 45.74 (1C, NH–*C*H$_2$), 44.40 (1C, *C*H$_{2\ propyl}$), 43.52 (1C, *C*H$_{2\ propyl}$), 30.19 (1C, CH_2–*C*H_2–$CH_{2\ propyl}$).

^{19}F NMR ($CDCl_3$, 376 MHz, ppm): δ_F = −111.73 (m, 1F), −115.27 (m, 1F).

(E)-N-(3-(1H-1,2,4-triazol-1-yl)propyl)-1-(2,4-dichlorophenyl)methanimine (13)

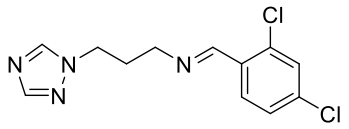

To a solution of **7** (1.255 g, 9.9 mmol) in 40 mL of dry toluene and 3 mL of absolute EtOH was added 2,4-dichlorobenzaldehyde (1.733 mg, 9.9 mmol). Some 4 Å molecular sieves and 10 drops of AcOH were added to the colorless solution, and the stirred mixture was heated to reflux over 1 day and after that to 80 ^{o}C for 3 days, during which time it turned yellow. The solids were filtered out, and the solution was evaporated and dried under vacuum to yield pure **13** as an orange oil (2.7 g, 96%).

^{1}H NMR ($CDCl_3$, 400 MHz, ppm): δ_H = 8.57 (s, 1H, C*H*$_{imine}$), 8.02 (s, 1H, C*H*$_{triazole}$), 7.90–7.88 (m, 2H), 7.34 (d, $^{4}J_{HH}$ = 2.0 Hz, 1H, C*H*$_{benzene}$), 7.22 (dd, $^{3}J_{HH}$ = 8.5, $^{4}J_{HH}$ = 1.7 Hz, 1H, C*H*$_{benzene}$), 4.27 (t, $^{3}J_{HH}$ = 6.8 Hz, 2H, C*H*$_{2\ propyl}$), 3.56 (t, $^{3}J_{HH}$ = 5.8 Hz, 2H, C*H*$_{2\ propyl}$), 2.23 (quint, $^{3}J_{HH}$ = 6.7 Hz, 2H, CH_2–C*H*$_2$–$CH_{2\ propyl}$).

^{13}C NMR ($CDCl_3$, 100 MHz, ppm): δ_C = 157.75 (1C, *C*H$_{imine}$), 152.08 (1C, *C*H$_{triazole}$), 143.18 (1C, *C*H$_{triazole}$), 137.18 (1C, *C*$_{q\ benzene}$), 135.63 (1C, *C*$_{q\ benzene}$), 131.46 (1C, *C*$_{q\ benzene}$), 129.63 (1C, *C*H$_{benzene}$), 129.14 (1C, *C*H$_{benzene}$), 127.56 (1C, *C*H$_{benzene}$), 57.68 (1C, *C*H$_{2\ propyl}$), 47.30 (1C, *C*H$_{2\ propyl}$), 30.65 (1C, CH_2–*C*H_2–$CH_{2\ propyl}$).

N-(2,4-dichlorobenzyl)-3-(1H-1,2,4-triazol-1-yl)propan-1-amine (14)

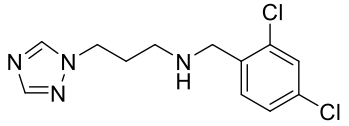

The oil of **13** (2.7 g, 9.5 mmol) was dissolved in 50 mL of dry MeOH and sodium borohydride ($NaBH_4$, 720 mg, 19 mmol) was added slowly. The light yellow solution was heated to reflux for 18 h, and then it was filtered and evaporated to dryness. The residue was taken in 100 mL of $CHCl_3$ and 50 mL of H_2O were added, with the pH adjusted to 10 by addition of KOH. The mixture was extracted, and the separated aqueous phase was further extracted with 2 x 40 mL of $CHCl_3$. The combined organic layers were dried with anhydrous Na_2SO_4, filtered, evaporated, and dried under vacuum to yield pure **14** as an orange oil (2.614 g, 97%).

^{1}H NMR ($CDCl_3$, 400 MHz, ppm): δ_H = 7.98 (s, 1H, C*H*$_{triazole}$), 7.87 (s, 1H, C*H*$_{triazole}$), 7.31 (d, $^{4}J_{HH}$ = 1.9 Hz, 1H, C*H*$_{benzene}$), 7.22 (d, $^{3}J_{HH}$ = 8.2 Hz, 1H, C*H*$_{benzene}$), 7.15 (dd, $^{3}J_{HH}$ = 8.2, $^{4}J_{HH}$ = 2.0 Hz, 1H, C*H*$_{benzene}$), 4.24 (t, $^{3}J_{HH}$ = 6.8 Hz, 2H, C*H*$_{2\ propyl}$), 3.74 (s, 2H, NH–C*H*$_2$), 2.52 (t, $^{3}J_{HH}$ = 6.5 Hz, 2H, C*H*$_{2\ propyl}$), 1.99 (quint, $^{3}J_{HH}$ *J* = 6.7 Hz, 2H, CH_2–C*H*$_2$–$CH_{2\ propyl}$).

^{13}C NMR ($CDCl_3$, 100 MHz, ppm): δ_C = 151.99 (1C, *C*H$_{triazole}$), 143.19 (1C, *C*H$_{triazole}$), 136.05 (1C, *C*$_{q\ benzene}$), 134.34 (1C, *C*$_{q\ benzene}$), 133.44 (1C, *C*$_{q\ benzene}$), 130.82 (1C, *C*H$_{benzene}$), 129.38 (1C, *C*H$_{benzene}$), 127.09 (1C, *C*H$_{benzene}$), 50.61 (1C, NH–*C*H$_2$), 47.18 (1C, *C*H$_{2\ propyl}$), 45.30 (1C, *C*H$_{2\ propyl}$), 29.82 (1C, CH$_2$–*C*H$_2$–CH$_{2\ propyl}$).

(E)-N-(2-(1H-1,2,4-triazol-1-yl)ethyl)-1-(pyridin-2-yl)methanimine (15)

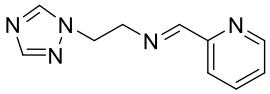

To a solution of **4** (112 mg, 1 mmol) in 10 mL of dry toluene and 5 mL of absolute EtOH was added 2-pyridinecarboxaldehyde (91 µL, 0.95 mmol). Some 4 Å molecular sieves and 3 drops of AcOH were added and the dark yellow solution was heated to reflux over 21 h. The solids were filtered out, and the solution was evaporated and dried under vacuum to yield pure **15** as a brown oil (191 mg, 100%).

^{1}H NMR ($CDCl_3$, 400 MHz, ppm): δ_H = 8.52 (d, $^3J_{HH}$ = 4.3 Hz, 1H, C*H*$_{pyridine}$), 8.11 (s, 1H, C*H*$_{imine}$), 8.02 (s, 1H, C*H*$_{triazole}$), 7.84 (s, 1H, C*H*$_{triazole}$), 7.78 (d, $^3J_{HH}$ = 7.9 Hz, 1H, C*H*$_{pyridine}$), 7.62 (td, $^3J_{HH}$ = 7.7, $^4J_{HH}$ = 1.5 Hz, 1H, C*H*$_{pyridine}$), 7.21 (ddd, $^3J_{HH}$ = 7.5, $^3J_{HH}$ = 4.8, $^4J_{HH}$ = 1.1 Hz, 1H, C*H*$_{pyridine}$), 4.47 (t, $^3J_{HH}$ = 5.8 Hz, 2H, C*H*$_{2\ ethyl}$), 3.98 (t, $^3J_{HH}$ = 5.1 Hz, 2H, C*H*$_{2\ ethyl}$).

^{13}C NMR ($CDCl_3$, 100 MHz, ppm): δ_C = 164.48 (1C, *C*H$_{imine}$), 153.61 (1C, *C*$_{q\ pyridine}$), 152.08 (1C, *C*H$_{triazole}$), 149.57 (1C, *C*H$_{pyridine}$), 143.73 (1C, *C*H$_{triazole}$), 136.58 (1C, *C*H$_{pyridine}$), 125.11 (1C, *C*H$_{pyridine}$), 121.47 (1C, *C*H$_{pyridine}$), 59.45 (1C, *C*H$_{2\ ethyl}$), 50.03 (1C, *C*H$_{2\ ethyl}$).

N-(pyridin-2-ylmethyl)-2-(1H-1,2,4-triazol-1-yl)ethan-1-amine (16)

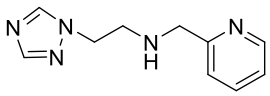

The oil of **15** (191 mg, 0.95 mmol) was dissolved in 10 mL of dry MeOH and sodium borohydride ($NaBH_4$, 76 mg, 2 mmol) was added slowly. The brown solution was stirred at room temperature for 2 h, then heated to reflux for 20 h during which time it became orange. The solution was evaporated to dryness, the residue was taken in 30 mL of $CHCl_3$, and 20 mL of H_2O were added with the pH adjusted to 10 by addition of KOH. The mixture was extracted, and the separated aqueous phase was further extracted with 2 x 30 mL of $CHCl_3$. The combined organic layers were dried with anhydrous Na_2SO_4, filtered, evaporated, and dried under vacuum to yield pure **16** as a brown oil (185 mg, 96%).

^{1}H NMR ($CDCl_3$, 400 MHz, ppm): δ_H = 8.44 (d, $^3J_{HH}$ = 4.6 Hz, 1H, C*H*$_{pyridine}$), 8.09 (s, 1H, C*H*$_{triazole}$), 7.86 (s, 1H, C*H*$_{triazole}$), 7.54 (td, $^3J_{HH}$ = 7.7, $^4J_{HH}$ = 1.7 Hz, 1H, C*H*$_{pyridine}$), 7.15 (d, $^3J_{HH}$ = 7.8 Hz, 1H,

C*H*$_{pyridine}$), 7.07 (td, $^{3}J_{HH}$ = 5.2, $^{4}J_{HH}$ = 1.7 Hz, 1H, C*H*$_{pyridine}$), 4.23 (t, $^{3}J_{HH}$ = 5.8 Hz, 2H, C*H*$_{2\ ethyl}$), 3.81 (s, 2H, NH–C*H*$_2$), 3.04 (t, $^{3}J_{HH}$ = 5.8 Hz, 2H, C*H*$_{2\ ethyl}$).

^{13}C NMR ($CDCl_3$, 100 MHz, ppm): δ_C = 157.98 (1C, *C*$_{q\ piridine}$), 150.95 (1C, *C*H$_{triazole}$), 148.29 (1C, *C*H$_{piridine}$), 142.60 (1C, *C*H$_{triazole}$), 135.48 (1C, *C*H$_{piridine}$), 121.16 (1C, *C*H$_{piridine}$), 121.13 (1C, *C*H$_{piridine}$), 53.60 (1C, *C*H$_{2\ ethyl}$), 48.83 (1C, NH–*C*H$_2$), 47.17 (1C, *C*H$_{2\ ethyl}$).

(E)-N-(2-(1H-1,2,4-triazol-1-yl)ethyl)-1-(2,4-dichlorophenyl)methanimine (17)

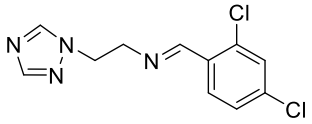

To a solution of **4** (623 mg, 5.56 mmol) in 20 mL of dry toluene and 6 mL of absolute EtOH was added 2,4-dichlorobenzaldehyde (973 mg, 5.56 mmol). Some 4 Å molecular sieves and 5 drops of AcOH were added to the colorless solution, and the stirred mixture was heated to reflux over 19 h, during which time it turned bright yellow. The solids were filtered out, the solution was evaporated and dried under vacuum to yield pure **17** as a yellow solid (1.406 g, 94%).

^{1}H NMR ($CDCl_3$, 400 MHz, ppm): δ_H = 8.40 (s, 1H, C*H*$_{imine}$), 8.00 (s, 1H, C*H*$_{triazole}$), 7.88 (s, 1H, C*H*$_{triazole}$), 7.81 (d, $^{3}J_{HH}$ = 8.5 Hz, 1H, C*H*$_{benzene}$), 7.31 (d, $^{4}J_{HH}$ = 2.0 Hz, 1H, C*H*$_{benzene}$), 7.19 (dd, $^{3}J_{HH}$ = 8.3, $^{4}J_{HH}$ = 1.9 Hz, 1H, C*H*$_{benzene}$), 4.48 (t, $^{3}J_{HH}$ = 5.6 Hz, 2H, C*H*$_{2\ ethyl}$), 4.00 (t, $^{3}J_{HH}$ = 6.0 Hz, 2H, C*H*$_{2\ ethyl}$).

^{13}C NMR ($CDCl_3$, 100 MHz, ppm): δ_C = 159.52 (1C, *C*H$_{imine}$), 152.19 (1C, *C*H$_{triazole}$), 143.74 (1C, *C*H$_{triazole}$), 137.51 (1C, *C*$_{q\ benzene}$), 135.82 (1C, *C*$_{q\ benzene}$), 131.08 (1C, *C*$_{q\ benzene}$), 129.66 (1C, *C*H$_{benzene}$), 129.00 (1C, *C*H$_{benzene}$), 127.58 (1C, *C*H$_{benzene}$), 59.70 (1C, *C*H$_{2\ ethyl}$), 50.07 (1C, *C*H$_{2\ ethyl}$).

N-(2,4-dichlorobenzyl)-2-(1H-1,2,4-triazol-1-yl)ethan-1-amine (18)

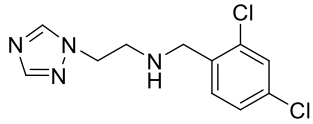

The solid of **17** (1.900 g, 7.06 mmol) was dissolved in 50 mL of dry MeOH and sodium borohydride ($NaBH_4$, 801 mg, 21.18 mmol) was added slowly. The light yellow solution was heated to reflux for 2 days, then filtered and evaporated to dryness. The residue was taken in 100 mL of $CHCl_3$ and 70 mL of H_2O were added, with the pH adjusted to 10 by addition of KOH. The mixture was extracted, and the separated aqueous phase was further extracted with 2 x 80 mL of $CHCl_3$. The combined organic layers were dried with anhydrous Na_2SO_4, filtered, evaporated, and dried under vacuum to yield pure **18** as a light yellow solid (1.797 g, 94%).

^{1}H NMR ($CDCl_3$, 400 MHz, ppm): δ_H = 8.06 (s, 1H, C$H_{triazole}$), 7.88 (s, 1H, C$H_{triazole}$), 7.30 (d, $^4J_{HH}$ = 2.0 Hz, 1H, C$H_{benzene}$), 7.19 (d, $^3J_{HH}$ = 8.2 Hz, 1H, C$H_{benzene}$), 7.14 (dd, $^3J_{HH}$ = 8.2, $^4J_{HH}$ = 2.0 Hz, 1H, C$H_{benzene}$), 4.22 (t, $^3J_{HH}$ = 5.7 Hz, 2H, C$H_{2\ ethyl}$), 3.77 (s, 2H, NH–CH_2), 3.01 (t, $^3J_{HH}$ = 5.2 Hz, 2H, C$H_{2\ ethyl}$).

^{13}C NMR ($CDCl_3$, 100 MHz, ppm): δ_C = 152.12 (1C, CH$_{triazole}$), 143.57 (1C, CH$_{triazole}$), 135.65 (1C, $C_{q\ benzene}$), 134.28 (1C, $C_{q\ benzene}$), 133.54 (1C, $C_{q\ benzene}$), 130.66 (1C, CH$_{benzene}$), 129.37 (1C, CH$_{benzene}$), 127.18 (1C, CH$_{benzene}$), 50.22 (1C, NH–CH$_2$), 49.81 (1C, CH$_{2\ ethyl}$), 47.89 (1C, CH$_{2\ ethyl}$).

2.1.2 Synthesis of target compounds

N-(2,4-dichlorobenzyl)-3-(1H-imidazol-1-yl)-N-(pyridin-2-ylmethyl)propan-1-amine (19a)

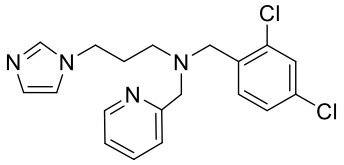

The oil of **10** (284 mg, 1 mmol) was dissolved in 11 mL of dry 1,2-dichloroethane (DCE), 2-pyridinecarboxaldehyde (95 µL, 1 mmol) and sodium triacetoxyborohydride ($NaBH(OAc)_3$, 426 mg, 2 mmol) were added, and the yellow solution was stirred at room temperature for 18 h. After that the solution was heated to reflux for 22 h, during which time it became amber with suspended solids. The solution was filtered and evaporated to dryness, the residue was taken in 30 mL of $CHCl_3$, and 20 mL of H_2O were added. The mixture was extracted, and the separated aqueous phase was further extracted with 2 x 30 mL of $CHCl_3$. The combined organic layers were dried with anhydrous Na_2SO_4, filtered, and evaporated to dryness. The crude compound was purified by silica column chromatography (60 Å, 230–400 mesh, 1.8 x 18 cm) using $CHCl_3$/MeOH (95:5) as eluent (R_f = 0.3). The combined pure fractions were evaporated and dried under vacuum to yield pure **19a** as a brown oil (154 mg, 41%).

^{1}H NMR ($CDCl_3$, 400 MHz, ppm): δ_H = 8.45 (d, $^3J_{HH}$ = 5.5 Hz, 1H, C$H_{pyridine}$), 7.57 (td, $^3J_{HH}$ = 7.7, $^4J_{HH}$ = 1.8 Hz, 1H, C$H_{pyridine}$), 7.36 (d, $^3J_{HH}$ = 8.3 Hz, 1H, C$H_{benzene}$), 7.31–7.24 (m, 3H), 7.14 (dd, $^3J_{HH}$ = 8.3, $^4J_{HH}$ =2.1 Hz, 1H, C$H_{benzene}$), 7.10 (td, $^3J_{HH}$ = 4.9, $^4J_{HH}$ = 2.4 Hz, 1H, C$H_{pyridine}$), 6.91 (s, 1H, C$H_{imidazole}$), 6.67 (s, 1H, C$H_{imidazole}$), 3.84 (t, $^3J_{HH}$ = 7.1 Hz, 2H, C$H_{2\ propyl}$), 3.67 (s, 2H, N–CH_2), 3.64 (s, 2H, N–CH_2), 2.48 (t, $^3J_{HH}$ = 6.7 Hz, 2H, C$H_{2\ propyl}$), 1.88 (quint, $^3J_{HH}$ = 6.8 Hz, 3H, CH_2–CH_2–$CH_{2\ propyl}$).

^{13}C NMR ($CDCl_3$, 100 MHz, ppm): δ_C = 159.00 (1C, $C_{q\ pyridine}$), 149.09 (1C, CH$_{pyridine}$), 136.87 (1C, CH$_{imidazole}$), 136.45 (1C, CH$_{pyridine}$), 135.13 (1C, $C_{q\ benzene}$), 134.82 (1C, $C_{q\ benzene}$), 133.40 (1C, $C_{q\ benzene}$), 131.69 (1C, CH$_{benzene}$), 129.36 (1C, CH$_{benzene}$), 128.99 (1C, CH$_{imidazole}$), 127.03 (1C,

*C*H$_{benzene}$), 123.06 (1C, *C*H$_{pyridine}$), 122.22 (1C, *C*H$_{pyridine}$), 118.69 (1C, *C*H$_{imidazole}$), 60.41 (1C, N–*C*H$_2$), 55.60 (1C, N–*C*H$_2$), 51.09 (1C, *C*H$_{2\ propyl}$), 44.84 (1C, *C*H$_{2\ propyl}$), 28.75 (1C, CH$_2$–*C*H$_2$–CH$_{2\ propyl}$).

ESI-HRMS (MeOH): Calculated for $[C_{19}H_{21}Cl_2N_4]^+$ (**19a** + H): m/z 375.1143. Found: m/z 375.1138.

N-(2,4-dichlorobenzyl)-3-(1H-imidazol-1-yl)-N-(quinolin-3-ylmethyl)propan-1-amine (19b)

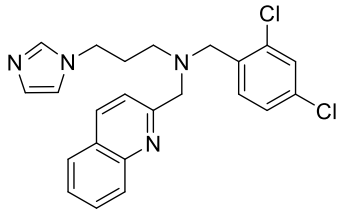

The oil of **10** (142 mg, 0.5 mmol) was dissolved in 7 mL of dry MeOH and 2-quinolinecarboxaldehyde (79 mg, 0.5 mmol) was added. The orange solution was stirred at room temperature for 1 h, then heated to reflux for 20h. The reaction was let to cool and 5 drops of AcOH, sodium cyanoborohydride ($NaBH_3CN$, 63 mg, 1 mmol), and another 3 mL of dry MeOH were added. The reaction was stirred at room temperature for another 4 days, and then evaporated to dryness. The residue was taken in 30 mL of $CHCl_3$ and 20 mL of H_2O were added, with the pH adjusted to 10 by addition of KOH. The mixture was extracted, and the separated aqueous phase was further extracted with 2 x 30 mL of $CHCl_3$. The combined organic layers were dried with anhydrous Na_2SO_4, filtered, and evaporated to dryness. The crude compound was purified by silica column chromatography (60 Å, 230–400 mesh, 1.8 x 15 cm) using $CHCl_3$/MeOH (96:4) as eluent (R_f = 0.3). The combined pure fractions were evaporated and dried under vacuum to yield pure **19b** as a bright yellow oil (57 mg, 27%).

^{1}H NMR ($CDCl_3$, 400 MHz, ppm): δ_H = 8.05 (d, $^3J_{HH}$ = 8.5 Hz, 1H, C*H*$_{quinoline}$), 7.97 (d, $^3J_{HH}$ = 8.5 Hz, 1H, C*H*$_{quinoline}$), 7.73 (d, $^3J_{HH}$ = 8.1 Hz, 1H, C*H*$_{quinoline}$), 7.64 (td, $^3J_{HH}$ = 7.0, $^4J_{HH}$ = 1.3 Hz, 1H, C*H*$_{quinoline}$), 7.51 – 7.40 (m, 3H), 7.36 (d, $^3J_{HH}$ = 8.3 Hz, 1H, C*H*$_{benzene}$), 7.30 (d, $^4J_{HH}$ = 2.1 Hz, 1H, C*H*$_{benzene}$), 7.14 (dd, $^3J_{HH}$ = 8.2, $^4J_{HH}$ = 2.1 Hz, 1H, C*H*$_{benzene}$), 6.88 (s, 1H, C*H*$_{imidazole}$), 6.64 (s, 1H, C*H*$_{imidazole}$), 3.86 (t, $^3J_{HH}$ = 7.1 Hz, 2H, C*H*$_{2\ propyl}$), 3.85 (s, 2H, N–C*H*$_2$), 3.70 (s, 2H, N–C*H*$_2$), 2.54 (t, $^3J_{HH}$ = 6.7 Hz, 2H, C*H*$_{2\ propyl}$), 1.92 (quint, $^3J_{HH}$ = 7.1 Hz, 2H, CH$_2$–C*H*$_2$–CH$_{2\ propyl}$).

^{13}C NMR ($CDCl_3$, 100 MHz, ppm): δ_C = 159.62 (1C, *C*$_{q\ quinoline}$), 147.46 (1C, *C*$_{q\ quinoline}$), 136.63 (1C, *C*H$_{imidazole}$), 136.54 (1C, *C*H$_{quinoline}$), 135.00 (1C, *C*$_{q\ benzene}$), 134.98 (1C, *C*$_{q\ benzene}$), 133.61 (1C, *C*$_{q\ benzene}$), 131.96 (1C, *C*H$_{benzene}$), 129.66 (1C, *C*H$_{quinoline}$), 129.47 (1C, *C*H$_{benzene}$), 128.93 (1C, *C*H$_{quinoline}$), 128.02 (1C, *C*H$_{imidazole}$), 127.60 (1C, *C*H$_{quinoline}$), 127.31 (1C, *C*$_{q\ quinoline}$), 127.07 (1C, *C*H$_{benzene}$), 126.42 (1C, *C*H$_{quinoline}$), 120.95 (1C, *C*H$_{quinoline}$), 118.86 (1C, *C*H$_{imidazole}$), 61.17 (1C, N–

CH_2), 55.89 (1C, N–CH_2), 51.30 (1C, $CH_{2\ propyl}$), 45.23 (1C, $CH_{2\ propyl}$), 28.66 (1C, CH_2–CH_2–$CH_{2\ propyl}$).

ESI-HRMS (MeOH): Calculated for $[C_{23}H_{23}Cl_2N_4]^+$ (**19b** + H): m/z 425.1299. Found: m/z 425.1287.

2-(((3-(1H-imidazol-1-yl)propyl)(2,4-dichlorobenzyl)amino)methyl)quinolin-8-ol (19c)

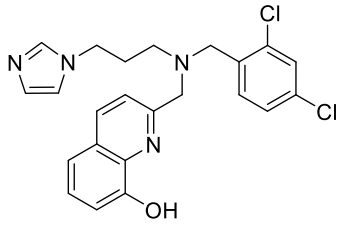

The oil of **10** (142 mg, 0.5 mmol) was dissolved in 7 mL of dry MeOH and **1** (113 mg, 0.65 mmol) was added. The dark yellow solution was stirred at room temperature for 1 h, then heated to reflux for 22 h. The reaction was let to cool and 5 drops of AcOH, $NaBH_3CN$ (63 mg, 1 mmol), and another 3 mL of dry MeOH were added. The reaction was stirred at room temperature for another 2 days, and then evaporated to dryness. The residue was taken in 30 mL of $CHCl_3$ and 20 mL of H_2O were added, with the pH adjusted to 10 by addition of KOH. The mixture was extracted, and the separated aqueous phase was further extracted with 2 x 30 mL of $CHCl_3$. The combined organic layers were dried with anhydrous Na_2SO_4, filtered, and evaporated to dryness. The crude compound was purified by silica column chromatography (60 Å, 230–400 mesh, 1.8 x 15.3 cm) using $CHCl_3$/MeOH (98:2) as eluent (R_f = 0.2). The combined pure fractions were evaporated and dried under vacuum to yield pure **19c** as a pink oil (33 mg, 15%).

^{1}H NMR ($CDCl_3$, 400 MHz, ppm): δ_H = 8.03 (d, $^3J_{HH}$ = 8.5 Hz, 1H, $CH_{quinoline}$), 7.43 (d, $^3J_{HH}$ = 8.5 Hz, 1H, $CH_{quinoline}$), 7.39–7.30 (m, 3H), 7.26 (s, 1H, $CH_{imidazole}$), 7.24 (dd, $^3J_{HH}$ = 8.3 Hz, $^4J_{HH}$ = 1.0 Hz, 2H, $CH_{benzene}$), 7.15 (dd, $^3J_{HH}$ = 8.2, $^4J_{HH}$ = 2.1 Hz, 1H, $CH_{benzene}$), 7.10 (dd, $^3J_{HH}$ = 7.6, $^4J_{HH}$ = 1.0 Hz, 1H, $CH_{quinoline}$), 6.89 (s, 1H, $CH_{imidazole}$), 6.65 (s, 1H, $CH_{imidazole}$), 3.84 (s, 2H, N–CH_2), 3.83 (t, $^3J_{HH}$ = 7.2 Hz, 2H, $CH_{2\ propyl}$), 3.70 (s, 2H, N–CH_2), 2.52 (t, $^3J_{HH}$ = 6.8 Hz, 2H, $CH_{2\ propyl}$), 1.90 (quint, $^3J_{HH}$ = 6.8 Hz, 2H, CH_2–CH_2–$CH_{2\ propyl}$).

^{13}C NMR ($CDCl_3$, 100 MHz, ppm): δ_C = 157.49 (1C, $C_{q\ quinoline}$), 151.91 (1C, $C_{q\ quinoline}$), 137.31 (1C, $C_{q\ quinoline}$), 136.91 (1C, $CH_{imidazole}$), 136.57 (1C, $CH_{quinoline}$), 134.98 (1C, $C_{q\ benzene}$), 134.94(1C, $C_{q\ benzene}$), 133.61 (1C, $C_{q\ benzene}$), 131.72 (1C, $CH_{quinoline}$), 129.49 (1C, $CH_{benzene}$), 129.40 (1C, $CH_{imidazole}$), 127.48 (1C, $CH_{quinoline}$), 127.45 (1C, $C_{q\ quinoline}$), 127.07 (1C, $CH_{benzene}$), 121.72 (1C, $CH_{quinoline}$), 118.61 (1C, $CH_{imidazole}$), 117.70 (1C, $CH_{benzene}$), 110.23 (1C, $CH_{quinoline}$), 60.71 (1C, N–

CH_2), 55.78 (1C, N–*C*H_2), 51.38 (1C, *C*$H_{2\ propyl}$), 44.82 (1C, *C*$H_{2\ propyl}$), 28.84 (1C, CH_2–*C*H_2–$CH_{2\ propyl}$).

ESI-HRMS (MeOH): Calculated for $[C_{23}H_{23}Cl_2N_4O]^+$ (**19c** + H): m/z 441.1249. Found: m/z 441.1241.

2-(((3-(1H-imidazol-1-yl)propyl)(2,4-dichlorobenzyl)amino)methyl)-6-methoxyphenol (19d)

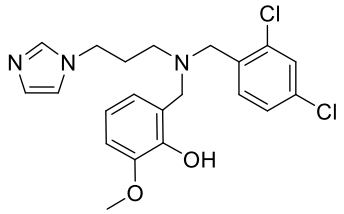

The oil of **10** (142 mg, 0.5 mmol) was dissolved in 5 mL of dry MeOH and *ortho*-vanillin (76 mg, 0.5 mmol) was added. The bright yellow solution was stirred at room temperature for 1 h, then heated to reflux for 21 h. The reaction was let to cool and 5 drops of AcOH, $NaBH_3CN$ (63 mg, 1 mmol), and another 5 mL of dry MeOH were added. The light yellow solution was stirred at room temperature for another 19 h, and then evaporated to dryness. The residue was taken in 30 mL of $CHCl_3$ and 20 mL of H_2O were added, with the pH adjusted to 9 by addition of KOH. The mixture was extracted, and the separated aqueous phase was further extracted with 2 x 30 mL of $CHCl_3$. The combined organic layers were dried with anhydrous Na_2SO_4, filtered, and evaporated to dryness. The crude compound was purified by silica column chromatography (60 Å, 230–400 mesh, 1.8 x 17 cm) using $CHCl_3$/MeOH (96:4) as eluent (R_f = 0.3). The combined pure fractions were evaporated and dried under vacuum to yield pure **19d** as a pink oil (115 mg, 55%).

^{1}H NMR ($CDCl_3$, 400 MHz, ppm): δ_H = 9.92 (br s, 1H, O*H*), 7.32 (d, $^4J_{HH}$ = 2.0 Hz, 1H, C*H*$_{benzene}$), 7.22–7.18 (m, 2H), 7.14 (dd, $^3J_{HH}$ = 8.2, $^4J_{HH}$ = 2.0 Hz, 1H, C*H*$_{benzene}$), 6.90 (s, 1H, C*H*$_{imidazole}$), 6.74 (dd, $^3J_{HH}$ = 8.1, $^4J_{HH}$ = 1.1 Hz, 1H, C*H*$_{phenol}$), 6.71–6.65 (m, 2H), 6.53 (d, $^3J_{HH}$ = 7.4 Hz, 1H, C*H*$_{phenol}$), 3.82–3.79 (m, 5H), 3.64 (s, 2H, N–C*H*$_2$), 3.63 (s, 2H, N–C*H*$_2$) 2.44 (t, $^3J_{HH}$ = 7.1 Hz, 2H, C*H*$_{2\ propyl}$), 1.96 (quint, $^3J_{HH}$ = 7.0 Hz, 2H, CH_2–C*H*$_2$–$CH_{2\ propyl}$).

^{13}C NMR ($CDCl_3$, 100 MHz, ppm): δ_C = 147.88 (1C, *C*$_{q\ phenol}$), 146.10 (1C, *C*$_{q\ phenol}$), 136.95 (1C, *C*H$_{imidazole}$), 135.34 (1C, *C*$_{q\ benzene}$), 134.53 (1C, *C*$_{q\ benzene}$), 133.03 (1C, *C*$_{q\ benzene}$), 132.61 (1C, *C*H$_{phenol}$), 129.86 (1C, *C*H$_{benzene}$), 129.53 (1C, *C*H$_{imidazole}$), 127.46 (1C, *C*H$_{benzene}$), 121.82 (1C, *C*$_{q\ phenol}$), 120.88 (1C, *C*H$_{phenol}$), 119.38 (1C, *C*H$_{benzene}$), 118.53 (1C, *C*H$_{imidazole}$), 111.13 (1C, *C*H$_{phenol}$), 57.13 (1C, N–*C*H_2), 55.84 (1C, O–*C*H_3), 55.64 (1C, N–*C*H_2), 50.67 (1C, *C*$H_{2\ propyl}$), 44.74 (1C, *C*$H_{2\ propyl}$), 28.10 (1C, CH_2–*C*H_2–$CH_{2\ propyl}$).

ESI-HRMS (MeOH): Calculated for $[C_{21}H_{24}Cl_2N_3O_2]^+$ (**19d** + H): m/z 420.1246. Found: m/z 420.1239.

2-(((3-(1H-imidazol-1-yl)propyl)(2,4-dichlorobenzyl)amino)methyl)-4-bromophenol (19e)

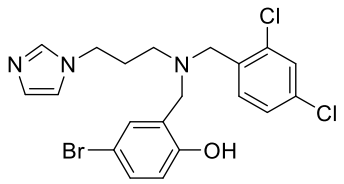

The oil of **10** (142 mg, 0.5 mmol) was dissolved in 5 mL of dry MeOH and 5-bromosalicylaldehyde (101 mg, 0.5 mmol) was added. The bright yellow solution was stirred at room temperature for 30 minutes, then heated to reflux for 21 h. The reaction was let to cool and 5 drops of AcOH, $NaBH_3CN$ (63 mg, 1 mmol), and another 5 mL of dry MeOH were added. The light yellow solution was stirred at room temperature for another 3 days, during which time it became almost colorless. The solution was evaporated to dryness, the residue was taken in 30 mL of $CHCl_3$, and 20 mL of H_2O were added, with the pH adjusted to 10 by addition of KOH. The mixture was extracted, and the separated aqueous phase was further extracted with 2 x 30 mL of $CHCl_3$. The combined organic layers were dried with anhydrous Na_2SO_4, filtered, and evaporated to dryness. The crude compound was purified by silica column chromatography (60 Å, 230–400 mesh, 1.8 x 14.5 cm) using $CHCl_3$/MeOH (97:3) as eluent (R_f = 0.3). The combined pure fractions were evaporated and dried under vacuum to yield pure **19e** as a brown oil (93 mg, 40%).

^{1}H NMR ($CDCl_3$, 400 MHz, ppm): δ_H = 10.18 (br s, 1H, O*H*), 7.36 (d, $^4J_{HH}$ = 2.0 Hz, 1H, C$H_{benzene}$), 7.27 (s, 1H, C$H_{imidazole}$), 7.22–7.10 (m, 5H), 7.02 (d, $^4J_{HH}$ = 2.4 Hz, 1H, CH_{phenol}), 6.94 (s, 1H, C$H_{imidazole}$), 6.69 (s, 1H, C$H_{imidazole}$), 6.62 (d, $^3J_{HH}$ = 8.6 Hz, 1H, CH_{phenol}), 3.82 (t, $^3J_{HH}$ = 7.0 Hz, 2H, C$H_{2\ propyl}$), 3.62 (s, 2H, N–CH_2), 3.61 (s, 2H, N–CH_2), 2.45 (t, $^3J_{HH}$ = 7.0 Hz, 2H, C$H_{2\ propyl}$), 1.97 (quint, $^3J_{HH}$ = 7.1 Hz, 2H, CH_2–CH_2–$CH_{2\ propyl}$).

^{13}C NMR ($CDCl_3$, 100 MHz, ppm): δ_C = 156.25 (1C, $C_{q\ phenol}$), 136.90 (1C, *C*H$_{imidazole}$), 135.37 (1C, $C_{q\ benzene}$), 134.87 (1C, $C_{q\ benzene}$), 132.72 (1C, *C*H$_{phenol}$), 132.59 (1C, $C_{q\ benzene}$), 131.91 (1C, *C*H$_{phenol}$), 131.38 (1C, *C*H$_{benzene}$), 130.02 (1C, *C*H$_{benzene}$), 129.62 (1C, *C*H$_{imidazole}$), 127.56 (1C, *C*H$_{benzene}$), 123.53 (1C, $C_{q\ phenol}$), 118.53 (1C, *C*H$_{imidazole}$), 118.05 (1C, *C*H$_{phenol}$), 111.28 (1C, $C_{q\ phenol}$), 56.99 (1C, N–*C*H_2), 55.71 (1C, N–*C*H_2), 50.73 (1C, *C*$H_{2\ propyl}$), 44.75 (1C, *C*$H_{2\ propyl}$), 27.95 (1C, CH_2–*C*H_2–$CH_{2\ propyl}$).

ESI-HRMS (MeOH): Calculated for $[C_{20}H_{21}Cl_2N_3OBr]^+$ (**19e** + H): m/z 468.0245. Found: m/z 468.0241.

2-(((3-(1H-imidazol-1-yl)propyl)(2,4-difluorobenzyl)amino)methyl)-4-bromophenol (20e)

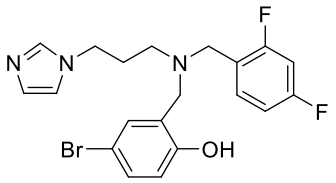

The oil of **12** (126 mg, 0.5 mmol) was dissolved in 10 mL of dry MeOH and 5-bromosalicylaldehyde (101 mg, 0.5 mmol) was added. The bright yellow solution was heated to 50 ^{o}C for 3 days, then heated to reflux for 9 h. The reaction was let to cool and 10 drops of AcOH, $NaBH_3CN$ (63 mg, 1 mmol), and another 5 mL of dry MeOH were added. The light yellow solution was stirred at room temperature for another 18 h, and then evaporated to dryness. The residue was taken in 30 mL of $CHCl_3$ and 20 mL of H_2O were added, with the pH adjusted to 10 by addition of KOH. The mixture was extracted, and the separated aqueous phase was further extracted with 2 x 30 mL of $CHCl_3$. The combined organic layers were dried with anhydrous Na_2SO_4, filtered, and evaporated to dryness. The crude compound was purified by silica column chromatography (60 Å, 230–400 mesh, 1.8 x 15 cm) using $CHCl_3$/MeOH (99:1) as eluent (R_f = 0.1). The combined pure fractions were evaporated and dried under vacuum to yield pure **20e** as a clear oil (56 mg, 26%).

^{1}H NMR ($CDCl_3$, 400 MHz, ppm): δ_H = 10.34 (br s, 1H, O*H*), 7.28 (s, 1H, C*H*$_{imidazole}$), 7.20 (dd, $^{3}J_{HH}$ = 8.6, $^{4}J_{HH}$ = 2.5 Hz, 1H, C*H*$_{phenol}$), 7.15–7.07 (m, 1H), 7.02 (d, $^{4}J_{HH}$ = 2.4 Hz, 1H, C*H*$_{phenol}$), 6.94 (s, 1H, C*H*$_{imidazole}$), 6.86–6.73 (m, 2H), 6.71 (s, 1H, C*H*$_{imidazole}$), 6.64 (d, $^{3}J_{HH}$ = 8.6 Hz, 1H, C*H*$_{phenol}$), 4.71 (s, 0H), 3.83 (t, $^{3}J_{HH}$ = 7.0 Hz, 2H, C*H*$_{2\ propyl}$), 3.62 (s, 2H, N–C*H*$_2$), 3.58 (s, 2H, N–C*H*$_2$), 2.43 (t, $^{3}J_{HH}$ = 7.2 Hz, 2H, C*H*$_{2\ propyl}$), 1.97 (quint, $^{3}J_{HH}$ = 7.1 Hz, 2H, CH$_2$–C*H*$_2$–CH$_{2\ propyl}$).

^{13}C NMR ($CDCl_3$, 100 MHz, ppm): δ_C = 162.87 (dd, $^{1}J_{CF}$ = 250.3 Hz, $^{3}J_{CF}$ = 12.2 Hz, 1C, *C*$_{q\ benzene}$), 161.56 (dd, $^{1}J_{CF}$ = 249.2 Hz, $^{3}J_{CF}$ = 11.9 Hz, 1C, *C*$_{q\ benzene}$), 156.48 (1C, *C*$_{q\ phenol}$), 136.94 (1C, *C*H$_{imidazole}$), 132.71 (dd, $^{3}J_{CF}$ = 9.3, $^{3}J_{CF}$ = 5.8 Hz, 1C, *C*H$_{benzene}$), 131.89 (1C, *C*H$_{phenol}$), 131.28 (1C, *C*H$_{phenol}$), 129.68 (1C, *C*H$_{imidazole}$), 123.46 (1C, *C*$_{q\ phenol}$), 118.92 (dd, $^{2}J_{CF}$ = 14.6, $^{4}J_{CF}$ = 3.2 Hz, 1C, *C*$_{q\ benzene}$), 118.53 (1C, *C*H$_{imidazole}$), 118.09 (1C, *C*H$_{phenol}$), 111.78 (dd, $^{2}J_{CF}$ = 21.3, $^{4}J_{CF}$ = 2.9 Hz, 1C, *C*H$_{benzene}$), 111.24 (1C, *C*$_{q\ phenol}$), 104.36 (t, $^{3}J_{CF}$ = 25.7 Hz, 1C, *C*H$_{benzene}$), 57.15 (1C, N–*C*H$_2$), 51.14 (1C, N–*C*H$_2$), 50.26 (1C, *C*H$_{2\ propyl}$), 44.61 (1C, *C*H$_{2\ propyl}$), 28.11 (1C, CH$_2$–*C*H$_2$–CH$_{2\ propyl}$).

^{19}F NMR ($CDCl_3$, 376 MHz, ppm): δ_F = −109.00 (m, 1F), −113.01 (m, 1F).

ESI-HRMS (MeOH): Calculated for $[C_{20}H_{21}F_2N_3O]^+$ (**20e** + H): m/z 436.0836. Found: m/z 436.0836.

N-(2,4-dichlorobenzyl)-N-(pyridin-2-ylmethyl)-3-(1H-1,2,4-triazol-1-yl)propan-1-amine (21a)

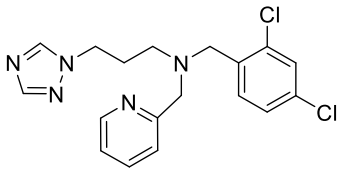

The oil of **14** (143 mg, 0.5 mmol) was dissolved in 10 mL of dry MeOH and 2-pyridinecarboxaldehyde (48 µL, 0.5 mmol) was added, and the orange solution was heated to reflux for 1 day. The reaction was let to cool, 10 drops of AcOH, $NaBH_3CN$ (63 mg, 1 mmol) and another 5 mL of dry MeOH were added. The yellow solution was stirred at room temperature for another day, and then was evaporated to dryness. The residue was taken in 30 mL of $CHCl_3$ and 20 mL of H_2O were added, with the pH adjusted to 10 by addition of KOH. The mixture was extracted, and the separated aqueous phase was further extracted with 2 x 30 mL of $CHCl_3$. The combined organic layers were dried with anhydrous Na_2SO_4, filtered, and evaporated to dryness. The crude compound was purified by silica column chromatography (60 Å, 230–400 mesh, 1.8 x 15 cm) using $CHCl_3$/MeOH (98:2) as eluent (R_f = 0.2). The combined pure fractions were evaporated and dried under vacuum to yield pure **21a** as a yellow oil (53 mg, 28%).

^{1}H NMR ($CDCl_3$, 400 MHz, ppm): δ_H = 8.45 (d, $^3J_{HH}$ = 4.8 Hz, 1H, C$H_{pyridine}$), 7.79 (s, 1H, C$H_{triazole}$), 7.73 (s, 1H, C$H_{triazole}$), 7.56 (td, $^3J_{HH}$ = 7.7, $^4J_{HH}$ = 1.6 Hz, 1H, C$H_{pyridine}$), 7.37 (d, $^3J_{HH}$ = 8.3 Hz, 1H, C$H_{benzene}$), 7.34–7.23 (m, 2H), 7.13 (dd, $^3J_{HH}$ = 8.3, $^4J_{HH}$ = 2.0 Hz, 1H, C$H_{benzene}$), 7.10 (dd, $^3J_{HH}$ = 7.2 Hz, $^4J_{HH}$ = 5.6 Hz, 1H, C$H_{pyridine}$), 4.07 (t, $^3J_{HH}$ = 7.0 Hz, 2H, C$H_{2\ propyl}$), 3.67 (s, 2H, N–CH_2), 3.64 (s, 2H, N–CH_2), 2.48 (t, $^3J_{HH}$ = 6.7 Hz, 2H, C$H_{2\ propyl}$), 2.01 (quint, $^3J_{HH}$ = 6.8 Hz, 2H, CH_2–CH_2–$CH_{2\ propyl}$).

^{13}C NMR ($CDCl_3$, 100 MHz, ppm): δ_C = 158.99 (1C, $C_{q\ pyridine}$), 151.84 (1C, CH$_{triazole}$), 149.10 (1C, CH$_{pyridine}$), 142.85 (1C, CH$_{triazole}$), 136.41 (1C, CH$_{pyridine}$), 135.12 (1C, $C_{q\ benzene}$), 134.82 (1C, $C_{q\ benzene}$), 133.38 (1C, $C_{q\ benzene}$), 131.68 (1C, CH$_{benzene}$), 129.35 (1C, CH$_{benzene}$), 127.00 (1C, CH$_{benzene}$), 123.08 (1C, CH$_{pyridine}$), 122.20 (1C, CH$_{pyridine}$), 60.31 (1C, N–CH$_2$), 55.48 (1C, N–CH$_2$), 50.80 (1C, CH$_{2\ propyl}$), 47.39 (1C, CH$_{2\ propyl}$), 27.32 (1C, CH_2–CH$_2$–$CH_{2\ propyl}$).

ESI-HRMS (H_2O): Calculated for $[C_{18}H_{20}Cl_2N_5]^+$ (**21a** + H): m/z 376.1096. Found: m/z 376.1093.

N-(2,4-dichlorobenzyl)-N-(quinolin-2-ylmethyl)-3-(1H-1,2,4-triazol-1-yl)propan-1-amine (21b)

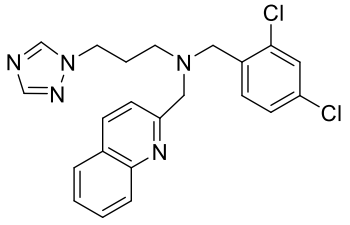

The oil of **14** (143 mg, 0.5 mmol) was dissolved in 10 mL of dry MeOH and 2-quinolinecarboxaldehyde (79 mg, 0.5 mmol) was added. The amber solution was heated to reflux for 1 day, during which time it became brown. The reaction was let to cool, 10 drops of AcOH, $NaBH_3CN$ (63 mg, 1 mmol), and another 5 mL of dry MeOH were added. The brown solution was stirred at room temperature for another day, during which time it became amber. The solution was evaporated to dryness, the residue was taken in 30 mL of $CHCl_3$ and 20 mL of H_2O were added, with the pH adjusted to 11 by addition of KOH. The mixture was extracted, and the separated aqueous phase was further extracted with 2 x 30 mL of $CHCl_3$. The combined organic layers were dried with anhydrous Na_2SO_4, filtered, and evaporated to dryness. The crude compound was purified by silica column chromatography (60 Å, 230–400 mesh, 1.8 x 15.5 cm) using $CHCl_3$/MeOH (99:1) as eluent (R_f = 0.1). The combined pure fractions were evaporated and dried under vacuum to yield pure **21b** as a bright yellow oil (37 mg, 17%).

^{1}H NMR ($CDCl_3$, 400 MHz, ppm): δ_H = 8.03 (d, $^3J_{HH}$ = 8.5 Hz, 1H, C$H_{quinoline}$), 7.97 (d, $^3J_{HH}$ = 8.5 Hz, 1H, C$H_{quinoline}$), 7.79–7.69 (m, 3H), 7.63 (t, $^3J_{HH}$ = 7.7 Hz, 1H, C$H_{quinoline}$), 7.49–7.42 (m, 2H), 7.36 (d, $^3J_{HH}$ = 8.3 Hz, 1H, C$H_{benzene}$), 7.29 (d, $^4J_{HH}$ = 2.0 Hz, 1H, C$H_{benzene}$), 7.12 (dd, $^3J_{HH}$ = 8.2, $^4J_{HH}$ = 2.0 Hz, 1H, C$H_{benzene}$), 4.06 (t, $^3J_{HH}$ = 7.1 Hz, 2H, C$H_{2\ propyl}$), 3.84 (s, 2H, N–CH_2), 3.69 (s, 2H, N–CH_2), 2.53 (t, $^3J_{HH}$ = 6.7 Hz, 2H, C$H_{2\ propyl}$), 2.03 (quint, $^3J_{HH}$ = 6.9 Hz, 2H, CH_2–CH_2–$CH_{2\ propyl}$).

^{13}C NMR ($CDCl_3$, 100 MHz, ppm): δ_C = 159.69 (1C, $C_{q\ quinoline}$), 151.86 (1C, $CH_{triazole}$), 147.48 (1C, $C_{q\ quinoline}$), 142.77 (1C, $CH_{triazole}$), 136.45 (1C, $CH_{quinoline}$), 135.04 (1C, $C_{q\ benzene}$), 134.99 (1C, $C_{q\ benzene}$), 133.53 (1C, $C_{q\ benzene}$), 131.90 (1C, $CH_{benzene}$), 129.60 (1C, $CH_{quinoline}$), 129.44 (1C, $CH_{benzene}$), 128.97 (1C, $CH_{quinoline}$), 127.57 (1C, $CH_{quinoline}$), 127.30 (1C, $C_{q\ quinoline}$), 127.01 (1C, $CH_{benzene}$), 126.38 (1C, $CH_{quinoline}$), 120.93 (1C, $CH_{quinoline}$), 61.13 (1C, N–CH_2), 55.74 (1C, N–CH_2), 51.16 (1C, $CH_{2\ propyl}$), 47.53 (1C, $CH_{2\ propyl}$), 27.41 (1C, CH_2–CH_2–$CH_{2\ propyl}$).

ESI-HRMS (MeOH): Calculated for $[C_{22}H_{22}Cl_2N_5]^+$ (**21b** + H): m/z 426.1252. Found: m/z 426.1248.

2-(((3-(1H-1,2,4-triazol-1-yl)propyl)(2,4-dichlorobenzyl)amino)methyl)quinolin-8-ol (21c)

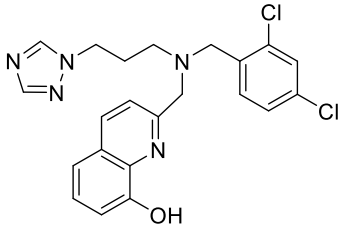

The oil of **14** (143 mg, 0.5 mmol) was dissolved in 10 mL of dry MeOH, and **1** (113 mg, 0.65 mmol) and 10 drops of AcOH were added. The bright yellow solution was heated to reflux for 1

day, during which time it became amber. The reaction was let to cool, and $NaBH_3CN$ (63 mg, 1 mmol) and another 5 mL of dry MeOH were added. The bright yellow solution was stirred at room temperature for another 18 h, and then evaporated to dryness. The residue was taken in 30 mL of $CHCl_3$ and 20 mL of H_2O were added, with the pH adjusted to 11 by addition of KOH. The mixture was extracted, and the separated aqueous phase was further extracted with 2 x 30 mL of $CHCl_3$. The combined organic layers were dried with anhydrous Na_2SO_4, filtered, and evaporated to dryness. The residue was treated with 10 mL of HCl 0.1 M and the insoluble matter was filtered off with a PTFE filter. The aqueous solution was then adjusted to pH 12 by addition of KOH and extracted with 3 x 20 mL of $CHCl_3$. The combined organic layers were dried with anhydrous Na_2SO_4, filtered, and evaporated to dryness. The crude compound was purified by silica column chromatography (60 Å, 230–400 mesh, 1.8 x 12.5 cm) using $CHCl_3$/MeOH (99.5:0.5) as eluent (R_f = 0.05). The combined pure fractions were evaporated and dried under vacuum to yield pure **21c** as a bright yellow oil (75 mg, 34%).

^{1}H NMR ($CDCl_3$, 400 MHz, ppm): δ_H = 8.12 (br s, 1H, O*H*), 8.00 (d, $^3J_{HH}$ = 8.4 Hz, 2H, C$H_{quinoline}$), 7.77 (s, 1H, C$H_{triazole}$), 7.74 (s, 1H, C$H_{triazole}$), 7.41 (d, $^3J_{HH}$ = 8.4 Hz, 1H, C$H_{quinoline}$), 7.36–7.25 (m, 3H), 7.21 (d, $^3J_{HH}$ = 8.1 Hz, 1H, C$H_{benzene}$), 7.14–7.02 (m, 2H), 4.05 (t, $^3J_{HH}$ = 7.0 Hz, 2H, C$H_{2\ propyl}$), 3.81 (s, 2H, N–CH_2), 3.67 (s, 2H, N–CH_2), 2.51 (t, $^3J_{HH}$ = 6.6 Hz, 2H, C$H_{2\ propyl}$), 2.03 (quint, $^3J_{HH}$ = 6.7 Hz, 2H, CH_2–CH_2–$CH_{2\ propyl}$).

^{13}C NMR ($CDCl_3$, 100 MHz, ppm): δ_C = 156.40 (1C, $C_{q\ quinoline}$), 150.86 (1C, $C_{q\ quinoline}$), 150.86 (1C, *C*H$_{triazole}$), 141.77 (1C, *C*H$_{triazole}$), 136.27 (1C, $C_{q\ benzene}$), 135.51 (1C, *C*H$_{quinoline}$), 133.92 (1C, $C_{q\ benzene}$), 133.89 (1C, $C_{q\ benzene}$), 132.52 (1C, $C_{q\ quinoline}$), 130.69 (1C, *C*H$_{quinoline}$), 128.41 (1C, *C*H$_{benzene}$), 126.43 (1C, $C_{q\ quinoline}$), 126.42 (1C, *C*H$_{quinoline}$), 126.00 (1C, *C*H$_{benzene}$), 120.73 (1C, *C*H$_{quinoline}$), 116.66 (1C, *C*H$_{benzene}$), 109.20 (1C, *C*H$_{quinoline}$), 59.48 (1C, N–*C*H$_2$), 54.62 (1C, N–*C*H$_2$), 50.04 (1C, *C*H$_{2\ propyl}$), 46.42 (1C, *C*H$_{2\ propyl}$), 26.37 (1C, CH_2–*C*H$_2$–$CH_{2\ propyl}$).

ESI-HRMS (H_2O): Calculated for $[C_{22}H_{22}Cl_2N_5O]^+$ (**21c** + H): m/z 442.1202. Found: m/z 442.1198.

2-(((3-(1H-1,2,4-triazol-1-yl)propyl)(2,4-dichlorobenzyl)amino)methyl)-6-methoxyphenol (21d)

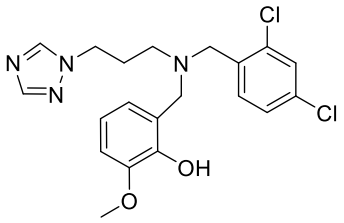

The oil of **14** (143 mg, 0.5 mmol) was dissolved in 10 mL of dry MeOH, and *ortho*-vanillin (76 mg, 0.5 mmol) and 10 drops of AcOH were added. The bright yellow solution was heated to

reflux for 1 day, the reaction was let to cool, and $NaBH_3CN$ (63 mg, 1 mmol) and another 5 mL of dry MeOH were added. The light yellow solution was stirred at room temperature for another 15 h, and then evaporated to dryness. The residue was taken in 30 mL of $CHCl_3$ and 20 mL of H_2O were added, with the pH adjusted to 11 by addition of KOH. The mixture was extracted, and the separated aqueous phase was further extracted with 2 x 30 mL of $CHCl_3$. The combined organic layers were dried with anhydrous Na_2SO_4, filtered, and evaporated to dryness. The residue was treated with 8 mL of HCl 0.1 M and the insoluble matter was filtered off with a PTFE filter. The aqueous solution was adjusted to pH 11 by addition of KOH and extracted with 3 x 20 mL of $CHCl_3$. The combined organic layers were dried with anhydrous Na_2SO_4, filtered, and evaporated to dryness. The crude compound was purified by silica column chromatography (60 Å, 230–400 mesh, 1.6 x 11 cm) using $CHCl_3$/MeOH (99:1) as eluent (R_f = 0.1). The combined pure fractions were evaporated and dried under vacuum to yield pure **21d** as a clear oil (89 mg, 42%).

^{1}H NMR ($CDCl_3$, 400 MHz, ppm): δ_H = 9.87 (br s, 1H, O*H*), 7.78 (s, 1H, C$H_{triazole}$), 7.71 (s, 1H, C$H_{triazole}$), 7.32 (d, $^4J_{HH}$ = 1.9 Hz, 1H, C$H_{benzene}$), 7.21 (d, $^3J_{HH}$ = 8.2 Hz, 1H, C$H_{benzene}$), 7.14 (dd, $^3J_{HH}$ = 8.2, $^4J_{HH}$ = 1.9 Hz, 1H, C$H_{benzene}$), 6.73 (d, $^3J_{HH}$ = 8.1 Hz, 1H, CH_{phenol}), 6.67 (t, $^3J_{HH}$ = 7.8 Hz, 1H, CH_{phenol}), 6.52 (d, $^3J_{HH}$ = 7.5 Hz, 1H, CH_{phenol}), 4.05 (t, $^3J_{HH}$ = 6.7 Hz, 2H, C$H_{2\ propyl}$), 3.79 (s, 3H, O–CH_3), 3.64, (s, 2H, N–CH_2), 3.63 (s, 2H, N–CH_2), 2.44 (t, $^3J_{HH}$ = 6.9 Hz, 2H, C$H_{2\ propyl}$), 2.10 (quint, $^3J_{HH}$ = 6.8 Hz, 2H, CH_2–CH_2–$CH_{2\ propyl}$).

^{13}C NMR ($CDCl_3$, 100 MHz, ppm): δ_C = 151.97 (1C, *C*H$_{triazole}$), 147.78 (1C, $C_{q\ phenol}$), 145.94 (1C, $C_{q\ phenol}$), 143.18 (1C, *C*H$_{triazole}$), 135.32 (1C, $C_{q\ benzene}$), 134.50 (1C, $C_{q\ benzene}$), 133.04 (1C, $C_{q\ benzene}$), 132.64 (1C, *C*H$_{benzene}$), 129.84 (1C, *C*H$_{benzene}$), 127.41 (1C, *C*H$_{benzene}$), 121.85 (1C, $C_{q\ phenol}$), 120.95 (1C, *C*H$_{phenol}$), 119.40 (1C, *C*H$_{phenol}$), 111.12 (1C, *C*H$_{phenol}$), 56.89 (1C, N–*C*H$_2$), 55.82 (1C, O–*C*H$_3$), 55.54 (1C, N–*C*H$_2$), 50.33 (1C, *C*H$_{2\ propyl}$), 47.20 (1C, *C*H$_{2\ propyl}$), 26.40 (1C, CH_2–*C*H$_2$–$CH_{2\ propyl}$).

ESI-HRMS (MeOH): Calculated for $[C_{20}H_{23}Cl_2N_4O_2]^+$ (**21d** + H): m/z 421.1198. Found: m/z 421.1196.

2-(((3-(1H-1,2,4-triazol-1-yl)propyl)(2,4-dichlorobenzyl)amino)methyl)-4-bromophenol (21e)

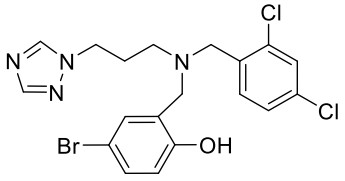

The oil of **14** (143 mg, 0.5 mmol) was dissolved in 10 mL of dry MeOH, and 5-bromosalicylaldehyde (101 mg, 0.5 mmol) and 10 drops of AcOH were added. The bright yellow solution was heated to reflux for 1 day, the reaction was let to cool, and $NaBH_3CN$ (63

mg, 1 mmol) and another 5 mL of dry MeOH were added. The light yellow solution was stirred at room temperature for 1 day, and then evaporated to dryness. The residue was taken in 30 mL of $CHCl_3$ and 20 mL of H_2O were added, with the pH adjusted to 10 by addition of KOH. The mixture was extracted, and the separated aqueous phase was further extracted with 2 x 30 mL of $CHCl_3$. The combined organic layers were dried with anhydrous Na_2SO_4, filtered, and evaporated to dryness. The crude compound was purified by silica column chromatography (60 Å, 230–400 mesh, 1.8 x 15 cm) using $CHCl_3$/MeOH (99.5:0.5) as eluent (R_f = 0.1). The combined fractions containing the target compound were evaporated, the residue was treated with 8 mL of HCl 0.1 M and the insoluble matter was filtered off with a PTFE filter. The aqueous solution was adjusted to pH 12 by addition of KOH and extracted with 3 x 20 mL of $CHCl_3$. The combined organic layers were dried with anhydrous Na_2SO_4, filtered, evaporated, and dried under vacuum to yield pure **21e** as a yellow oil (30 mg, 22%).

^{1}H NMR ($CDCl_3$, 400 MHz, ppm): δ_H = 10.09 (br s, 1H, O*H*), 7.82 (s, 2H, C*H*$_{triazole}$), 7.36 (d, $^4J_{HH}$ = 1.8 Hz, 1H, C*H*$_{benzene}$), 7.21–7.12 (m, 3H), 7.01 (d, $^4J_{HH}$ = 2.4 Hz, 1H, C*H*$_{phenol}$), 6.62 (d, $^3J_{HH}$ = 8.6 Hz, 1H, C*H*$_{phenol}$), 4.06 (t, $^3J_{HH}$ = 6.8 Hz, 2H, C*H*$_{2\ propyl}$), 3.64 (s, 2H, N–C*H*$_2$), 3.61 (s, 2H, N–C*H*$_2$), 2.47(t, $^3J_{HH}$ = 7.0 Hz, 2H, C*H*$_{2\ propyl}$), 2.12 (quint, $^3J_{HH}$ = 6.9 Hz, 2H, CH$_2$–C*H*$_2$–CH$_{2\ propyl}$).

^{13}C NMR ($CDCl_3$, 100 MHz, ppm): δ_C = 155.18 (1C, *C*$_{q\ phenol}$), 151.12 (1C, *C*H$_{triazole}$), 142.11 (1C, *C*H$_{triazole}$), 134.37 (1C, *C*$_{q\ benzene}$), 133.86 (1C, *C*$_{q\ benzene}$), 131.73 (1C, *C*H$_{phenol}$), 131.52 (1C, *C*$_{q\ benzene}$), 130.91 (1C, *C*H$_{benzene}$), 130.36 (1C, *C*H$_{phenol}$), 129.00 (1C, *C*H$_{benzene}$), 126.51 (1C, *C*H$_{benzene}$), 122.39 (1C, *C*$_{q\ phenol}$), 117.01 (1C, *C*H$_{phenol}$), 110.27 (1C, *C*$_{q\ phenol}$), 55.90 (1C, N–*C*H$_2$), 54.52 (1C, N–*C*H$_2$), 49.43 (1C, *C*H$_{2\ propyl}$), 46.22 (1C, *C*H$_{2\ propyl}$), 25.24 (1C, CH$_2$–*C*H$_2$–CH$_{2\ propyl}$).

ESI-HRMS (MeOH): Calculated for $[C_{19}H_{20}Cl_2N_4OBr]^+$ (**21e** + H): m/z 469.0198. Found: m/z 469.0196.

N-(2,4-dichlorobenzyl)-N-(pyridin-2-ylmethyl)-2-(1H-1,2,4-triazol-1-yl)ethan-1-amine (22a)

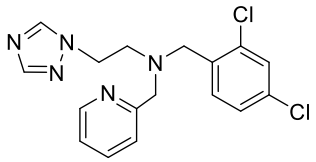

The oil of **16** (136 mg, 0.67 mmol) was dissolved in 12 mL of dry DCE, and 2,4-dichlorobenzaldehyde (117 mg, 0.67 mmol) and $NaBH(OAc)_3$ (287 mg, 1.34 mmol) were added. The brown solution was stirred at room temperature for 21 h and then heated to reflux for 1 day. The solution was filtered and evaporated to dryness, the residue was taken in 30 mL of $CHCl_3$ and 20 mL of H_2O were added, with the pH adjusted to 10 by addition of KOH. The mixture was extracted, and the separated aqueous phase was further extracted with 2 x 30 mL

of $CHCl_3$. The combined organic layers were dried with anhydrous Na_2SO_4, filtered, and evaporated to dryness. The crude compound was purified by silica column chromatography (60 Å, 230–400 mesh, 1.8 x 15.7 cm) using $CHCl_3$/MeOH (97:3) as eluent (R_f = 0.3). The combined pure fractions were evaporated and dried under vacuum to yield pure **22a** as a brown oil (165 mg, 68%).

^{1}H NMR ($CDCl_3$, 400 MHz, ppm): δ_H = 8.45 (d, $^3J_{HH}$ = 4.9 Hz, 1H, C$H_{pyridine}$), 7.99 (s, 1H, C$H_{triazole}$), 7.76 (s, 1H, C$H_{triazole}$), 7.53 (td, $^3J_{HH}$ = 7.7, $^4J_{HH}$ = 1.8 Hz, 1H, C$H_{pyridine}$), 7.25 (s, 1H, C$H_{benzene}$), 7.12 – 7.05 (m, 4H), 4.15 (t, $^3J_{HH}$ = 6.4, 5.1 Hz, 2H, C$H_{2\ ethyl}$), 3.75 (s, 2H, N–CH_2), 3.69 (s, 2H, N–CH_2), 2.95 (t, $^3J_{HH}$ = 6.4 Hz, 2H, C$H_{2\ ethyl}$).

^{13}C NMR ($CDCl_3$, 100 MHz, ppm): δ_C = 158.29 (1C, $C_{q\ pyridine}$), 151.61 (1C, CH$_{triazole}$), 148.95 (1C, CH$_{pyridine}$), 143.68 (1C, CH$_{triazole}$), 136.78 (1C, CH$_{pyridine}$), 134.62 (1C, $C_{q\ benzene}$), 134.50 (1C, $C_{q\ benzene}$), 133.49 (1C, $C_{q\ benzene}$), 131.26 (1C, CH$_{benzene}$), 129.30 (1C, CH$_{benzene}$), 127.14 (1C, CH$_{benzene}$), 122.94 (1C, CH$_{pyridine}$), 122.39 (1C, CH$_{pyridine}$), 60.22 (1C, CH$_{2\ ethyl}$), 55.52 (1C, N–CH$_2$), 53.45 (1C, N–CH$_2$), 47.85 (1C, CH$_{2\ ethyl}$).

ESI-HRMS (MeOH): Calculated for $[C_{17}H_{18}Cl_2N_5]^+$ (**22a** + H): m/z 362.0939. Found: m/z 362.0930.

2-(((2-(1H-1,2,4-triazol-1-yl)ethyl)(2,4-dichlorobenzyl)amino)methyl)quinolin-8-ol (23c)

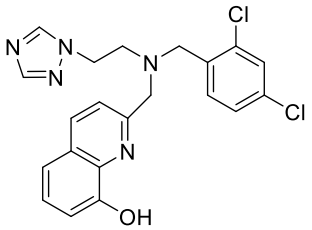

The solid of **18** (136 mg, 0.5 mmol) was dissolved in 10 mL of dry MeOH and **1** (113 mg, 0.65 mmol) was added. The dark yellow solution was stirred at room temperature for 30 minutes and then heated to reflux for 1 day, during which time it turned amber. The reaction was cooled and 5 drops of AcOH, $NaBH_3CN$ (63 mg, 1 mmol), and another 5 mL of dry MeOH were added. The bright yellow solution was stirred at room temperature for another 18 h, and then evaporated to dryness. The residue was taken in 30 mL of $CHCl_3$ and 20 mL of H_2O were added, with the pH adjusted to 9 by addition of KOH. The mixture was extracted, and the separated aqueous phase was further extracted with 2 x 30 mL of $CHCl_3$. The combined organic layers were dried with anhydrous Na_2SO_4, filtered, and evaporated to dryness. The crude compound was purified by silica column chromatography (60 Å, 230–400 mesh, 1.8 x 15 cm) using $CHCl_3$/MeOH (99:1) as eluent (R_f = 0.1). The combined fractions containing the target compound were evaporated, the residue was treated with 4 mL of HCl 0.1 M and the insoluble

matter was filtered off with a PTFE filter. The aqueous solution was adjusted to pH 12 by addition of KOH and extracted with 2 x 20 mL of $CHCl_3$. The combined organic layers were dried with anhydrous Na_2SO_4, filtered, evaporated, and dried under vacuum to yield pure **23c** as a yellow oil (60 mg, 28%).

^{1}H NMR ($CDCl_3$, 400 MHz, ppm): δ_H = 8.11 (br s, 1H, O*H*), 7.96 (d, $^3J_{HH}$ = 8.5 Hz, 1H, C$H_{quinoline}$), 7.90 (s, 1H, C$H_{triazole}$), 7.76 (s, 1H, C$H_{triazole}$), 7.34 (t, $^3J_{HH}$ = 7.9 Hz, 1H, C$H_{quinoline}$), 7.27 (d, $^4J_{HH}$ = 1.6 Hz, 1H, C$H_{benzene}$), 7.23–7.16 (m, 2H), 7.14–7.06 (m, 3H), 4.13 (t, $^3J_{HH}$ = 5.8 Hz, 2H, C$H_{2\ ethyl}$), 3.86 (s, 2H, N–CH_2), 3.73 (s, 2H, N–CH_2), 3.00 (t, $^3J_{HH}$ = 5.8 Hz, 2H, C$H_{2\ ethyl}$).

^{13}C NMR ($CDCl_3$, 100 MHz, ppm): δ_C = 155.78 (1C, $C_{q\ quinoline}$), 150.87 (1C, $C_{q\ quinoline}$), 150.75 (1C, $CH_{triazole}$), 142.48 (1C, $CH_{triazole}$), 136.29 (1C, $C_{q\ quinoline}$), 135.74 (1C, $CH_{quinoline}$), 133.72 (1C, $C_{q\ benzene}$), 133.40 (1C, $C_{q\ benzene}$), 132.67 (1C, $C_{q\ benzene}$), 130.31 (1C, $C_{q\ quinoline}$), 128.41 (1C, $CH_{benzene}$), 126.52 (1C, $CH_{quinoline}$), 126.49 (1C, $CH_{benzene}$), 126.18 (1C, $CH_{quinoline}$), 120.41 (1C, $CH_{benzene}$), 116.71 (1C, $CH_{quinoline}$), 109.29 (1C, $CH_{quinoline}$), 59.65 (1C, N–CH_2), 54.66 (1C, N–CH_2), 52.59 (1C, $CH_{2\ ethyl}$), 46.87 (1C, $CH_{2\ ethyl}$).

ESI-HRMS (H_2O): Calculated for $[C_{21}H_{19}Cl_2N_5O]^+$ (**23c** + H): m/z 428.1045. Found: m/z 428.1043.

2-(((2-(1H-1,2,4-triazol-1-yl)ethyl)(2,4-dichlorobenzyl)amino)methyl)-6-methoxyphenol (23d)

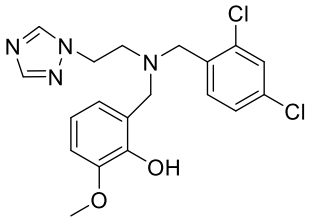

The solid of **18** (136 mg, 0.5 mmol) was dissolved in 6 mL of dry MeOH and *ortho*-vanillin (76 mg, 0.5 mmol) was added. The bright yellow solution was stirred at room temperature for 1 h, then heated to reflux for 22 h. The reaction was cooled and 5 drops of AcOH, $NaBH_3CN$ (63 mg, 1 mmol), and another 3 mL of dry MeOH were added. The light yellow solution was stirred at room temperature for 1 day, and then evaporated to dryness. The residue was taken in 30 mL of $CHCl_3$ and 20 mL of H_2O were added, with the pH adjusted to 10 by addition of KOH. The mixture was extracted, and the separated aqueous phase was further extracted with 2 x 30 mL of $CHCl_3$. The combined organic layers were dried with anhydrous Na_2SO_4, filtered, and evaporated to dryness. The crude compound was purified by silica column chromatography (60 Å, 230–400 mesh, 1.8 x 15 cm) using $CHCl_3$/MeOH (98:2) as eluent (R_f = 0.3). The combined fractions containing the target compound were evaporated, the residue was treated with 4 mL of HCl 0.1 M and the insoluble matter was filtered off with a PTFE syringe filter. The aqueous solution was adjusted to pH 10 by addition of KOH and extracted with 3 x 20 mL of $CHCl_3$. The

combined organic layers were dried with anhydrous Na_2SO_4, filtered, evaporated, and dried under vacuum to yield pure **23d** as a yellow oil (99 mg, 49%).

^{1}H NMR ($CDCl_3$, 400 MHz, ppm): δ_H = 8.57 (br s, 1H, O*H*), 7.99 (s, 1H, C$H_{triazole}$), 7.79 (s, 1H, C$H_{triazole}$), 7.26 (d, $^3J_{HH}$ = 1.7 Hz, 1H, C$H_{benzene}$), 7.09–7.00 (m, 2H), 6.75–6.67 (m, 2H), 6.58 (dd, $^3J_{HH}$ = 7.4, $^4J_{HH}$ = 1.4 Hz, 1H, CH_{phenol}), 4.17 (t, $^3J_{HH}$ = 6.2 Hz, 2H, C$H_{2\ ethyl}$), 3.78 (s, 3H, O–CH_3), 3.72 (s, 2H, N–CH_2), 3.64 (s, 2H, N–CH_2), 2.93 (t, $^3J_{HH}$ = 6.2 Hz, 2H, C$H_{2\ ethyl}$).

^{13}C NMR ($CDCl_3$, 100 MHz, ppm): δ_C = 151.06 (1C, *C*H$_{triazole}$), 146.64 (1C, $C_{q\ phenol}$), 144.61 (1C, $C_{q\ phenol}$), 142.65 (1C, *C*H$_{triazole}$), 133.95 (1C, $C_{q\ benzene}$), 133.11 (1C, $C_{q\ benzene}$), 132.32 (1C, $C_{q\ benzene}$), 131.01 (1C, *C*H$_{benzene}$), 128.55 (1C, *C*H$_{benzene}$), 126.38 (1C, *C*H$_{benzene}$), 120.98 (1C, $C_{q\ phenol}$), 120.53 (1C, *C*H$_{phenol}$), 118.50 (1C, *C*H$_{phenol}$), 110.10 (1C, *C*H$_{phenol}$), 55.32 (1C, N–*C*H$_2$), 54.89 (1C, O–*C*H$_3$), 54.73 (1C, N–*C*H$_2$), 52.20 (1C, *C*H$_{2\ ethyl}$), 46.39 (1C, *C*H$_{2\ ethyl}$).

ESI-HRMS (MeOH): Calculated for $[C_{19}H_{21}Cl_2N_4O_2]^+$ (**23d** + H): m/z 407.1042. Found: m/z 407.1038.

2-(((2-(1H-1,2,4-triazol-1-yl)ethyl)(2,4-dichlorobenzyl)amino)methyl)-4-bromophenol (23e)

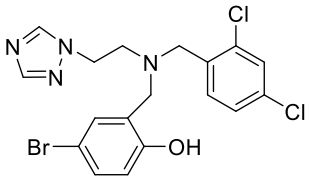

The solid of **18** (136 mg, 0.5 mmol) was dissolved in 6 mL of dry MeOH and 5-bromosalicylaldehyde (101 mg, 0.5 mmol) was added. The bright yellow solution was stirred at room temperature for 30 minutes, then heated to reflux for 1 day. The reaction was cooled and 5 drops of AcOH, $NaBH_3CN$ (63 mg, 1 mmol), and another 5 mL of dry MeOH were added. The light yellow solution was stirred at room temperature for 1 day, and then evaporated to dryness. The residue was taken in 30 mL of $CHCl_3$ and 20 mL of H_2O were added, with the pH adjusted to 10 by addition of KOH. The mixture was extracted, and the separated aqueous phase was further extracted with 2 x 30 mL of $CHCl_3$. The combined organic layers were dried with anhydrous Na_2SO_4, filtered, and evaporated to dryness. The crude compound was purified by silica column chromatography (60 Å, 230–400 mesh, 1.6 x 9.5 cm) using $CHCl_3$/MeOH (99.5:0.5) as eluent (R_f = 0.1). The combined pure fractions were evaporated and dried under vacuum to yield pure **23e** as a brown oil (43 mg, 19%).

^{1}H NMR ($CDCl_3$, 400 MHz, ppm): δ_H = 9.30 (br s, 1H, O*H*), 7.92 (s, 1H, C$H_{triazole}$), 7.83 (s, 1H, C$H_{triazole}$), 7.32 (d, $^4J_{HH}$ = 2.0 Hz, 1H, C$H_{benzene}$), 7.20 (dd, $^3J_{HH}$ = 8.5 Hz, $^4J_{HH}$ = 2.4 Hz, 1H, C$H_{benzene}$), 7.12 (dd, $^3J_{HH}$ = 8.2, $^4J_{HH}$ = 2.1 Hz, 1H, CH_{phenol}), 7.06 (d, $^4J_{HH}$ = 2.3 Hz, 1H, CH_{phenol}), 7.02 (d, $^3J_{HH}$ =

8.3 Hz, 1H, C$H_{benzene}$), 6.63 (d, $^3J_{HH}$ = 8.6 Hz, 1H, CH_{phenol}), 4.19 (t, $^3J_{HH}$ = 6.1 Hz, 2H, C$H_{2\ ethyl}$), 3.69 (s, 2H, N–CH_2), 3.66 (s, 2H, N–CH_2), 2.99 (t, $^3J_{HH}$ = 6.1 Hz, 2H, C$H_{2\ ethyl}$).

^{13}C NMR ($CDCl_3$, 100 MHz, ppm): δ_C = 156.05 (1C, $C_{q\ phenol}$), 152.18 (1C, $CH_{triazole}$), 143.45 (1C, $CH_{triazole}$), 135.17 (1C, $C_{q\ benzene}$), 134.74 (1C, $C_{q\ benzene}$), 132.46 (1C, $C_{q\ benzene}$), 132.39 (1C, $CH_{benzene}$), 132.22 (1C, $CH_{benzene}$), 131.70 (1C, CH_{phenol}), 129.82 (1C, $CH_{benzene}$), 127.62 (1C, CH_{phenol}), 123.33 (1C, $C_{q\ phenol}$), 118.28 (1C, CH_{phenol}), 111.44 (1C, $C_{q\ phenol}$), 57.43 (1C, N–CH_2), 55.80 (1C, N–CH_2), 53.47 (1C, $CH_{2\ ethyl}$), 47.13 (1C, $CH_{2\ ethyl}$).

ESI-HRMS (MeOH): Calculated for $[C_{18}H_{18}Cl_2N_4OBr]^+$ (**23e** + H): m/z 455.0041. Found: m/z 455.0038.

2.2 Copper(II) binding studies

The interaction of the target azole compounds with copper(II) was studied by UV spectrophotometric titrations at 25 ^oC in MeOH/H_2O (1:1) solution buffered with 10 mM of MOPS (pH = 7.00). A solution of $CuCl_2$ (at 20-100 µM) was titrated with a solution of each azole compound (at 200-500 µM) until 1.3–4 equivalents of azole was added, in the range of wavelengths of 230-320 nm. The UV spectra were acquired on a PerkinElmer Lambda 650 UV–visible spectrophotometer in Hellma 114-QS quartz cuvettes of 1400 µL volume. The particular concentrations of copper and azoles, and the number of equivalents added in each case are detailed in **Table 2.1**. Conditional binding constants for each copper(II)-azole system were determined with the software HypSpec,[88,89] which uses the combined titration data to determine the equilibrium constant for each stoichiometry present. The fitting of titration data is achieved using the least-squares approach, meaning that the sum of squared residuals is minimized. To better compare the binding properties of the ligands towards copper(II), the value of pCu was also calculated (pCu = −log $[Cu]_{free}$), corresponding to the concentration of free copper in equilibrium at pH = 7.00. The calculation of pCu values was done with the software HySS,[90] which is capable of computing the concentration of any equilibrium species in solution by considering all the species found and their equilibrium constants together with the total concentration of each equilibrium reagent.

Table 2.1 – Experimental conditions used in the copper(II) titration of each compound.

Target compound	Copper sol. concentration (μM)	Azole sol. concentration (μM)	Azole equivalents added
19a	50	400	2.5
19b	100	400	1.3
19c	20	160	3.5
19d	60	250	3.0
19e	75	500	3.0
20e	50	250	3.0
21a	50	400	2.5
21b	75	400	2.5
21c	20	160	3.6
21d	60	300	3.0
21e	50	320	3.0
22a	100	500	2.5
23c	20	200	3.5
23d	60	300	3.0
23e	50	320	3.0

2.3 Biological activity studies

All assays were performed in RPMI-1640 medium buffered with 165 M of MOPS (pH 7.00). *Candida glabrata* wild-type strain ATCC CBS138 was stored at −80 ^{o}C. For biological assays *Candida glabrata* was kept in Yeast Peptone Dextrose (YPD) agar plates and grown at 37 ^{o}C. OD_{600} were measured with a Biochrom Ultraspec 10 Cell Density Meter.

2.3.1 Minimal inhibitory concentration

The minimal inhibitory concentration (MIC) of the target compounds in *Candida glabrata* were determined by dilution assays of the compounds in the absence and in presence of copper(II), in accordance to the CLSI (Clinical Laboratory and Standards Institute) standard methods M27-A3 for yeasts.[91] The assays were performed in 96-well plates, and the concentrations of the compounds applied ranged from 200 to 800 μM with sequential dilutions in H_2O or H_2O/DMSO (75:25), depending on the preparation of the compound's solution. Copper(II) was added from an aqueous $CuCl_2$ solution (51.2 mM) in equimolar amount relative to the azole compounds. The OD_{600} of *Candida glabrata* in RPMI medium was set to 0.2 and 1.5 μL/mL RPMI of this solution was used. Each well had 20 μL of target compound, 80 μL of RPMI medium and 100 μL of cells. Growth in RPMI medium at 37 ^{o}C was recorded after 24 h and 48 h by measuring the OD_{600} of the plates, using a BioTek Epoch Microplate Spectrophotometer. The growth condition without drug was used as the normalization condition, after background (RPMI medium) subtraction. The concentrations of the compound between which the relative ODs fall below 50% are called the MIC_{50}.

2.3.2 Measurement of ergosterol levels

The intracellular ergosterol levels of *Candida glabrata* were determined by HPLC. A pre-culture of RPMI medium inoculated with *Candida glabrata* (15–25 mL) was grown overnight at 37 ^{o}C and 180 rpm (incubator shaker HT INFORS AG CH-4103 Bottmingen). The OD_{600} was set to 0.2 and cultures were left to grow to early exponential phase (OD_{600} 0.8) in RPMI medium, at 37 ^{o}C and 180 rpm. The cells were then left overnight at 37 ^{o}C and 180 rpm, untreated or treated with the higher concentration of the MIC_{50} range of each target compound, at 24 h and in the absence of copper(II). The medium was removed, the OD_{600} was normalized to the lowest OD_{600} (18–20), and sterols were extracted using methanol. After 30 seconds of vortex agitation with glass beads, samples were incubated at 30 ^{o}C for 1 h at 180 rpm. Samples were then centrifuged at 4000 g for 7 minutes at 4 ^{o}C. The supernatant was recovered and centrifuged again at 9500 g for 10 minutes. Analysis was performed on a Waters e2695 HPLC System (Waters Chromatography, USA) with a 2998 Photodiode Array Detector, by injecting a volume of 30–50 µL of each sample into a Symmetry C18 column (4.6 × 250 mm, 5 µm particle size, Waters Chromatography, USA), using a MeOH/H_2O (95:5) mixture as eluent. Column temperature was 30 ^{o}C and samples were kept at 10 ^{o}C. A standard curve prepared with ergosterol (Sigma-Aldrich) was plotted to determine the amount of ergosterol present in each sample.

3. Results and discussion

In this work three different families of target compounds were synthesized, all based on a similar structural design. All target compounds are composed of a central tertiary amine that is functionalized with three separate functional groups: a dihalogenobenzyl group, a 1-alkyl substituted imidazole or 1,2,4-triazole chain, and a copper(II)-binding function (**Figure 3.1**). The differences between families are on the azole group and the length of the carbon chain between the azole and central amine, while the difference within each family lies on the copper(II)-binding function appended and, in one case, on the halogen substituents of the benzyl group. The goal of these structural variations was to perform a structure-activity relationship discussion based on the biological activity results, in order to understand the influence of the different azole and dihalogenobenzyl functions, alkyl chain lengths, and copper(II)-binding functions on the antifungal properties of the compounds. The design of the target compounds was based on a tertiary amine since amines are excellent donor functions for the coordination of copper(II) and also because they are synthetically versatile and easily functionalized with the different functional groups desired.

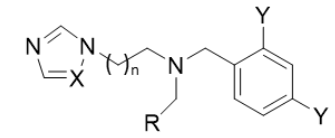

X = N, C
Y = Cl, F
n = 1, 2
R = copper(II)-binding function

Figure 3.1 – General structure of the target azole compounds.

3.1 Synthesis

The main synthetic pathway to obtain the target compounds is similar for all compounds. It starts from a primary alkylamine scaffold already containing the selected azole function, and proceeds in three steps using consecutive indirect and direct reductive aminations to append the two remaining functional groups desired for each particular target compound.

The copper(II)-binding functions were appended using aldehyde reagents, which are all commercially available. Nonetheless, the 8-hydroxy-2-quinolinecarboxaldehyde used was synthesized since it is quite expensive and may be easily synthesized in one step from

inexpensive reagents (**Figure 3.2**). The synthetic step is a selenium dioxide (SeO_2) mediated oxidation in dioxane/water at 95 ^oC, in which the methyl group of 8-hydroxy-2-methylquinoline is partially oxidized to an aldehyde. The compound was isolated in moderate yield (57%) by chromatography, with the overall procedure adapted from Tallec et al.[86]

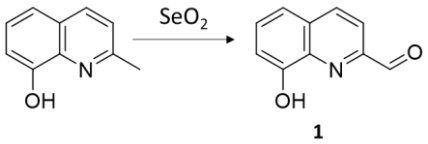

1

Figure 3.2 – Synthesis of 8-hydroxy-2-quinolinecarboxaldehyde (**1**).

The primary amines used for the three families varied in the azole group, which could be an imidazole in one family or a triazole in the other two families, and in the length of the carbon chain separating the azole from the amine, which could be an ethylene chain in also one family or a propylene chain in the remaining two families. The particular primary amines used were then 1-(3-aminopropyl)imidazole (**8**), 1-(3-aminopropyl)-1,2,4-triazole (**7**), and 1-(2-aminoethyl)-1,2,4-triazole (**4**). Although these amines are all commercially available, only the imidazole-containing amine was obtained commercially, while the two triazole-containing ones were synthesized. The synthesis of such primary amines was performed using a Gabriel synthesis appproach in three steps starting from phthalimide (**Figure 3.3**). In the first step phthalimide was reacted with excess dibromopropane or dibromoethane,[92] by a procedure adapted from Krchová et al. using dry dimethylformamide as solvent, potassium carbonate as base, and tetrabutylammonium bromide (TBAB) as a phase-transfer catalyst.[87] Both reactions were heated at 40 ^oC and the *N*-(2-bromoethyl)phthalimide compound (**2**) was isolated in excellent yield just by extraction from ethyl acetate/water, whereas the *N*-(3-bromopropyl)phthalimide compound (**5**) was purified in good yield by chromatography after the extraction. The second step was a nucleophilic substitution of the previous phthalimide derivatives with 1,2,4-triazole. In this step 1,2,4-triazole was initially deprotonated with potassium *tert*-butoxide in acetonitrile solution at room temperature, and then compounds **2** or **5** were added and the reactions heated to reflux. Compound **3** was obtained by precipitation in ethanol, while compound **6** was isolated by chromatography, both in moderate yields. The third step was the deprotection of the phthalimide moiety of the previous triazole derivatives to yield the primary amines **4** and **7**, using hydrazine monohydrate in ethanol. These reactions were achieved in excellent yields and the by-product formed in both cases (phthalhydrazide) is a solid that is easily removed by precipitation with chloroform.

Having in hand all the aldehydes and primary amine reagents, the target compounds were then synthesized in three more steps (**Figure 3.4**). The first synthetic step was a condensation of the primary amine containing the selected azole with an aldehyde to form an imine appended with the desired functional group. This step was always performed in toluene in presence of molecular sieves to adsorb the formed water and acetic acid as a catalyst, and produced excellent yields of the intermediate imines after isolation simply by filtration. This procedure was used instead of the more usual reflux in an alcohol with isolation by precipitation from the reaction mixture, as we found that this way we could maximize the reaction yields while obtaining pure imines without the need for any purification method. The second synthetic step was the reduction of the imine to form a secondary amine. This step was performed in standard conditions using sodium borohydride as reducer in methanol, with the amines isolated by extraction from chloroform/water typically in near-quantitative yield. In this synthetic pathway, the combined first and second steps are in fact an indirect reductive amination which, although possible to undertake in a direct (one-pot) procedure, were performed separately to better understand the reactivity of each individual reaction and also check the purity of the imine intermediates. Additionally, reductive aminations were selected over nucleophilic substitutions to append both functional groups on the starting primary amine not only because substitutions typically have lower yields than reductive aminations of primary amines, but mainly because substitutions can lead to multiple reactions of the starting amine to form undesired higher order side-products (tertiary or quaternary amines, respectively for the first and second functional groups to be appended), which would need to be purified in order to isolate the desired compound.

The third synthetic step was a direct reductive amination of the intermediate secondary amines with an aldehyde to form the target tertiary amines. Reductive aminations with secondary amines are two-stage reactions in which the amine and the aldehyde first react to form an iminium ion intermediate that is subsequently reduced to a tertiary amine.[93] These reactions do not usually present such high yields as the indirect reductive aminations of primary amines since they are never complete, and typically result in relatively simple reaction mixtures containing mostly the target tertiary amine together with some starting reactants and also an alcohol side-product resulting from the undesired reduction of the starting aldehyde. These reactions were performed in two different ways in an attempt to find the best conditions, as follows: in a few cases, the secondary amine was dissolved in dichloroethane and the aldehyde and sodium triacetoxyborohydride ($NaBH(OAc)_3$) as reducer were added simultaneously, with the mixture reacting first at room temperature and finally in reflux. In

most cases the secondary amine was dissolved in methanol and left to react first with the aldehyde alone for an initial period. After that, the reducer sodium cyanoborohydride ($NaBH_3CN$) was added and the mixture reacted for an additional period. The conditions of the various reactions of this type were changed slightly while trying to optimize the yields. The differences found for the two separate reducers and conditions used are meaningful as seen by the ^1H NMR of the reaction mixtures after extraction from chloroform/water, in which the reactions with $NaBH(OAc)_3$ did not show clear signals of the three expected components possibly due to higher degradation of the reagents, whereas the reactions with $NaBH_3CN$ clearly display the signals of the three expected components and there were not many unknown signals.

All target compounds but one were appended with a 2,4-dichlorobenzyl function in order to simplify the understanding of the reactions by NMR, since the fluorine atoms of the 2,4-fluorobenzyl function display coupling interactions with proton and carbon atoms and thus significantly complicate the assignment of NMR signals. For all target compounds but one, the aldehyde used on the first synthetic step was 2,4-dichlorobenzaldehyde or 2,4-difluorobenzaldehyde, while the third step was done with the aldehydes containing the copper(II)-binding functions. The order of employment of the two types of aldehydes was tested to understand which order would be better to synthesize the target compounds. In the end, it became clear that by first using the aldehyde containing the dihalogenobenzyl function, the first and second synthetic steps can be performed on a larger scale and each intermediate could be used for various third-step reactions within each family of target compounds. Additionally, the purification of target compounds by silica column chromatography is also slightly easier using this order, since the secondary amine intermediates obtained have a higher polarity difference to the target compounds than when using the reverse order. It should be emphasized that the main goal of this work was not to study in detail and optimize the used reactions, but to synthesize as many target compounds as possible to perform antifungal activity tests. For this reason, each specific reaction used was only performed the small number of times necessary to obtain each desired compound or intermediate, and thus it may well be possible to improve some of the lower yields reported by investing additional time on reaction optimization.

The synthetic scheme in **Figure 3.4** shows the detailed pathway adopted to obtain the target compounds. The first family of compounds was based on the 1-(3-aminopropyl)imidazole (**8**) primary amine intermediate, from which two secondary amine intermediates were obtained containing a 2,4-dichlorobenzyl (**10**) or 2,4-fluorobenzyl (**12**)

function. The former was then appended with five different copper(II)-binding functions (**19a-e**), while the latter was only appended with one (**20e**). The second family was based on the 1-(3-aminopropyl)-1,2,4-triazole (**7**) previously obtained, from which a single secondary amine intermediate (**14**) was obtained containing a 2,4-dichlorobenzyl function. This intermediate was then appended with the same five copper(II)-binding functions used on the first family (**21a-e**). The third family was based on the 1-(2-aminoethyl)-1,2,4-triazole (**4**) previously obtained, from which two different orders of aldehyde employment were adopted. In the first order, 2-pyridinecarboxaldehyde was first used to form the secondary amine intermediate (**16**), which was then further substituted with 2,4-dichlorobenzaldehyde to produce one of the target compounds in the family (**22a**). The rest of the compounds of the third family were synthesized by reaction of 1-(2-aminoethyl)-1,2,4-triazole first with 2,4-dichlorobenzaldehyde to form the secondary amine intermediate (**18**), which was then appended with three other copper(II)-binding functions (**23c-e**) similar to the ones used for the first and second families.

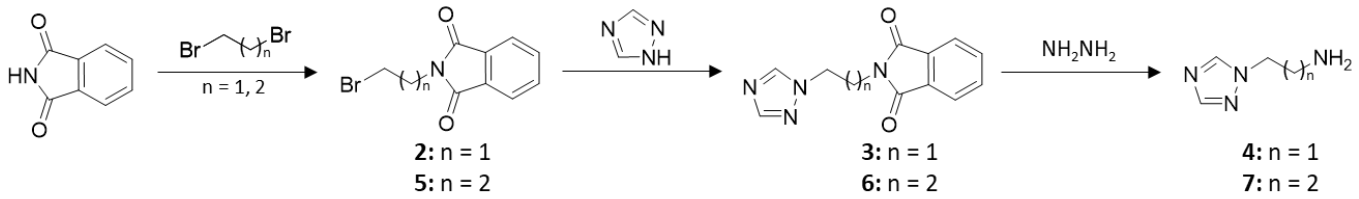

Figure 3.3 – Scheme of the synthesis of primary amine intermediates 1-(3-aminoethyl)-1,2,4-triazole and 1-(2-aminopropyl)-1,2,4-triazole.

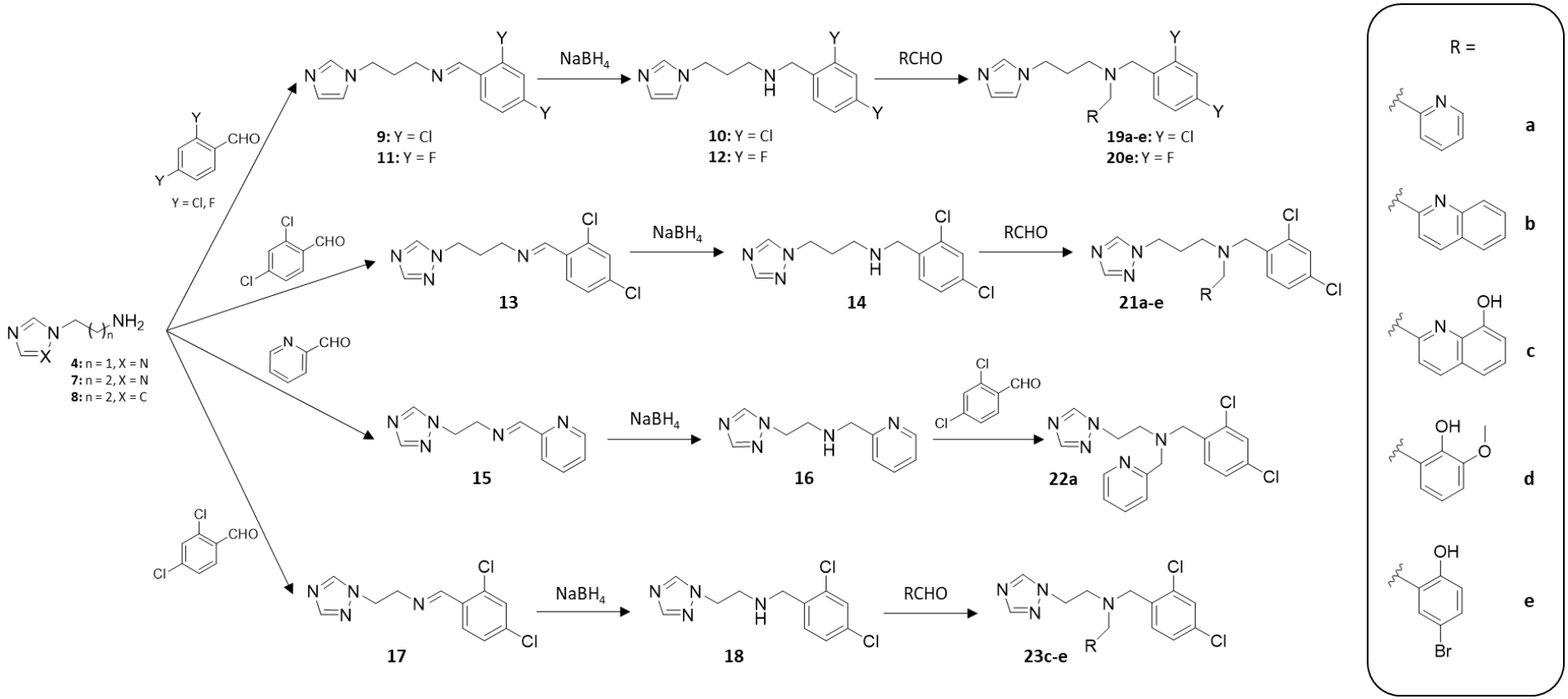

Figure 3.4 – Scheme of the synthesis of target compounds starting from the primary amine intermediates.

Each synthetic step was followed by NMR since all the compounds, including the imine intermediates, were stable and could be isolated and characterized. Some spectral features of both intermediate and target compounds of the main synthetic pathway are worth mentioning, particularly the signals of the ^{1}H spectra. The formation of the imine intermediate is characterized by the appearance of a singlet around 8.50 ppm integrating for one proton, highlighted in **Figure 3.5.A**. Upon reduction of the imines to secondary amines, the imine singlet is replaced by an aliphatic singlet around 3.70 ppm integrating for two protons, highlighted in **Figure 3.5.B**. The formation of the tertiary amine target compound is identified by the appearance of a second aliphatic singlet also around 3.70 ppm and integrating for two protons, highlighted in **Figure 3.5.C**.

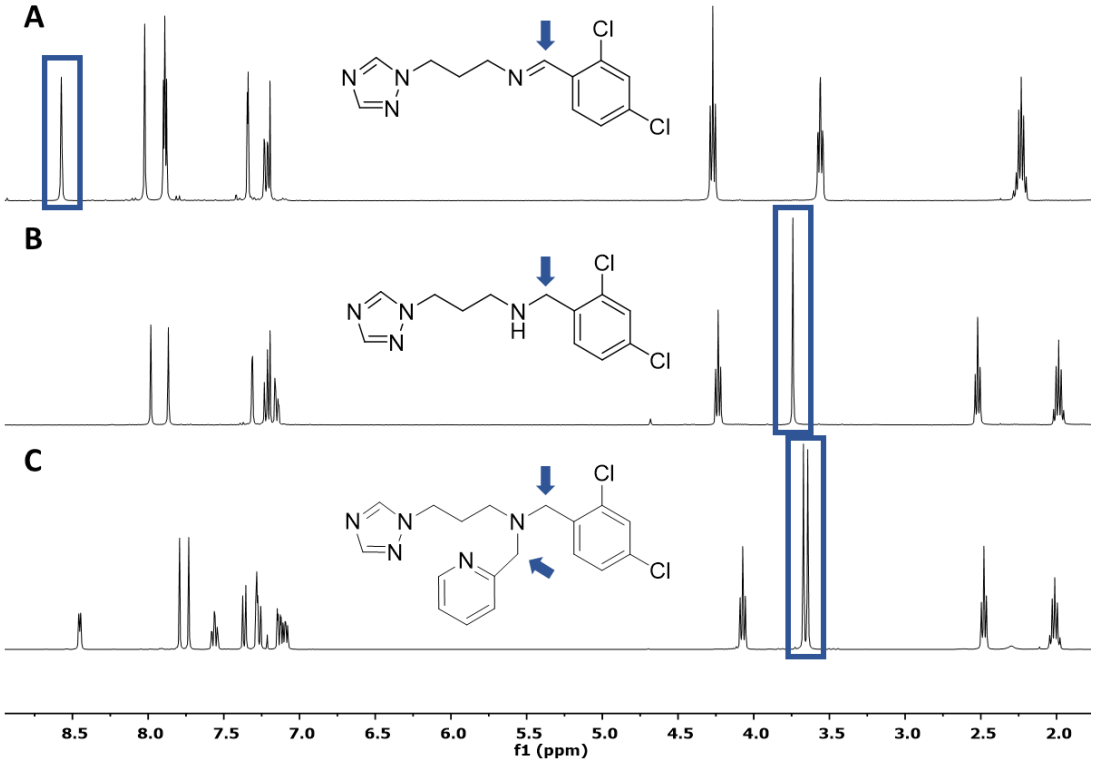

Figure 3.5 – Stacking of the ^{1}H NMR spectra (in $CDCl_3$) of each synthetic step for an example of target compound: (A) imine **13**, (B) secondary amine **14**, (C) tertiary amine **21a**.

Each intermediate secondary amine has a typical ^{1}H NMR spectrum, but since the structural differences between these compounds are small, their spectra are fairly similar overall (**Figure 3.6)**. Starting by the aliphatic region, compound **10** (**Figure 3.6.A**) shows a quintuplet and two triplets from the propylene chain, and a singlet from the methylene next to the secondary amine. Compound **12** (**Figure 3.6.B**) only differs from **10** in the halogen atoms in the benzyl, so there is no major difference on its aliphatic signals. Compound **14** (**Figure 3.6.C**) differs from **10** in the azole group, a triazole instead of an imidazole, and since this azole is attached to the propylene chain there is a downfield shift in two of the corresponding

propylene signals. Compound **18** (**Figure 3.6.D**) differs from **14** in having an ethylene chain linking the triazole and the secondary amine, thus it shows only two triplets corresponding to the ethylene chain and the expected singlet. The differences in the aromatic region are more prominent due to the azole function (**Figure 3.7)**. In compound **10** (**Figure 3.7.A**) the three singlets expected for imidazole can be seen at around 6.8, 7.0 and 7.4 ppm. The dichlorobenzyl function also shows three signals, two doublets and a doublet of doublets (dd), which display the particular H–H *J*-coupling features arising from the substitution pattern of the benzyl ring. One of the doublets at around 7.23 ppm displays a minimal coupling constant assigned to a four-bond coupling, the other at around 7.20 ppm displays a higher coupling constant assigned to a three-bond coupling. The doublet of doublets at around 7.08 ppm displays both a three- and four-bond coupling constant. In compound **12** (**Figure 3.7.B**) the imidazole signals are relatively similar to compound **10**, but the difluorobenzyl signals are much more complex than for **10** since fluorine atoms also couple with the protons in ^{1}H NMR. This effect is evident on one of the previous doublets at around 7.20 ppm that is now a triplet of doublets (td), since it displays two similar H–F coupling constants with the two fluorine atoms besides the single H-H coupling constant. The two other multiplet signals expected are overlapping at 6.7–6.8 ppm so is not possible to do a detailed analysis. In compound **14** (**Figure 3.7.C**) the imidazole is replaced by a triazole function that shows two singlets quite downfield shifted compared to the imidazole signals, but the dichlorobenzyl signals are quite similar to compound **10**. There are no significant differences between compound **14** and **18** (**Figure 3.7.D**) in the aromatic region except for a small downfield shift of one triazole singlet, the difference between these compounds lying almost exclusively on the aliphatic region due to the different alkyl chain.

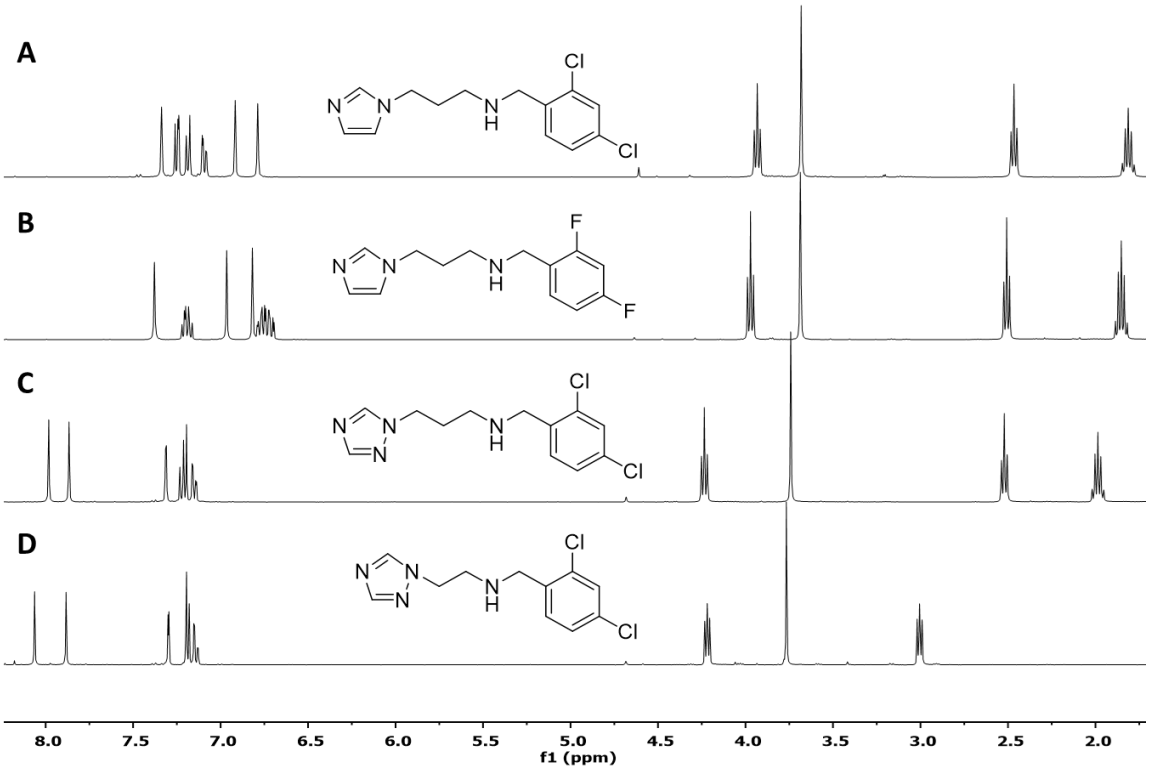

Figure 3.6 – Stacking of ^{1}H NMR spectra (in $CDCl_3$) of the different secondary amine intermediates: (A) **10**, (B) **12**, (C) **14**, (D) **18**.

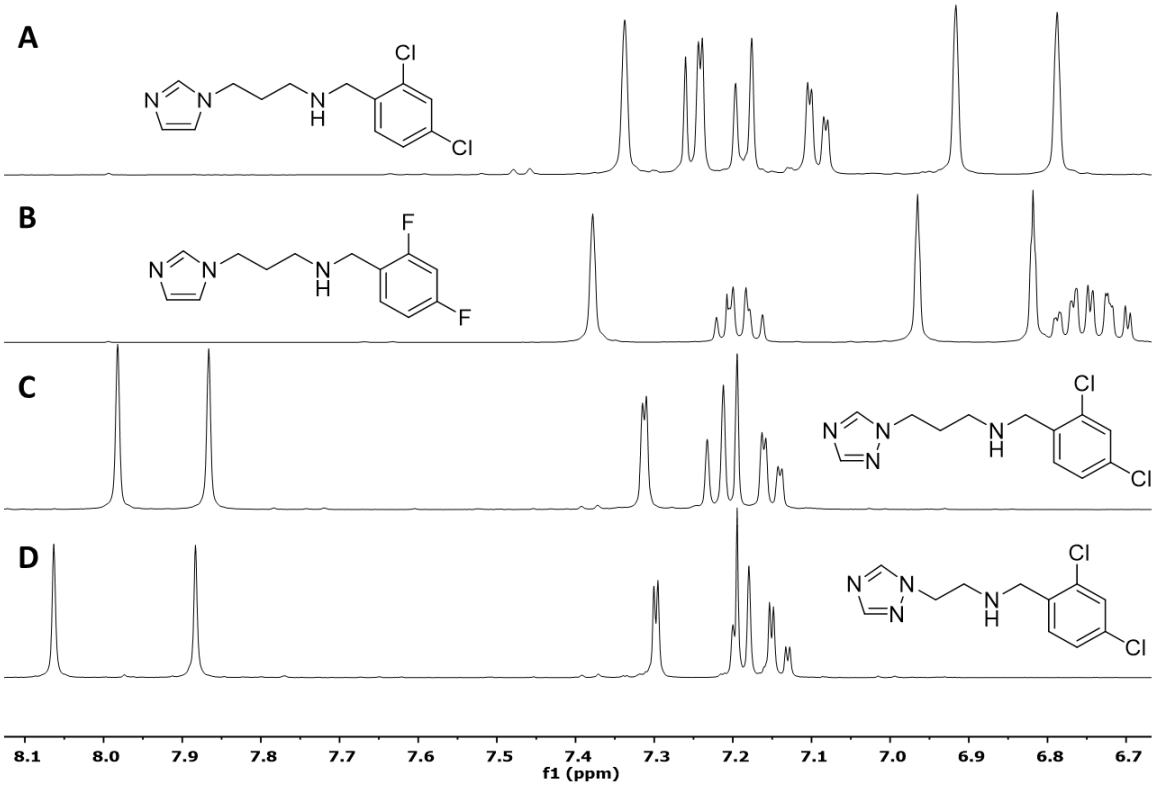

Figure 3.7 – Stacking of the aromatic region of the ^{1}H NMR spectra (in $CDCl_3$) of the different intermediates: (A) **10**, (B) **12**, (C) **14**, (D) **18**.

In each structural family, the differences between target compounds arise essentially from the varying copper(II)-binding functions appended on the central tertiary amine. The selected copper(II)-binding functions were pyridine (**Figure 3.8.a**), quinoline (**Figure 3.8.b**), 8-hydroxyquinoline (**Figure 3.8.c**), 2-methoxyphenol (**Figure 3.8.d**) and 4-bromophenol (**Figure 3.8.e**). As previously mentioned, the goal was that each target compound had at least two good donor atoms for copper(II) coordination, one being the tertiary amine and another being positioned within a distance of three to four bonds such that the target compounds could act as polydentate ligands for copper(II). This metal binds preferably to nitrogen atoms of both aliphatic and aromatic amines, so pyridine was the first choice as binding function. As the nitrogen of pyridine is at a 3-bond distance from the tertiary amine, copper(II) can coordinate through formation of a 5-membered chelate ring. As a pyridine derivative, the quinoline function has a copper(II) coordination mode similar to pyridine, with the main difference lying on an additional aromatic ring attached, which is expected to increase the lipophilicity of the target compounds. In contrast, 8-hydroxyquinoline is itself a known bidentate metal chelator that should be able to bind copper(II) more strongly than the previous functions, especially if the hydroxyl deprotonates upon coordination. Also, this group enables the target compounds to bind as tridentate chelators overall when considering the tertiary amine of the target compounds, by coordinating copper(II) through two 5-membered chelate rings. On the other hand, and since it is not known how strong a copper(II) coordination is best suited to promote antifungal activity, some target compounds were synthesized with copper(II)-binding function not containing nitrogen atoms. On a different note, oxygen atoms of hydroxyl groups are good donor atoms to copper(II) when deprotonated, because the electron donating power increases and the negative charge also helps to compensate the positive charge of copper(II). Thus, the last copper(II)-binding functions selected were 2-methoxyphenol and 4-bromophenol, between which the difference lies on the additional heteroatoms present on the phenol ring. These heteroatoms will not participate directly in the coordination of copper(II) but may nonetheless affect it. Indeed, the bromine substituent is very electronegative so it could favor the deprotonation of the hydroxyl and thus strengthen the copper(II) coordination by the target compounds, and a weaker effect of the same type might also be expected from the methoxy substituents. Another difference in these phenol derivatives is that the potential oxygen donor atom will be at a 4-bond distance from the tertiary amine of the target compounds, and so copper(II) would bind through a 6-membered chelate ring instead of the 5-membered chelate ring of the previous copper(II)-binding groups based on pyridine.

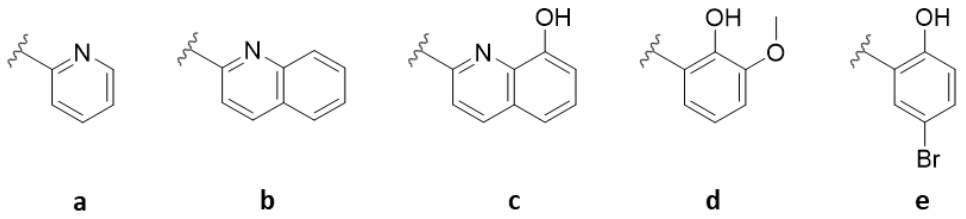

Figure 3.8 – Selected copper(II)-binding functions used in the synthesis: (a) pyridine, (b) quinoline, (c) 8-hydroxyquinoline, (d) 2-methoxyphenol, (e) 4-bromophenol.

Each copper(II)-binding function produces unique ^{1}H NMR signals on the spectra of the target compounds mostly seen on the aromatic region, as seen on the spectra of the second family of compounds **(Figure 3.9)**. These signals are additional to the already present signals of the triazole (one or two singlets at 7.7–7.9 ppm) and of the dichlorobenzene (two doublets and a doublet of doublets at 7.1–7.4 ppm). In the case of **21a** (**Figure 3.9.a**), a distinctive doublet is seen at around 8.5 ppm, which corresponds to the most deshielded proton of the pyridine ring. The rest of the signals appear as one triplet of doublets (7.55 ppm), one doublet of doublets (7.10 ppm), and a doublet (7.35 ppm). In the case of **21b** (**Figure 3.9.b**) it is not possible to do a full assignment of the spectrum, but there are some relevant peaks such as the two doublets at 7.9-8.1 ppm that could correspond to the protons at a 3-bond distance from the nitrogen atom of quinoline. A similar effect happens for **21c** (**Figure 3.9.c**), with only one assignable doublet at 8.0 ppm that should also correspond to the single proton at a 3-bond distance from the nitrogen atom. Another relevant signal in this case is the barely visible broadened peak downfield from this doublet (around 8.1 ppm), which corresponds to the proton of the hydroxyl group that as an exchangeable proton is not as well defined as the protons bound to carbon atoms. In the spectrum of **21d** (**Figure 3.9.d**) there are three signals from the methoxyphenol shifted upfield compared to the previous copper(II)-binding functions, two doublets and a triplet at 6.50–6.75 ppm. There are also some signals not seen in this range, such as a broad singlet at 9.9 ppm from the hydroxyl and an aliphatic singlet from the methoxy substituent in the phenol function. The spectrum of compound **21e** (**Figure 3.9.e**) only shows two visible signals from the bromophenol, as the third signal is overlapping one of the dichlorobenzyl signals. The visible signals are two doublets that similarly to the previous case are upfield shifted compared to the first three copper(II)-binding functions. There is also a signal outside of this range appearing as a broad singlet at 10.1 ppm that corresponds to the hydroxyl group from the phenol.

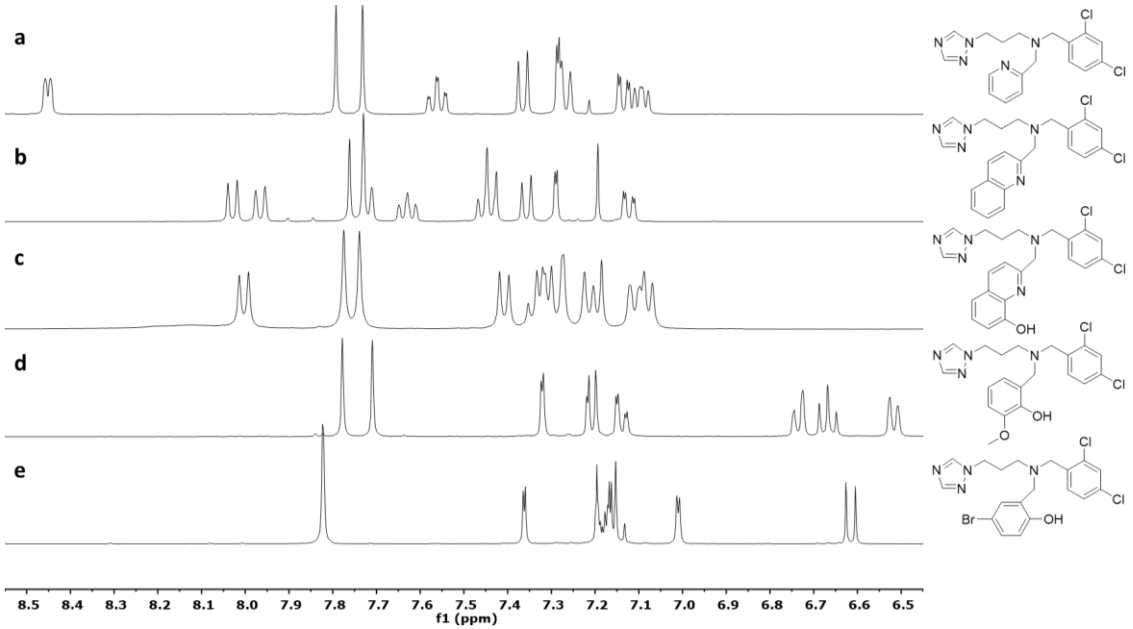

Figure 3.9 – Stacking of the aromatic region of the ^{1}H NMR spectra (in $CDCl_3$) of the second family of target compounds (**21**), each containing a different copper(II)-binding function: (a) pyridine, (b) quinoline, (c) hydroxyquinoline, (d) methoxyphenol, (e) bromophenol.

The structures of all the target compounds are shown in **Figure 3.10** organized in the three structural families described previously. The overall number of synthetic steps and yields obtained for each target compound are summarized in **Table 3.1**. Considering that the synthesis of each compound required between three and seven synthetic steps, the yields may be described as good in roughly half of the cases but only modest in the other half. However, it should also be noticed that the least yielding step in all cases is the final reductive amination one that, as mentioned before, may be possible to optimize in the future if more time is available both in the synthesis and isolation parts.

Table 3.1 – Total number of steps and global yields of the synthesis of each target compound.

Target compound	Total synthetic steps	Overall yield (%)
19a	3	41
19b	3	27
19c	4	8
19d	3	54
19e	3	40
20e	3	24
21a	6	7
21b	6	4
21c	7	5
21d	6	11
21e	6	6
22a	6	32
23c	7	7
23d	6	21
23e	6	8

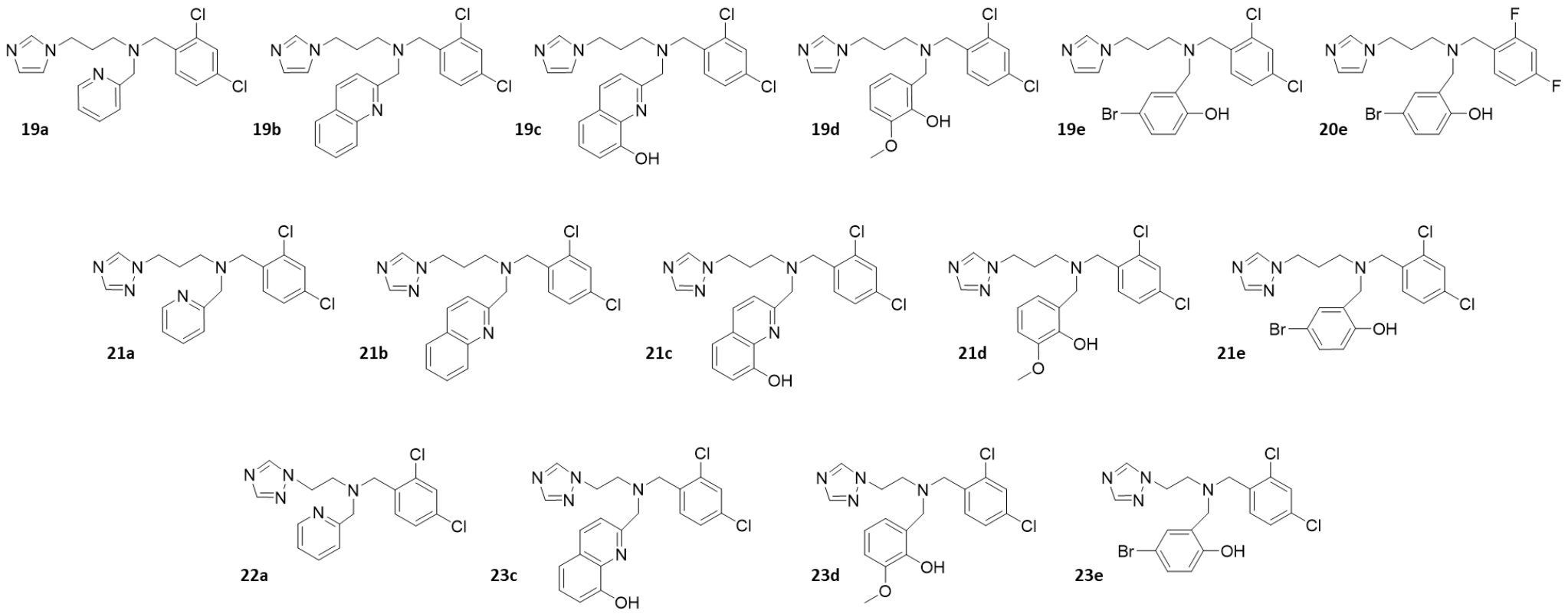

Figure 3.10 – Structures of the target compounds of the first (top row), second (middle row), and third (bottom row) families.

3.2 Copper(II) binding studies

To study the interaction of the target compounds with copper(II), UV spectrophotometric titrations were performed in aqueous methanol (1:1) solutions buffered at pH = 7 with 10 mM of MOPS. The main goal of these titrations was to determine the binding strength of each azole towards copper(II), so that this property may be compared between each azole compound within a given structural family or from different families. The adoption of a solvent mixture as medium was due to the limited solubility of most synthesized azoles in neat water, and methanol appeared as an appropriate co-solvent given that it freely dissolved all azoles and is also commonly used in the literature for such mixed-solvent studies. Since these binding studies aimed to compare all azoles and not to determine their full complexation properties throughout the pH range, we chose to carry them out at a fixed pH that was relevant for possible biological applications, thus pH = 7 was selected. In these conditions, the binding constants determined are conditional since the concentration of protons was kept constant during each titration by use of a buffer substance. The choice of buffer was restricted to those not interfering with the binding phenomenon as much as possible, since it is known that many commonly used buffers are also able to bind metal cations. Indeed, many buffers such as Good's buffers are based on functionalized amines, which by nature are good copper(II) donor functions. A few literature studies have searched for non-binding buffers, and MOPS (3-(*N*-morpholino)propanesulfonic acid) arises as the least interfering one among those suitable for the neutral pH region.[94] After running a few preliminary experiments, we found that MOPS was indeed suitable to determine the binding of the azoles to copper(II), so it was finally adopted as the buffer substance in all our equilibrium studies and used in a concentration that is 40–145 times higher than any other reagent. It should be noted that MOPS was also the buffer used in the subsequent biological studies.

The conditional equilibrium binding constants were determined with the software HypSpec,[88,89] which uses the least-squares fitting approach, meaning that the sum of squared residuals is minimized where the residuals are the difference between the experimental or observed value and the value calculated from the model. For the software to be able to determine a binding constant, there must be a relevant change in the amount of complex formed and free ligand.

A solution of copper(II) chloride ($CuCl_2$) buffered with MOPS (pH = 7.00) and contained in a spectrophotometric cuvette was titrated with each of the ligands at addition intervals of 0.1 equivalents until excess of ligand was reached, and the UV spectra were recorded at each titration point. The spectra of the free ligand and of $CuCl_2$ in the same buffered medium were

also recorded and are inserted in the software as known spectra, thus requiring that the software refines the spectra of only the other species present in equilibrium. After all the data is inserted in the software, a relevant range of wavelengths is chosen centered at the main absorption bands of the reagents and formed complex.

In the beginning of the titration there is an excess of copper(II) in comparison to the ligand, and the higher the binding constant, the higher is the relative amount of complex formed. As the ligand reaches an excess over copper, the relative amount of free ligand will increase, and the amount of complex will reach a plateau depending on the magnitude of the constant. In **Figure 3.11** is shown an example of a titration with **21c**, in which the beginning of the titration (bottom curve) displays absorbance only below 230 nm. As the ligand is added, a band centered around 265 nm appears corresponding to the formation of the complex between the ligand and copper(II). After some additions of ligand, this band increases less than before, and a new band centered around 245 nm starts appearing. This latter band corresponds to the free ligand in equilibrium and increases more intensely towards the end of the titration.

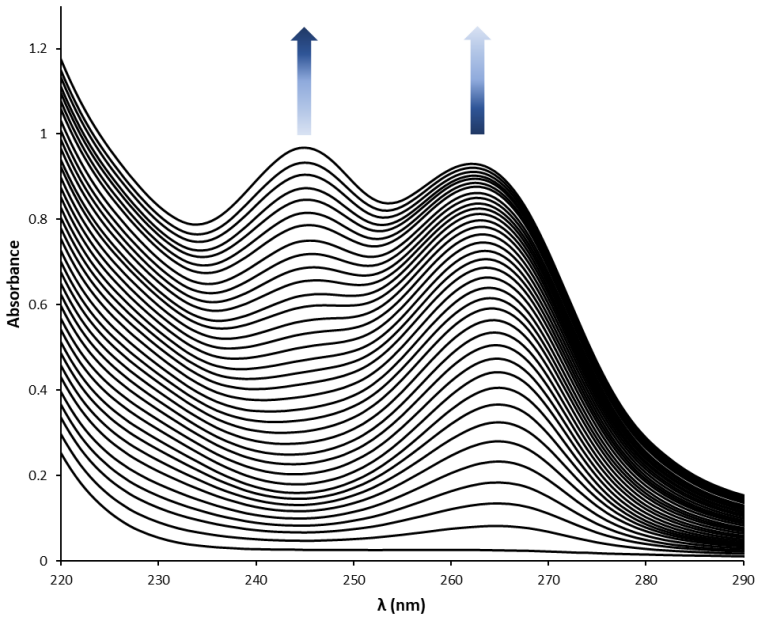

Figure 3.11 – UV titration of copper(II) with **21c**, with the appearing absorption bands highlighted.

Since there are different functional groups on the target compounds, the binding mode of each compound to copper(II) may likely also be different. One of the donor atoms in all compounds must be the central tertiary amine, while the other donor atoms depend on the family of the compound and on the copper(II)-binding functions present. The first family contains an imidazole, for which coordination to copper(II) is not structurally favored, but the second and third families contain a triazole, for which there is a possibility that the *N*-2

nitrogen atom could also bind copper(II) even if only weakly. In case there is effectively copper(II) coordination through the triazole *N*-2 nitrogen, the potential complexes would form 7-membered or 6-membered chelate rings involving this nitrogen and the tertiary amine for compounds of the second or third family, respectively. The structure of the complexes formed is hypothesized as being generally of square planar geometry, where the coordinated donor atoms form a plane with copper(II), but the exact geometry or additional donor atoms were not determined. To try and determine these geometries it would have been necessary to record absorption spectra at wavelengths above 350 nm, where the more informative *d*-*d* absorption bands are visible, and/or electron paramagnetic resonance (EPR) studies to probe the metal center structural environment. Both of these studies would require much higher concentrations of the target compounds than those used in the UV studies, which were impracticable in the present case given the small scale in which the compounds were isolated.

The determination of the conditional binding constants for each target compound has provided binding constants not only for the 1:1 metal-to-ligand stoichiometry but in some cases also for the 1:2 and 2:1 stoichiometries as well. Since during all titrations an excess of copper(II) or of ligand are alternately present in some of the points, multiple stoichiometries may appear if such complexes are stable enough and their relative amounts in equilibrium are relevant. Since the conditional binding constants determined did not always found the expected 1:1 stoichiometry for all complexes, the results cannot be directly compared between all target compounds. To better compare the binding ability of the ligands towards copper, we resorted to the calculation of the more general parameter pCu. The pCu is equal to the negative logarithm of the concentration of free copper(II) in solution, meaning the copper(II) that did not form any complex species. The better the compound's ability in binding copper(II), the lower is the concentration of free metal in solution and so the higher is the pCu. It is important to notice that lower concentrations of free copper(II) do not necessarily correspond to more stable complex species, but only that such species consumed more metal to be formed. The calculation of the pCu values was done using the software HySS.[90] This software is capable of computing the concentration of free copper in solution by taking into account all equilibrium species formed and their equilibrium constants together with the total concentrations of copper and ligand. To directly compare the results, the same total concentrations of copper and ligand were used for every system. The concentrations chosen were 100 µM of each component, a concentration that is closely related to the magnitude of the minimum inhibitory concentrations calculated for the compounds. The conditional binding constants and the pCu values obtained for each target compound are presented in **Table 3.2**.

Table 3.2 – Conditional binding constants and calculated pCu values for each target compound.

Target compound	log $\beta(M_2L)$	log $\beta(ML)$	log $\beta(ML_2)$	pCu
19a	-	3.93(1)	-	4.19
19b	-	3.83(4)	-	4.17
19c	-	6.39(1)	10.85(2)	4.97
19d	-	ND	7.03(3)	4.03
19e	-	ND	7.23(1)	4.05
20e	-	ND	7.66(5)	4.08
21a	-	4.50(1)	-	4.37
21b	-	4.38(3)	-	4.33
21c	11.14(3)	6.02(2)	10.64(2)	5.40
21d	-	ND	7.44(1)	4.06
21e	-	ND	7.96(3)	4.11
22a	-	5.67(1)	-	4.87
23c	11.81(3)	6.48(2)	10.19(5)	5.86
23d	-	3.35(1)	-	4.07
23e	-	3.89(1)	-	4.18

In the first family of compounds, the pyridine- and quinoline-containing compounds, **19a** and **19b** respectively, only formed complexes of 1:1 stoichiometry. Both compounds have the same potentially good donor atoms for copper(II), a tertiary amine nitrogen and the pyridine/quinoline nitrogen. These nitrogen atoms are also separated by three bonds in both cases, so both compounds may act as bidentate ligands by forming complexes with 5-membered chelate rings. The compound **19a** has a higher log β(ML) by only 0.1 log units, which suggests that the binding mode of the compounds is similar, and **19a** has the higher log β(ML) of the two possibly due to a lower electron donating power of the quinoline nitrogen of **19b** arising from a higher electronic delocalization effect in the quinoline function.

For **19c** the log β(ML) is 6.39, which is much higher than for the previous two compounds. Hydroxyquinoline is a known bidentate chelator for copper, coordinating strongly through the nitrogen and oxygen atoms of the function after hydroxyl deprotonation by forming a 5-membered chelate ring with the metal. The tertiary amine of **19c** should also coordinate copper(II) by forming another 5-membered chelate ring. By having three good donor atoms the complex formed will be very stable, explaining the higher conditional binding constant determined. For this compound it was also possible to find a binding constant for the 1:2 stoichiometry, the log $\beta(ML_2)$ determined at 10.85. In this case it is possible that the complex forms between two hydroxyquinoline functions from two different ligand molecules to form a tetracoordinated complex species.

For the phenol-containing ligands of the first family, **19d**, **19e** and **20e**, only the binding constant for the 1:2 stoichiometry could be determined, which means that the 1:1 complex species is too weak to be found in significant amount and thus it cannot be determined. As the phenol functions only have an oxygen donor atom that is weak unless deprotonated, this suggests that the formation of complex could require a second ligand molecule, by having four donor atoms to coordinate copper, two strong and two weak. The log $\beta(ML_2)$ for **19d** is about 0.2 log units lower than for **19e**, meaning that the compound containing bromophenol binds more strongly to copper(II) than the compound containing methoxyphenol. For compound **20e**, which is similar to **19e** but with a difluorobenzyl instead of a dichlorobenzyl function, the binding constant determined is more than 0.4 log units higher than **19e**, showing that the fluorine atoms have a positive influence in the copper(II) complex formation despite not being directly involved in metal coordination.

In the second family of compounds, the pyridine- and quinoline-containing compounds, **21a** and **21b** respectively, formed only complexes of 1:1 stoichiometry such that the log $\beta(ML)$ is about 0.1 log units higher for the pyridine compound compared to the quinoline one, explained as previously by the higher electronic delocalization on quinoline. When compared with the first family of compounds, the only structural difference is the replacement of the imidazole with a triazole. Since the log $\beta(ML)$ increased in both cases by more than 0.5 log units between families, it is possible that the triazole has a role in the coordination of copper(II). In such event, the coordination would occur through three donor atoms, the tertiary amine, the nitrogen of the pyridine/quinoline functions and the *N*-2 nitrogen atom of the triazole by forming one 5-membered and one 7-membered chelate rings.

For compound **21c**, containing an hydroxyquinoline function, it was possible to determine binding constants for the stoichiometries of 2:1, 1:1, and 1:2. This means that this compound can also bind two different copper(II) cations, likely one through the hydroxyquinoline function and another through the tertiary amine and the *N*-2 nitrogen atom of the triazole. Both log $\beta(ML)$ and log $\beta(ML_2)$ decreased in comparison to the first family of compounds, maybe due to the presence of the competing 2:1 stoichiometry.

As in the first family, for the compounds with the phenol functions, **21d** and **21e**, it was only possible to determine the binding constant for the 1:2 stoichiometry. Also similarly, the bromophenol-containing compound shows a higher log $\beta(ML_2)$ than the methoxyphenol one, with a difference of 0.52 log units. These log $\beta(ML_2)$ values also increased by 0.41 and 0.73 log units between families, suggesting once again that the triazole might participate in the coordination of copper(II).

In the third family of compounds, the pyridine-containing compound **22a** has a log β(ML) significantly higher when compared with the first and second families. In this case the compound has three suitable nitrogen donor atoms for the coordination of copper(II), the tertiary amine, the nitrogen of the pyridine, and the *N*-2 nitrogen of the triazole. Indeed, the possible formation of a 6-membered chelate ring between the *N*-2 nitrogen of the triazole and the tertiary amine would explain the increase by more than 1.1 units for the log β(ML) when compared with compound **21a** from the second family.

For compound **23c**, containing an hydroxyquinoline function, it was again possible to determine binding constants for the 2:1, 1:1, and 1:2 stoichiometries. The log β(ML) determined is the highest of all studied compounds, which may be explained by the high chelating ability of the hydroxyquinoline function together with the potential coordination of the *N*-2 nitrogen atom of the triazole. In such an event, the complex formed would be tetracoordinated to one ligand molecule with all 5- or 6-membered chelate rings. As for **21c**, this compound can also bind two different copper(II) cations, and since the log $\beta(M_2L)$ of **23c** is higher by 0.67 log units compared to **21c** it also suggests that coordination through the *N*-2 nitrogen atom of the triazole is favorable for copper(II) binding. On the contrary, the log $\beta(ML_2)$ is the lowest of all three families, which is justified by the stronger overall coordination ability of compound **23c**.

For compounds **23d** and **23e**, unlike in the first and second families, the only binding constants determined were for the 1:1 stoichiometry, which prevents any direct comparison with compounds from the previous families. This change could also be explained by the possible copper(II) coordination through the *N*-2 nitrogen atom of the triazole, something that would disfavor the use of a second ligand molecule to stabilize the formed complex. On the other hand, as previously seen, the bromophenol-containing compound forms a more stable complex than the methoxyphenol one, even though the coordination mode should be similar.

Since the conditional binding constants determined cannot be directly compared for all target compounds due to the different stoichiometries involved, it is possible to make such a comparison by using the pCu parameter that was calculated and which applies to all occurring stoichiometries combined. For a better perception of the pCu values, a bar graph of the results was plotted (**Figure 3.12**) with the results organized by structural family and color-coded according to the copper(II)-binding function present.

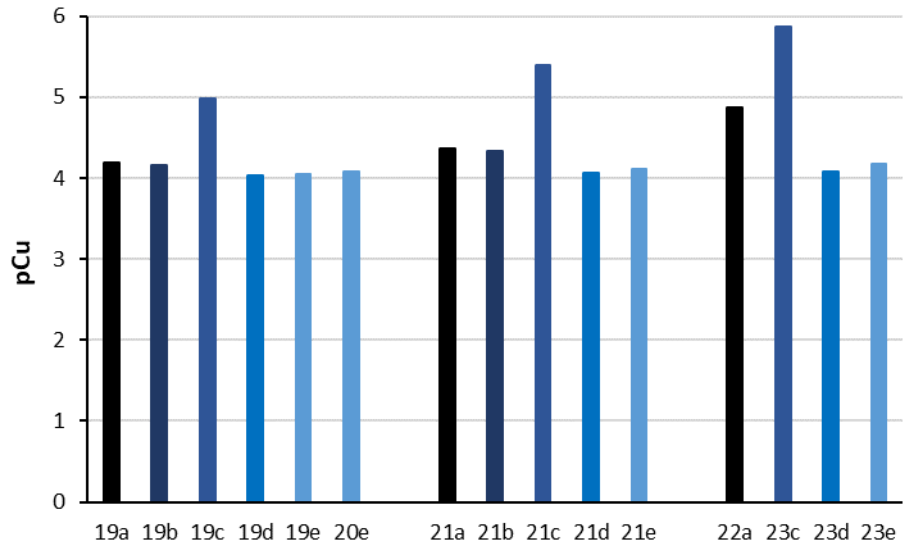

Figure 3.12 – Graphical representation of the pCu values of the studied compounds at pH = 7 and 100 µM concentration of total copper and ligand. Each color represents the copper(II)-binding function (black – pyridine, dark blue – quinoline, navy blue – hydroxyquinoline, turquoise – methoxyphenol, and light blue – bromophenol).

There is a trend of increasing pCu values from the first family to the third family, although less apparent for the phenol-containing compounds, which evidences an increasing ability of binding copper(II) by the target compounds. The third family has a higher ability to bind copper(II) than the second one, suggesting once again that the ethylene chain separating the triazole and the tertiary amine aids the coordination of the triazole to copper(II). The second family has a higher capability for binding copper than the first one, showing that using a propylene chain and replacing imidazole by triazole also assists the overall coordination of copper(II). This fact strongly suggests that triazole may well be involved in copper(II) coordination for compounds of both second and third families. The hydroxyquinoline-containing compounds have higher pCu values than those containing the remaining copper(II)-binding functions, since it is the only chelating functional group used. The pyridine and quinoline-containing compounds are the next best compounds with high pCu, likely due to the better electron donor nitrogen atoms in comparison with the oxygen donor atoms of the bromophenol- and methoxyphenol-containing compounds. Between the two phenol functions, the pCu values are not as different from family to family as for the other copper(II)-binding functions, but bromophenol compounds have slightly higher pCu than methoxyphenol ones in all families. As for the single compound containing a 2,4-difluorobenzyl function, **20e** has a slightly higher pCu than **19e**, pointing to the fluorine atoms having an influence, albeit indirect, in the coordination of copper(II).

3.3 Biological activity studies

To study the susceptibility of *Candida glabrata* to the target compounds, the minimum inhibitory concentration (MIC) was determined. MICs are defined as the lowest concentration of a drug that will inhibit the visible growth of a microorganism after incubation, and MIC_{50} is the range of concentrations that inhibits the growth of 50% of a microorganism compared to a non-treated control. The MIC_{50} for *Candida glabrata* for each target compound was determined after 24 h and 48 h of incubation with the target compound and the copper(II) complex. Compound **23e** could not be studied since it was not soluble in water. The results for the remaining compounds are presented in **Table 3.3**.

Table 3.3 – MIC_{50} values for *Candida glabrata*, at 24 and 48 h in RPMI at 37 ^{o}C for each target compound, in the absence and in the presence of copper(II).

Target Compound	MIC_{50} 24h (μM)		MIC_{50} 48h (μM)	
	Without copper	With copper	Without copper	With copper
Cu	-	100–200	-	100–200
Fluconazole	-	-	52.5–105	-
19a	100–200	100–200	200–400	100–200
19b	25–50	25–50	50–100	25–50
19c	1.563-3.125	1.563-3.125	6.25-12.5	6.25-12.5
19d	50–100	12.5–25	50–100	12.5–25
19e	0.781–1.563	0.781–1.563	3.125–6.25	1.563–3.125
20e	1.563–3.125	0.781–1.563	25–50	6.25–12.5
21a	400–800	200–400	200–400	200–400
21b	50–100	12.5–25	50–100	25–50
21c	3.125–6.25	3.125–6.25	12.5–25	12.5–25
21d	200–400	100–200	200–400	100–200
21e	50–100	1.563–6.25	25–50	25–50
22a	ND	400–800	ND	400–800
23c	3.125–6.25	3.125–6.25	12.5–25	12.5–25
23d	200–400	100–200	200–400	100–200

Most azole drugs are fungistatic, meaning that they prevent fungal growth but do not cause fungal cell death. In biological studies this is shown by a phenomenon called trailing growth in which fungal cells gain tolerance to the azole drug and restart growth after some time, which corresponds to an increased MIC_{50} value at 48 h when compared to the one at 24 h. Whenever the MIC_{50} is equal at both timepoints the drug may still be fungistatic, and to confirm this the MIC_{50} would need to be determined for longer time periods to check if the cells restart to grow. Of the 14 target compounds studied, 12 had no difference in MIC_{50} or an increase at 48 h, meaning that they are fungistatic drugs. The two target compounds that had a decrease in MIC_{50} from 24 to 48 h are **21a** and **21e**, but this decrease was only seen in the MIC_{50} determined in the absence of copper(II).

The synthesis of these target compounds was based on the pharmacophore groups of fluconazole and the goal was for the target compounds to have higher antifungal activity than fluconazole, meaning a lower MIC_{50} value. Fluconazole's MIC_{50} is 52.5–105 μM at 48 h for *Candida glabrata*,[55] which is a high MIC_{50} compared with other *Candida* species like *Candida albicans*.[51] For a better perception of the MIC_{50} values determined at 48 h without copper, a bar graph of the results was plotted (**Figure 3.13**), with the results organized by structural family and color-coded according to the copper(II)-binding function present. From the 14 target compounds studied, four had MIC_{50} values higher than fluconazole (**19a**, **21a**, **21d**, **23d**), three had MIC_{50} values in a similar range of concentrations of fluconazole (50–100 μM) (**19b**, **19d**, **21b**) and six had lower MIC_{50} values than fluconazole (**19c**, **19e**, **20e**, **21c**, **21e**, **23c**). Compound **22a** was not active in the range of concentrations studied (≤800 μM), but interestingly the complex had antifungal activity in the range of 400–800 μM. From these results it can be concluded that the pyridine compounds (**19a**, **21a** and **22a**) are not very active as compared to fluconazole. Both quinoline compounds (**19b** and **21b**) had an antifungal activity similar to that of fluconazole. The target compounds with the hydroxyquinoline copper(II)-binding function (**19c**, **21c** and **23c**) had higher activities than fluconazole, and among them, the target compound from the first family had the lowest MIC_{50}. From the target compounds with the methoxyphenol copper(II)-binding group, two had a lower activity than fluconazole (**21d** and **23d**) and the compound from the first family (**19d**) had a similar MIC_{50} to fluconazole. All the compounds with the bromophenol copper(II)-binding group studied (**19e**, **20e** and **21e**) had higher antifungal activities compared to fluconazole, and the target compound from the first family with the dichlorobenzyl group was the more active compound, with a MIC_{50} value of 3.125–6.25 μM. The target compound with difluorobenzyl (**20e**) has a higher MIC_{50} value than the similar target compound dichlorobenzyl (**19e**) as observed in the literature.[58–60] These comparisons indicate that the copper(II)-binding group has an effect on the antifungal activity, since even in the absence of copper(II) the hydroxyquinoline- and bromophenol-containing compounds have lower MIC_{50} values than the rest of the compounds. There is a slight tendency for the MIC_{50} values to increase from the first to the third family, which means that the imidazole and propylene chain could be advantageous for antifungal activity against *Candida glabrata*. The higher activity of imidazole-containing compounds and of the dichlorobenzyl over difluorobenzyl compounds has to be further studied since these are two groups known for higher toxicity in human cells, so to confirm any of the target compounds as lead compounds, toxicity studies must be done.

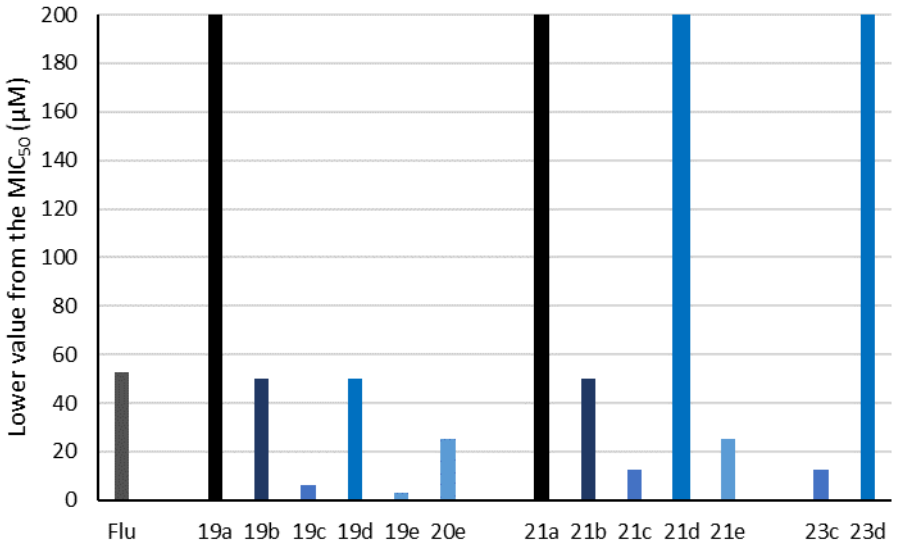

Figure 3.13 – Graphical representation of the lower concentration value from the MIC_{50} interval of each target compound determined for *Candida glabrata* at 48 h in RPMI at 37 °C in the absence of copper(II). Each color represents the copper(II)-binding function (black – pyridine, dark blue – quinoline, navy blue – hydroxyquinoline, turquoise – methoxyphenol, and light blue – bromophenol).

Comparing the results from the MIC_{50} determined at 48 h in the absence and presence of copper(II) (**Figure 3.14**), compounds can be divided into two groups: those for which the presence of copper does not impact the MIC_{50} value and those for which copper decreases this value. The first group includes compounds **19c**, **21a**, **21c**, **21e** and **23c**. There seems to be a tendency for the target compounds containing hydroxyquinoline to maintain their antifungal activity regardless of the presence of the metal.

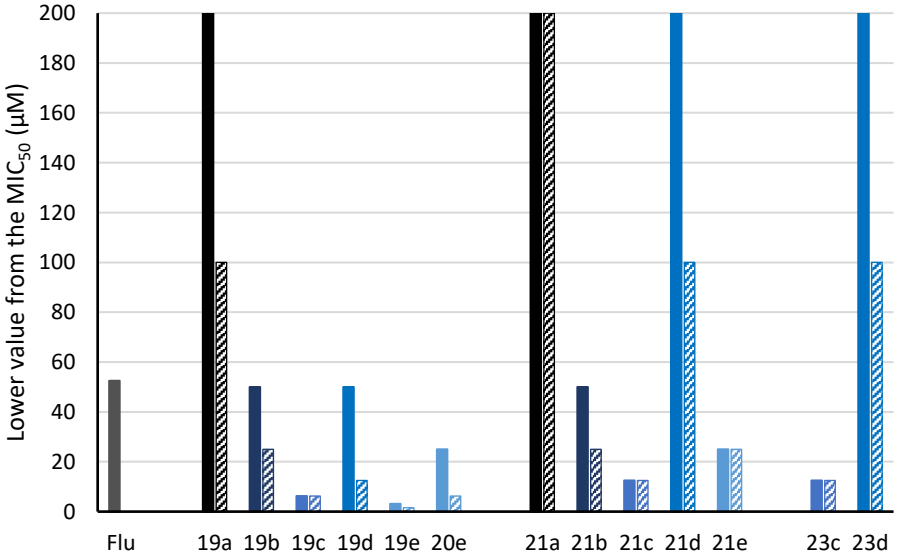

Figure 3.14 – Graphical representation of the lower value from the interval of concentrations of the MIC_{50} for each target compound, determined for *Candida glabrata* at 48 h in RPMI at 37 °C, in the absence (solid) and presence (striped) of copper(II). Each color represents the copper(II)-binding function (black – pyridine, dark blue – quinoline, navy blue – hydroxyquinoline, turquoise – methoxyphenol, and light blue – bromophenol).

We next tested whether the target compounds were able to inhibit the Erg11 enzyme and, consequently, ergosterol biosynthesis. For that, *C. glabrata* was grown for an overnight period in the presence of each target compound at the highest concentration of its MIC_{50} interval at 24 h, always in the absence of copper(II). Cells left untreated (control) or treated with the target compounds or fluconazole were harvested, disrupted and ergosterol was extracted with methanol and quantified by HPLC (**Figure 3.15**). To compare the results between assays performed on different days, all ergosterol levels were plotted as a ratio of the ergosterol amount after incubation with the target compound over the ergosterol amount under control conditions. In order to obtain quantitative data, assays with the most interesting compounds would need to be repeated using quintuplicate (n = 5) samples in the same experiment. Nevertheless, as described below, this assay proved to be useful as a pre-screening to identify promising target compounds whose activity mechanism involves Erg11 inhibition.

For the first family, compounds **19a**, **19b**, and **19c** do not inhibit the synthesis of ergosterol, whereas **19d**, **19e**, and **20e** appear to do so, although not as much as fluconazole. Among these last target compounds, those with the bromophenol copper(II)-binding function appear to have a more pronounced effect than with methoxyphenol (**19d**). In the second family of target compounds only **21a** does not inhibit the ergosterol synthesis. Target compounds **21b** and **21c** show signs of similar and lower inhibition of Erg11, respectively, when compared to fluconazole, whilst **21d** and **21e** seem to strongly inhibit Erg11. For the third family of target compounds, only **23c** and **23d** were studied; **23c** did not affect ergosterol levels, but **23d** should decrease ergosterol biosynthesis. These results suggest that compounds containing methoxyphenol and bromophenol are more active in inhibiting Erg11, possibly due to the presence of heteroatoms in these groups that may allow the formation of additional weak interactions between the compounds and the active site of Erg11 and thus increase binding to Erg11.

It also seems that target compounds of the second family are more efficient in depleting ergosterol than those of the first family, for all copper(II)-binding functions except pyridine, which may be related to the substitution of the imidazole for a triazole that has an extra heteroatom for potential weak binding at the active site of Erg11. Although only two compounds from the third family were tested, our preliminary results suggest that members of this family are more effective in reducing ergosterol levels than those of the first family, but less effective than those of the second family. This could mean that the propylene chain between the tertiary amine and the azole group of the second family could be beneficial over

the ethylene chain of the third family for the binding of the target compounds at the active site of Erg11.

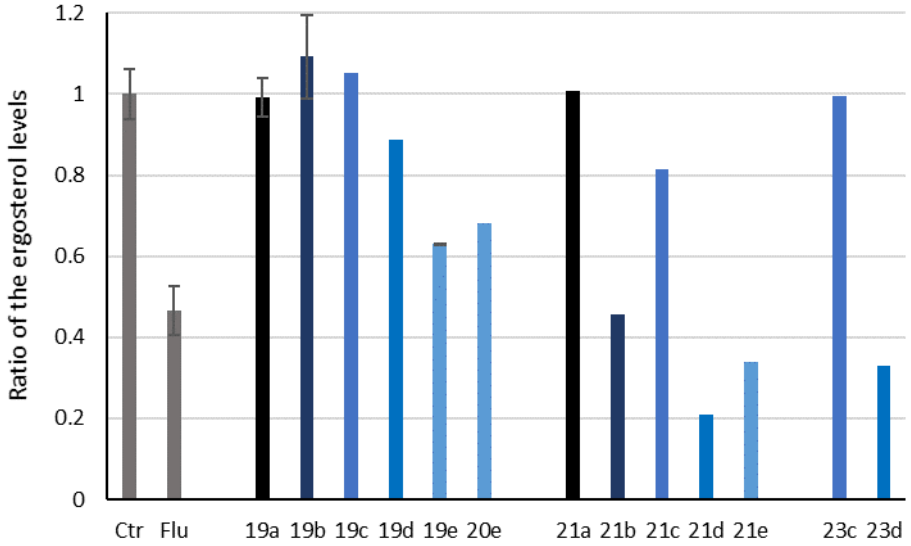

Figure 3.15 – Intracellular ergosterol levels in *Candida glabrata* after overnight incubation with the target compounds at the highest concentration of their MIC_{50} at 24 h. Ctr – Control (non-treated cells), Flu – Fluconazole.

3.4 Structure-activity relationship discussion

To get a deeper insight about the possible mechanisms of the antifungal effect found for the compounds with regard to their structures, it is useful to consider all the discussed experimental results as a whole. From the three families of azole compounds synthesized, the first family based on the 1-(3-aminopropyl)imidazole scaffold tends to have the lowest MIC_{50} values, followed by the second family based on the 1-(3-aminopropyl)-1,2,4-triazole scaffold, and finally the third family based on the 1-(2-aminoethyl)-1,2,4-triazole scaffold, which suggests that the imidazole group and the propylene chain are advantageous for antifungal activity. Nevertheless, the first family appears to have the lowest levels of ergosterol inhibition and pCu values, which indicates that the higher antifungal activity cannot be explained by the inhibition of Erg11. The second family has higher or similar MIC_{50} values compared with the first family and shows the highest inhibition of Erg11, suggesting that replacing the imidazole with triazole compromises the MIC_{50} values but could increase the specificity of the drug towards the targeted enzyme, thus decreasing potential side effects.

Of all copper(II)-binding functions, the hydroxyquinoline- and bromophenol-containing compounds have the lowest MIC_{50} values in the absence of copper(II). Since the ergosterol biosynthesis in the hydroxyquinoline-containing compounds does not seem to be inhibited by the compounds of the first and third families, and it is only slightly inhibited by members of the second family, it is possible that the antifungal activity from these target compounds arises mainly from their chelating function, which may affect metal homeostasis. In order to confirm this hypothesis, the intracellular copper levels after inoculation would need to be measured by ICP-AES. On the contrary, the bromophenol-containing compounds seem to strongly inhibit ergosterol synthesis, indicating that the activity mechanism of the compounds depends on the copper(II)-binding functions present. Interestingly, while pyridine-containing compounds were ineffective against *Candida glabrata* or have high MIC_{50} values that did not correlate with Erg11 inhibition, quinoline-containing compounds have MIC_{50} values similar to that of fluconazole and one of them showed to promote inhibition of Erg11. The difference in antifungal activities between these copper(II)-binding groups is possibly related to the additional aromatic ring of the quinoline function that adds lipophilicity to the target compound, thus being beneficial for the drug permeation into the fungal cells and/or promoting stabilizing interactions within the active site of Erg11 like van der Waals or π interactions.

One of the goals of this work was to correlate the biological activity of the target compounds with their copper(II) binding ability, in order to understand how strong the copper(II) binding should be to benefit the antifungal activity. In most cases, the MIC_{50} value in the presence of copper(II) is lower than the value in its absence, which means that the metal may potentially have a synergistic effect with such compounds, especially for **19d** and **20e** that are methoxyphenol- and bromophenol-containing compounds, respectively. These two copper(II)-binding functions are not associated with high pCu values, which implies that such compounds have a weaker copper(II) binding ability than the others. On the contrary, hydroxyquinoline-containing compounds do not show a decrease in MIC_{50} values in the presence of copper(II), despite the copper(II)-binding function being associated with higher pCu values, which suggest that compounds with a lower binding ability towards copper(II) could have higher synergistic effects with the metal.

The structure of the second family of target compounds seems to be the best candidate for the synthesis of new antifungal drugs, together with copper(II)-binding functions containing heteroatoms capable of establishing a higher number of weak interactions within the Erg11 active site.

From the 15 target compounds synthesized, there are a few that display properties worth highlighting. Compound **19e** has the lowest MIC_{50} values at 48 h both in the absence and in presence of copper(II) (**Table 3.3**), and compound **21d** showed the highest Erg11 inhibition ability (**Figure 3.15**). Compound **21e** seems to be particularly promising because, although it does not have a MIC_{50} value as low as **19e** (**Table 3.3**), it showed a strong inhibition of the ergosterol biosynthesis (**Figure 3.15**) and so the higher concentration of drug required when compared to **19e** might not be more toxic since it has higher target specificity. Compounds **19e**, **20e**, and **21b** all have MIC_{50} values in the absence of copper(II) that are similar or lower than fluconazole and that decrease in the presence of copper(II) (**Table 3.3**), showing that the metal is enhancing the activity of these compounds in a synergistic way. These compounds also seem to inhibit the ergosterol biosynthesis (**Figure 3.15**), suggesting that in the presence of copper(II) there are two different activity mechanisms occurring simultaneously, and such dual activity may be useful to overcome fungal resistance.

4. Conclusion and outlook

In this work, we have designed novel compounds based on a central tertiary amine substituted with the main pharmacophore functions of the antifungal drug fluconazole – the azole and dihalogenophenyl functions – and additionally containing a copper(II)-binding function to explore a potential synergy between the activity of azole compounds and copper(II) binding. A total of 15 target compounds were synthesized divided into three structural families, which differ in the azole used and the length of the alkyl chain linking the central amine to the azole. Within each structural family, a range of five different copper(II)-binding functions were employed to vary the copper(II)-binding ability of the target compounds.

The study of the interaction of the compounds with copper(II) revealed that complexes are formed for all compounds with variable stoichiometry depending on the particular compound structure and mainly on the copper(II)-binding function contained, so the pCu parameter was calculated and used for a direct comparison. The pCu values show that the strongest binding ability is obtained with the compounds containing the hydroxyquinoline function. The compounds containing pyridine and quinoline functions have an intermediate binding ability for copper(II), while the compounds containing phenol functions have the lowest binding ability. The pCu values also evidence that the binding ability increases from the first to the second structural family, and also from the second to the third family.

The susceptibility of *Candida glabrata* to the synthesized compounds was studied in the absence and presence of copper(II), with the exception of **23e** that was not soluble enough and thus could not be studied. Comparing the MIC_{50} values in the absence of copper(II) with those of fluconazole, it was found that four of the compounds have higher values than fluconazole, three had similar values, six had lower values, and one did not show a MIC_{50} value in the range of concentrations tested. The target compounds with lower MIC_{50} values are the ones containing the hydroxyquinoline and bromophenol copper(II)-binding functions. There is a slight tendency for the MIC_{50} values to increase from the first to the third family, which means that the imidazole group could be more active than triazole against *Candida glabrata*, but since it is known to have higher toxicity than triazole against human cells, it actually may not be advantageous overall. The compound containing a difluorobenzyl function has a higher MIC_{50} value than the similar compound containing dichlorobenzyl, but the latter is also known for higher toxicity against human cells so it may not be the most suitable option. Both of these points would need to be examined further through toxicity studies. In the presence of

copper(II) there is a decrease of MIC_{50} values for most of the target compounds, suggesting a synergistic effect between the organic compounds and the metal. In particular, compounds **19d** and **20e**, respectively containing methoxyphenol or bromophenol functions, showed the highest difference in MIC_{50} values in the absence and presence of copper(II). In contrast, hydroxyquinoline-containing compounds did not show any decrease in MIC_{50} values.

To ascertain if the target compounds displaying antifungal activity do really inhibit the ergosterol biosynthesis, the levels of this sterol were measured by HPLC in *Candida glabrata* after induction with each of these compounds and compared with non-treated and fluconazole-treated cells. It was possible to observe a higher tendency of inhibition by the compounds containing the methoxyphenol and bromophenol functions, maybe due to the heteroatoms present in these groups potentially enhancing the binding of such compounds in the active site of Erg11. The compounds of the second family containing quinoline and hydroxyquinoline functions also appear to inhibit the ergosterol biosynthesis. Overall, the structure of the second family, which is based on the 1-(3-aminopropyl)-1,2,4-triazole scaffold, appears to be the most effective for achieving Erg11 inhibition.

To summarize the structure-activity relationships, it seems that the first family of compounds has lower MIC_{50} values, the second family has higher inhibition of the ergosterol biosynthesis, and the third family has a higher ability to bind copper(II). Based on this, the structure of the second family of compounds seems to be the strongest candidate for developing new antifungal drugs; although it does not show the lowest MIC_{50} values it has higher specificity to the target, which could decrease side effects. The hydroxyquinoline- and bromophenol-containing compounds are the ones that show the highest antifungal activities, possibly having different activity mechanisms on the basis of their activity. In the first case it could be related with the disruption of the cellular copper homeostasis, and in the second case with the higher levels of Erg11 inhibition. The copper(II)-binding functions that seem to show a synergistic effect with the metal are also the ones with lower pCu values (methoxyphenol and bromophenol), which could indicate that a weaker binding ability to copper is beneficial. One of the most promising compounds belongs to the second family and contains the bromophenol function (**21e**), and even if it does not have the lowest MIC_{50} value, it seems to significantly inhibit the ergosterol biosynthesis. Compounds **19e**, **20e,** and **21b** have lower MIC_{50} values in the presence of copper(II) than in its absence, and also inhibit the ergosterol biosynthesis, displaying a dual activity that could potentially be useful to overcome fungal resistance.

Finally, additional studies need to be performed to fully disclose the activity mechanisms of the target compounds. These may include determining the levels of intracellular copper by ICP-AES, before and after treatment with the compounds to find if they are acting as copper(II) shuttles or ionophores, and measuring the levels of ROS to check if the antifungal activity arises from copper toxicity. Finally, the toxicity towards human cells of the most promising compounds must be evaluated before any of them can be selected as a lead compound for further development.

5. Bibliography

(1) Perfect, J. R. The Antifungal Pipeline: A Reality Check. *Nat. Rev. Drug Discov.* **2017**, *16* (9), 603–616. https://doi.org/10.1038/nrd.2017.46.

(2) Stop Neglecting Fungi. *Nat. Microbiol.* **2017**, *2* (8), 17120. https://doi.org/10.1038/nmicrobiol.2017.120.

(3) Hajdu, S.; Obradovic, A.; Presterl, E.; Vécsei, V. Invasive Mycoses Following Trauma. *Injury* **2009**, *40* (5), 548–554. https://doi.org/10.1016/j.injury.2008.03.034.

(4) Rodrigues, J.; Caruthers, C.; Azmeh, R.; Dykewicz, M. S.; Slavin, R. G.; Knutsen, A. P. The Spectrum of Allergic Fungal Diseases of the Upper and Lower Airways. *Expert Rev. Clin. Immunol.* **2016**. https://doi.org/10.1586/1744666X.2016.1142874.

(5) Moyes, D. L.; Naglik, J. R.; Riera, C. M. Mucosal Immunity and Candida Albicans Infection. *Clin. Dev. Immunol.* **2011**. https://doi.org/10.1155/2011/346307.

(6) Hope, W.; Natarajan, P.; Goodwin, L. Invasive Fungal Infections. *Clin. Med. (Northfield. Il).* **2013**, *13* (5), 507–517. https://doi.org/https://doi.org/10.7861/clinmedicine.13-5-507.

(7) Pfaller, M. A.; Diekema, D. J. Epidemiology of Invasive Candidiasis: A Persistent Public Health Problem. *Clin. Microbiol. Rev.* **2007**, *20* (1), 133–163. https://doi.org/10.1128/CMR.00029-06.

(8) Lamoth, F.; Lockhart, S. R.; Berkow, E. L.; Calandra, T. Changes in the Epidemiological Landscape of Invasive Candidiasis. *J. Antimicrob. Chemother.* **2018**, *73* (1), i4–i13. https://doi.org/10.1093/jac/dkx444.

(9) McCarty, T. P.; Pappas, P. G. Invasive Candidiasis. *Infect. Dis. Clin. North Am.* **2016**, *30* (1), 103–124. https://doi.org/10.1016/j.idc.2015.10.013.

(10) Park, B. J.; Wannemuehler, K. A.; Marston, B. J.; Govender, N.; Pappas, P. G.; Chiller, T. M. Estimation of the Current Global Burden of Cryptococcal Meningitis among Persons Living with HIV/AIDS. *AIDS* **2009**, *23* (4), 525–530. https://doi.org/10.1097/QAD.0b013e328322ffac.

(11) Denning, D. W.; Bromley, M. J. How to Bolster the Antifungal Pipeline: Few Drugs Are Coming to Market, but Opportunities for Drug Development Exist. *Science* **2015**, *347* (6229), 1414–1416. https://doi.org/10.1126/science.aaa6097.

(12) Howard, K. C.; Dennis, E. K.; Watt, D. S.; Garneau-Tsodikova, S. A Comprehensive Overview of the Medicinal Chemistry of Antifungal Drugs: Perspectives and Promise. *Chem. Soc. Rev.* **2020**, *49* (8), 2426–2480. https://doi.org/10.1039/c9cs00556k.

(13) Chandrasekar, P. H.; Sobel, J. D. Micafungin: A New Echinocandin. *Clin. Infect. Dis.* **2006**, *42* (8), 1171–1178. https://doi.org/10.1086/501020.

(14) Shukla, P. K.; Singh, P.; Yadav, R. K.; Pandey, S.; Bhunia, S. S. Past, Present, and Future of Antifungal Drug Development. *Top. Med. Chem.* **2018**, *29*, 125–167. https://doi.org/10.1007/7355_2016_4.

(15) Vermes, A.; Guchelaar, H. J.; Dankert, J. Flucytosine: A Review of Its Pharmacology, Clinical Indications, Pharmacokinetics, Toxicity and Drug Interactions. *J. Antimicrob. Chemother.* **2000**, *46* (2), 171–179. https://doi.org/10.1093/jac/46.2.171.

(16) Campoy, S.; Adrio, J. L. Antifungals. *Biochem. Pharmacol.* **2017**, *133*, 86–96. https://doi.org/10.1016/j.bcp.2016.11.019.

(17) Bowman, S. M.; Free, S. J. The Structure and Synthesis of the Fungal Cell Wall. *BioEssays* **2006**, *28* (8), 799–808. https://doi.org/10.1002/bies.20441.

(18) Joffrion, T. M.; Cushion, M. T. Sterol Biosynthesis and Sterol Uptake in the Fungal Pathogen Pneumocystis Carinii. *FEMS Microbiol. Lett.* **2010**, *311* (1), 1–9. https://doi.org/10.1111/j.1574-6968.2010.02007.x.

(19) Hildenbrand, M. F.; Bayerl, T. M. Differences in the Modulation of Collective Membrane Motions by Ergosterol, Lanosterol, and Cholesterol: A Dynamic Light Scattering Study. *Biophys. J.* **2005**, *88* (5), 3360–3367. https://doi.org/10.1529/biophysj.104.050112.
(20) Aggarwal, R.; Sumran, G. An Insight on Medicinal Attributes of 1,2,4-Triazoles. *Eur. J. Med. Chem.* **2020**, *205*, 112652. https://doi.org/10.1016/j.ejmech.2020.112652.
(21) Gonzalez, F. J.; Gelboin, H. V. Human Cytochromes P450: Evolution and CDNA-Directed Expression. *Environ. Health Perspect.* **1992**, *98*, 81–85. https://doi.org/10.1289/ehp.929881.
(22) P.B. Danielson, B. S. P. The Cytochrome P450 Superfamily: Biochemistry, Evolution and Drug Metabolism in Humans. *Curr. Drug Metab.* **2005**, *3* (6), 561–597. https://doi.org/10.2174/1389200023337054.
(23) Lepesheva, G. I.; Waterman, M. R. Sterol 14α-Demethylase Cytochrome P450 (CYP51), a P450 in All Biological Kingdoms. *Biochim. Biophys. Acta, Gen. Subj.* **2007**, *1770* (3), 467–477. https://doi.org/10.1016/j.bbagen.2006.07.018.
(24) Sagatova, A. A.; Keniya, M. V.; Wilson, R. K.; Monk, B. C.; Tyndall, J. D. A. Structural Insights into Binding of the Antifungal Drug Fluconazole to Saccharomyces Cerevisiae Lanosterol 14α-Demethylase. *Antimicrob. Agents Chemother.* **2015**, *59* (8), 4982–4989. https://doi.org/10.1128/AAC.00925-15.
(25) Pore, V. S.; Agalave, S. G.; Singh, P.; Shukla, P. K.; Kumar, V.; Siddiqi, M. I. Design and Synthesis of New Fluconazole Analogues. *Org. Biomol. Chem.* **2015**, *13* (23), 6551–6561. https://doi.org/10.1039/c5ob00590f.
(26) Berger, S.; Chazli, Y. El; Babu, A. F.; Coste, A. T. Azole Resistance in Aspergillus Fumigatus: A Consequence of Antifungal Use in Agriculture? *Front. Microbiol.* **2017**, *8* (JUN). https://doi.org/10.3389/fmicb.2017.01024.
(27) Sagatova, A. A.; Keniya, M. V.; Wilson, R. K.; Sabherwal, M.; Tyndall, J. D. A.; Monk, B. C. Triazole Resistance Mediated by Mutations of a Conserved Active Site Tyrosine in Fungal Lanosterol 14α-Demethylase. *Sci. Rep.* **2016**, *6*. https://doi.org/10.1038/srep26213.
(28) Flowers, S. A.; Colón, B.; Whaley, S. G.; Schuler, M. A.; David Rogers, P. Contribution of Clinically Derived Mutations in ERG11 to Azole Resistance in Candida Albicans. *Antimicrob. Agents Chemother.* **2015**, *59* (1), 450–460. https://doi.org/10.1128/AAC.03470-14.
(29) Price, C. L.; Parker, J. E.; Warrilow, A. G.; Kelly, D. E.; Kelly, S. L. Azole Fungicides - Understanding Resistance Mechanisms in Agricultural Fungal Pathogens. *Pest Manag. Sci.* **2015**, *71* (8), 1054–1058. https://doi.org/10.1002/ps.4029.
(30) Sanglard, D.; Ischer, F.; Monod, M.; Bille, J. Cloning of Candida Albicans Genes Conferring Resistance to Azole Antifungal Agents: Characterization of CDR2, a New Multidrug ABC Transporter Gene. *Microbiology* **1997**, *143* (2), 405–416. https://doi.org/10.1099/00221287-143-2-405.
(31) Hennigar, S. R.; McClung, J. P. Nutritional Immunity: Starving Pathogens of Trace Minerals. *Am. J. Lifestyle Med.* **2016**, *10* (3), 170. https://doi.org/10.1177/1559827616629117.
(32) García-Santamarina, S.; Thiele, D. J. Copper at the Fungal Pathogen-Host Axis. *J. Biol. Chem.* **2015**, *290* (31), 18945–18953. https://doi.org/10.1074/jbc.R115.649129.
(33) Morton, V.; Staub, T. A Short History of Fungicides. *APSnet Feature Articles.* **2008**. https://doi.org/10.1094/apsnetfeature-2008-0308.
(34) Pearson, R. G. The HSAB Principle - More Quantitative Aspects. *Inorg. Chim. Acta* **1995**, *240*, 93–98. https://doi.org/https://doi.org/10.1016/0020-1693(95)04648-8.
(35) Pearson, R. G.; Busch, D. H. Hard and Soft Acids and Bases. *J. Am. Chem. Soc.* **1963**, *85* (22), 3533–3539. https://doi.org/https://doi.org/10.1021/ja00905a001.

(36) Nicholls, D. *Complexes and First-Row Transition Elements*; Macmillan Education UK: Palgrave, London, **1974**. https://doi.org/10.1007/978-1-349-02335-6.
(37) Liu, S. Bifunctional Coupling Agents for Radiolabeling of Biomolecules and Target-Specific Delivery of Metallic Radionuclides. *Adv. Drug Deliv. Rev.* **2008**, *60*, 1347–1370. https://doi.org/10.1016/j.addr.2008.04.006.
(38) Wadas, T. J.; Wong, E. H.; Weisman, G. R.; Anderson, C. J. Copper Chelation Chemistry and Its Role in Copper Radiopharmaceuticals. *Curr. Pharm. Des.* **2007**, *13*, 3–16. https://doi.org/10.2174/138161207779313768.
(39) Martell, A. E.; Hancock, R. D.; Motekaitis, R. J. Factors Affecting Stabilities of Chelate, Macrocyclic and Macrobicyclic Complexes in Solution. *Coord. Chem. Rev.* **1994**, *133*, 39–65. https://doi.org/https://doi.org/10.1016/0010-8545(94)80056-1.
(40) Chung, C.-S. Entropy Effects in Chelation Reactions. *J. Chem. Educ.* **1984**, *61* (12), 1062–1064. https://doi.org/https://doi.org/10.1021/ed061p1062.
(41) Rie Vallet, V.; Wahlgren, U.; Grenthe, I. Chelate Effect and Thermodynamics of Metal Complex Formation in Solution: A Quantum Chemical Study. *J. Am. Chem. Soc.* **2003**, *125* (48), 14941–14950. https://doi.org/10.1021/ja036646j.
(42) Oliveri, V. Biomedical Applications of Copper Ionophores. *Coord. Chem. Rev.* **2020**, *422*. https://doi.org/10.1016/j.ccr.2020.213474.
(43) Helsel, M. E.; Franz, K. J. Pharmacological Activity of Metal Binding Agents That Alter Copper Bioavailability. *Dalton Trans.* **2015**, *44* (19), 8770. https://doi.org/10.1039/c5dt00634a.
(44) Valko, M.; Morris, H.; Cronin, M. T. D. Metals, Toxicity and Oxidative Stress. *Curr. Med. Chem.* **2005**, *12* (10), 1161–1208. https://doi.org/https://doi.org/10.2174/0929867053764635.
(45) Brancaccio, D.; Gallo, A.; Piccioli, M.; Novellino, E.; Ciofi-Baffoni, S.; Banci, L. [4Fe-4S] Cluster Assembly in Mitochondria and Its Impairment by Copper. *J. Am. Chem. Soc.* **2017**, *139* (2), 719–730. https://doi.org/10.1021/jacs.6b09567.
(46) Macomber, L.; Imlay, J. A. The Iron-Sulfur Clusters of Dehydratases Are Primary Intracellular Targets of Copper Toxicity. *Proc. Natl. Acad. Sci. U.S.A.* **2009**, *106* (20), 8344–8349. https://doi.org/10.1073/pnas.0812808106.
(47) Yuan, S.; Chen, S.; Xi, Z.; Liu, Y. Copper-Finger Protein of Sp1: The Molecular Basis of Copper Sensing. *Metallomics* **2017**, *9* (8), 1169–1175. https://doi.org/10.1039/c7mt00184c.
(48) Predki, P. F.; Sarkar, B. Metal Replacement in "zinc Finger" and Its Effect on DNA Binding. *Environ. Health Perspect.* **1994**, *102* (3), 195–198. https://doi.org/10.1289/ehp.94102s3195.
(49) Tidow, H.; Andreeva, A.; Rutherford, T. J.; Fersht, A. R. Solution Structure of the U11-48K CHHC Zinc-Finger Domain That Specifically Binds the 5′ Splice Site of U12-Type Introns. *Structure* **2009**, *17* (2), 294–302. https://doi.org/10.1016/j.str.2008.11.013.
(50) Ząbek, A.; Nagaj, J.; Grabowiecka, A.; Dworniczek, E.; Nawrot, U.; Młynarz, P.; Jezowska-Bojczuk, M. Activity of Fluconazole and Its Cu(II) Complex towards Candida Species. *Med. Chem. Res.* **2015**, *24* (5), 2005–2010. https://doi.org/10.1007/s00044-014-1275-7.
(51) Hunsaker, E. W.; Franz, K. J. Copper Potentiates Azole Antifungal Activity in a Way That Does Not Involve Complex Formation. *Dalton Trans.* **2019**, *48* (26), 9654–9662. https://doi.org/10.1039/c9dt00642g.
(52) Hunsaker, E. W.; Franz, K. J. Emerging Opportunities To Manipulate Metal Trafficking for Therapeutic Benefit. *Inorg. Chem.* **2019**, *58* (20), 13528–13545. https://doi.org/10.1021/ACS.INORGCHEM.9B01029.
(53) Prachayasittikul, V.; Prachayasittikul, S.; Ruchirawat, S.; Prachayasittikul, V. 8-Hydroxyquinolines: A Review of Their Metal Chelating Properties and Medicinal Applications. *Drug Des. Devel. Ther.* **2013**, *7*, 1157–1178. https://doi.org/10.2147/DDDT.S49763.

(54) Hunsaker, E. W.; McAuliffe, K. J.; Franz, K. J. Fluconazole Analogues with Metal-Binding Motifs Impact Metal-Dependent Processes and Demonstrate Antifungal Activity in Candida Albicans. *J. Biol. Inorg. Chem.* **2020**, *25* (5), 729–745. https://doi.org/10.1007/s00775-020-01796-x.

(55) Gaspar-Cordeiro, A.; da Silva, S.; Aguiar, M.; Rodrigues-Pousada, C.; Haas, H.; Lima, L. M. P.; Pimentel, C. A Copper(II)-Binding Triazole Derivative with Ionophore Properties Is Active against Candida Spp. *J. Biol. Inorg. Chem.* **2020**, *25* (8), 1117–1128. https://doi.org/10.1007/s00775-020-01828-6.

(56) Gaspar-Cordeiro, A.; Amaral, C.; Pobre, V.; Antunes, W.; Petronilho, A.; Paixão, P.; Matos, A. P.; Pimentel, C. Copper Acts Synergistically with Fluconazole in Candida Glabrata by Compromising Drug Efflux, Sterol Metabolism, and Zinc Homeostasis. *bioRxiv* **2021**, 2021.12.22.473865. https://doi.org/10.1101/2021.12.22.473865.

(57) Nam, N. H.; Sardari, S.; Selecky, M.; Parang, K. Carboxylic Acid and Phosphate Ester Derivatives of Fluconazole: Synthesis and Antifungal Activities. *Bioorganic Med. Chem.* **2004**, *12* (23), 6255–6269. https://doi.org/10.1016/j.bmc.2004.08.049.

(58) Sadeghpour, H.; Khabnadideh, S.; Zomorodian, K.; Pakshir, K.; Hoseinpour, K.; Javid, N.; Faghih-Mirzaei, E.; Rezaei, Z. Design, Synthesis, & Biological Activity of New Triazole & Nitro-Triazole Derivatives as Antifungal Agents. *Molecules* **2017**, *22* (7), 1150. https://doi.org/10.3390/molecules22071150.

(59) Hashemi, S. M.; Badali, H.; Faramarzi, M. A.; Samadi, N.; Afsarian, M. H.; Irannejad, H.; Emami, S. Novel Triazole Alcohol Antifungals Derived from Fluconazole: Design, Synthesis, and Biological Activity. *Mol. Divers.* **2014**, *19* (1), 15–27. https://doi.org/10.1007/s11030-014-9548-0.

(60) Lebouvier, N.; Pagniez, F.; Duflos, M.; Le Pape, P.; Na, Y. M.; Le Baut, G.; Le Borgne, M. Synthesis and Antifungal Activities of New Fluconazole Analogues with Azaheterocycle Moiety. *Bioorganic Med. Chem. Lett.* **2007**, *17* (13), 3686–3689. https://doi.org/10.1016/j.bmcl.2007.04.038.

(61) Warrilow, A. G. S.; Hull, C. M.; Parker, J. E.; Garvey, E. P.; Hoekstra, W. J.; Moore, W. R.; Schotzinger, R. J.; Kelly, D. E.; Kellya, S. L. The Clinical Candidate VT-1161 Is a Highly Potent Inhibitor of Candida Albicans CYP51 but Fails to Bind the Human Enzyme. *Antimicrob. Agents Chemother.* **2014**, *58* (12), 7121–7127. https://doi.org/10.1128/AAC.03707-14.

(62) Benhamou, R. I.; Bibi, M.; Steinbuch, K. B.; Engel, H.; Levin, M.; Roichman, Y.; Berman, J.; Fridman, M. Real-Time Imaging of the Azole Class of Antifungal Drugs in Live Candida Cells. *ACS Chem. Biol.* **2017**, *12* (7), 1769–1777. https://doi.org/10.1021/acschembio.7b00339.

(63) Benhamou, R. I.; Bibi, M.; Berman, J.; Fridman, M. Localizing Antifungal Drugs to the Correct Organelle Can Markedly Enhance Their Efficacy. *Angew. Chem. Int. Ed.* **2018**, *57* (21), 6230–6235. https://doi.org/10.1002/anie.201802509.

(64) Benhamou, R. I.; Jaber, Q. Z.; Herzog, I. M.; Roichman, Y.; Fridman, M. Fluorescent Tracking of the Endoplasmic Reticulum in Live Pathogenic Fungal Cells. *ACS Chem. Biol.* **2018**, *13* (12), 3325–3332. https://doi.org/10.1021/acschembio.8b00782.

(65) Lin, Y.; Betts, H.; Keller, S.; Cariou, K.; Gasser, G. Recent Developments of Metal-Based Compounds against Fungal Pathogens. *Chem. Soc. Rev.* **2021**, *50* (18), 10346–10402. https://doi.org/10.1039/d0cs00945h.

(66) Zhang, L.; Ling, Y.; Du, M. Synthesis, Crystal Structures and in Vitro Anti-Fungal Activities of Two Silver(I) Coordination Polymers with Fluconazole. *Inorg. Chim. Acta* **2007**, *360* (10), 3182–3188. https://doi.org/10.1016/j.ica.2007.03.033.

(67) Martínez, A.; Carreon, T.; Iniguez, E.; Anzellotti, A.; Sánchez, A.; Tyan, M.; Sattler, A.; Herrera, L.; Maldonado, R. A.; Sánchez-Delgado, R. A. Searching for New Chemotherapies for Tropical Diseases: Ruthenium-Clotrimazole Complexes Display High in Vitro Activity against Leishmania Major and Trypanosoma Cruzi and Low Toxicity toward Normal Mammalian Cells. *J. Med. Chem.* **2012**, *55* (8), 3867–3877. https://doi.org/10.1021/jm300070h.

(68) Kljun, J.; Scott, A. J.; Lanišnik Rižner, T.; Keiser, J.; Turel, I. Synthesis and Biological Evaluation of Organoruthenium Complexes with Azole Antifungal Agents. First Crystal Structure of a Tioconazole Metal Complex. *Organometallics* **2014**, *33* (7), 1594–1601. https://doi.org/10.1021/om401096y.

(69) Gagini, T.; Colina-Vegas, L.; Villarreal, W.; Borba-Santos, L. P.; De Souza Pereira, C.; Batista, A. A.; Kneip Fleury, M.; De Souza, W.; Rozental, S.; Costa, L. A. S.; et al. Metal-Azole Fungistatic Drug Complexes as Anti-Sporothrix Spp. Agents. *New J. Chem.* **2018**, *42* (16), 13641–13650. https://doi.org/10.1039/c8nj01544a.

(70) Rafique, S.; Idrees, M.; Nasim, A.; Akbar, H.; Athar, A. Transition Metal Complexes as Potential Therapeutic Agents. *Biotechnol. Mol. Biol. Rev.* **2010**, *5* (2), 38–45. https://doi.org/https://doi.org/10.5897/BMBR2010.0003.

(71) Vinay Kumar, B.; Bhojya Naik, H. S.; Girija, D.; Sharath, N.; Pradeepa, S. M.; Joy Hoskeri, H.; Prabhakara, M. C. Synthesis, DNA-Binding, DNA-Photonuclease Profiling and Antimicrobial Activity of Novel Tetra-Aza Macrocyclic Ni(II), Co(II) and Cu(II) Complexes Constrained by Thiadiazole. *Spectrochim. Acta Part A Mol. Biomol. Spectrosc.* **2012**, *94*, 192–199. https://doi.org/10.1016/j.saa.2012.03.071.

(72) Haddad, R.; Yousif, E.; Ahmed, A. Synthesis and Characterization of Transition Metal Complexes of 4-Amino-5-Pyridyl-4H-1,2,4-Triazole-3-Thiol. *SpringerPlus* **2013**, *2* (1), 1–6. https://doi.org/10.1186/2193-1801-2-510.

(73) Hussain Sumrra, S.; Imran, M.; Ibrahim, M.; Ambreen, S.; Mehmood, R.; Assiri, M. A.; Irfan, A.; Hussain Sumrra, S.; Imran, M.; Ibrahim, M.; et al. In-Vitro Antimicrobial Screening and Coordination Behavior of Metals Based Bidentate Compounds. *J. Chil. Chem. Soc.* **2021**, *66* (1), 5057–5062. https://doi.org/10.4067/S0717-97072021000105057.

(74) Sumrra, S. H.; Mushtaq, F.; Khalid, M.; Raza, M. A.; Faizan Nazar, M.; Ali, B.; Braga, A. A. C.; Technology, I.; Khan, R. Y. Synthesis, Spectral Characterization and Computed Optical Analysis of Potent Triazole Based Compounds, Spectrochimica Acta Part A: Molecular and Biomolecular Spectroscopy Synthesis, Spectral Characterization and Computed Optical Analysis of Potent Triazol. *Spectrochim. Acta Part A Mol. Biomol. Spectrosc.* **2017**, *190*, 197–207. https://doi.org/10.1016/j.saa.2017.09.019.

(75) Li, S.; Chen, J. X.; Xiang, Q. X.; Zhang, L. Q.; Zhou, C. H.; Xie, J. Q.; Yu, L.; Li, F. Z. The Synthesis and Activities of Novel Mononuclear or Dinuclear Cyclen Complexes Bearing Azole Pendants as Antibacterial and Antifungal Agents. *Eur. J. Med. Chem.* **2014**, *84*, 677–686. https://doi.org/10.1016/J.EJMECH.2014.07.075.

(76) Aly, H. M.; Moustafa, M. E.; Nassar, M. Y.; Abdelrahman, E. A. Synthesis and Characterization of Novel Cu(II) Complexes with 3-Substituted-4-Amino-5-Mercapto-1,2,4-Triazole Schiff Bases: A New Route to CuO Nanoparticles. *J. Mol. Struct.* **2015**, *Complete* (1086), 223–231. https://doi.org/10.1016/J.MOLSTRUC.2015.01.017.

(77) Li, J.; Ren, G. Y.; Zhang, Y.; Yang, M. Y.; Ma, H. X. Two Cu(II) Complexes of 1,2,4-Triazole Fungicides with Enhanced Antifungal Activities. *Polyhedron* **2019**, *157*, 163–169. https://doi.org/10.1016/J.POLY.2018.09.052.

(78) Graham L, P. *An Introduction to Medicinal Chemistry*, 5th ed.; Oxford University Press: Oxford, United Kingdom, **2013**.

(79) Tillement, J. P.; Tremblay, D. Clinical Pharmacokinetic Criteria for Drug Research. *Compr. Med. Chem. II* **2006**, *5*, 11–30. https://doi.org/10.1016/b0-08-045044-x/00117-6.

(80) Abuhelwa, A. Y.; Williams, D. B.; Upton, R. N.; Foster, D. J. R. Food, Gastrointestinal PH, and Models of Oral Drug Absorption. *Eur. J. Pharm. Biopharm.* **2017**, *112*, 234–248. https://doi.org/10.1016/j.ejpb.2016.11.034.
(81) Parasuraman S. Toxicological Screening. *J. Pharmacol. Pharmacother.* **2011**, *2* (2), 74–79. https://doi.org/10.4103/0976-500X.81895.
(82) Hennessy, S. Postmarketing Drug Surveillance: An Epidemiologic Approach. *Clin. Ther.* **1998**, *20*, 32–39. https://doi.org/https://doi.org/10.1016/S0149-2918(98)80006-4.
(83) Richardson, K.; Cooper, K.; Marriott, M. S.; Tarbit, M. H.; Troke, F.; Whittle, P. J. Discovery of Fluconazole, a Novel Antifungal Agent. *Rev. Infect. Dis.* **1990**, *12* (Supplement_3), S267–S271. https://doi.org/10.1093/clinids/12.Supplement_3.S267.
(84) Richardson, K. The Discovery of Fluconazole. *Contemp. Org. Synth.* **1996**, *3*, 125–132. https://doi.org/10.1039/co9960300125.
(85) Armarego, W. L. F.; Chai, C. L. L. *Purification of Laboratory Chemicals*, 6th ed.; Butterworth-Heinemann: Burlington, USA, **2009**.
(86) Tallec, G.; Imbert, D.; Fries, P. H.; Mazzanti, M. Highly Stable and Soluble Bis-Aqua Gd, Nd, Yb Complexes as Potential Bimodal MRI/NIR Imaging Agents. *Dalton Trans.* **2010**, *39* (40), 9490–9492. https://doi.org/10.1039/c0dt00994f.
(87) Krchová, T.; Kotek, J.; Jirák, D.; Havlíčková, J.; Císařová, I.; Hermann, P. Lanthanide(III) Complexes of Aminoethyl-DO3A as PARACEST Contrast Agents Based on Decoordination of the Weakly Bound Amino Group. *Dalton Trans.* **2013**, *42* (44), 15735–15747. https://doi.org/10.1039/c3dt52031e.
(88) Gans, P.; Sabatini, A.; Vacca, A. Determination of Equilibrium Constants from Spectrophotometric Data Obtained from Solutions of Known PH: The Program PHab. *Ann. Chim.* **1999**, *89*, 45–49.
(89) Gans, P.; Sabatini, A.; Vacca, A. Investigation of Equilibria in Solution. Determination of Equilibrium Constants with the HYPERQUAD Suite of Programs. *Talanta* **1996**, *43*, 1739–1753. https://doi.org/https://doi.org/10.1016/0039-9140(96)01958-3.
(90) Alderighi, L.; Gans, P.; Ienco, A.; Peters, D.; Sabatini, A.; Vacca, A. Hyperquad Simulation and Speciation (HySS): A Utility Program for the Investigation of Equilibria Involving Soluble and Partially Soluble Species. *Coord. Chem. Rev.* **1999**, *184*, 311–318. https://doi.org/https://doi.org/10.1016/S0010-8545(98)00260-4.
(91) Institute CLSICaLS. Reference method for broth dilution antifungal susceptibility testing of yeasts. CLSI standard M27, 4th ed., **2017** https://clsi.org/standards/products/microbiology/documents/m27/ (accessed Feb 8, 2022).
(92) Gibson, M. S.; Bradshaw, R. W. The Gabriel Synthesis of Primary Amines. *Angew. Chemie Int. Ed. Eng.* **1968**, *7* (12), 919–930. https://doi.org/10.1002/ANIE.196809191.
(93) Podyacheva, E.; Afanasyev, O. I.; Tsygankov, A. A.; Makarova, M.; Chusov, D. Hitchhiker's Guide to Reductive Amination. *Synthesis (Stuttg).* **2019**, *51* (13), 2667–2677. https://doi.org/10.1055/S-0037-1611788.
(94) Yu, Q.; Kandegedara, A.; Xu, Q.; Rorabacher, D. B. Avoiding Interferences from Good's Buffers: A Contiguous Series of Noncomplexing Tertiary Amine Buffers Covering the Entire Range of PH 3–11. *Anal. Biochem.* **1997**, *253* (1), 50–56. https://doi.org/https://doi.org/10.1006/abio.1997.2349.

6. Annexes

NMR spectra of synthesized target compounds

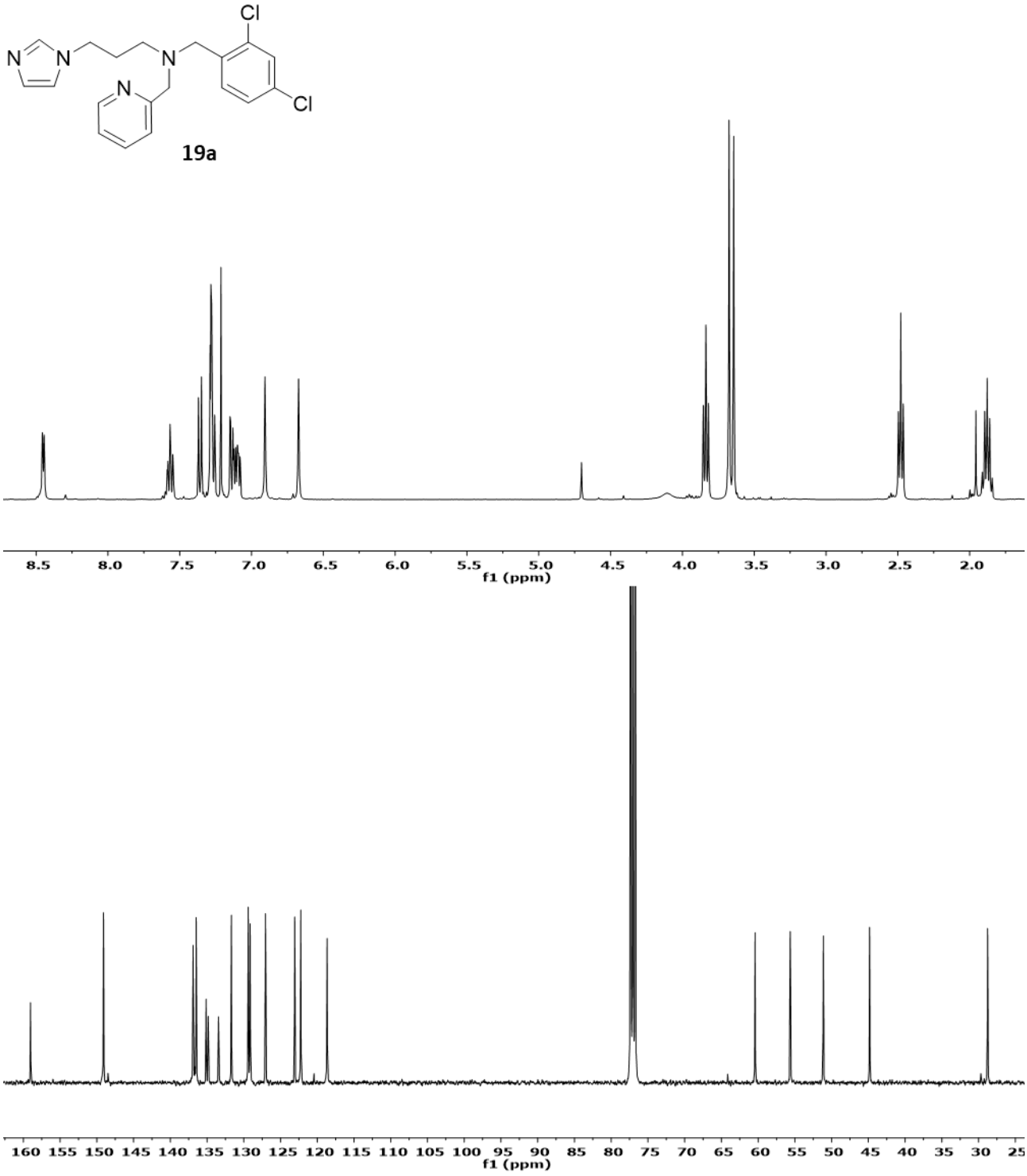

Figure 6.1 – ^{1}H (top) and ^{13}C (bottom) NMR of compound **19a**.

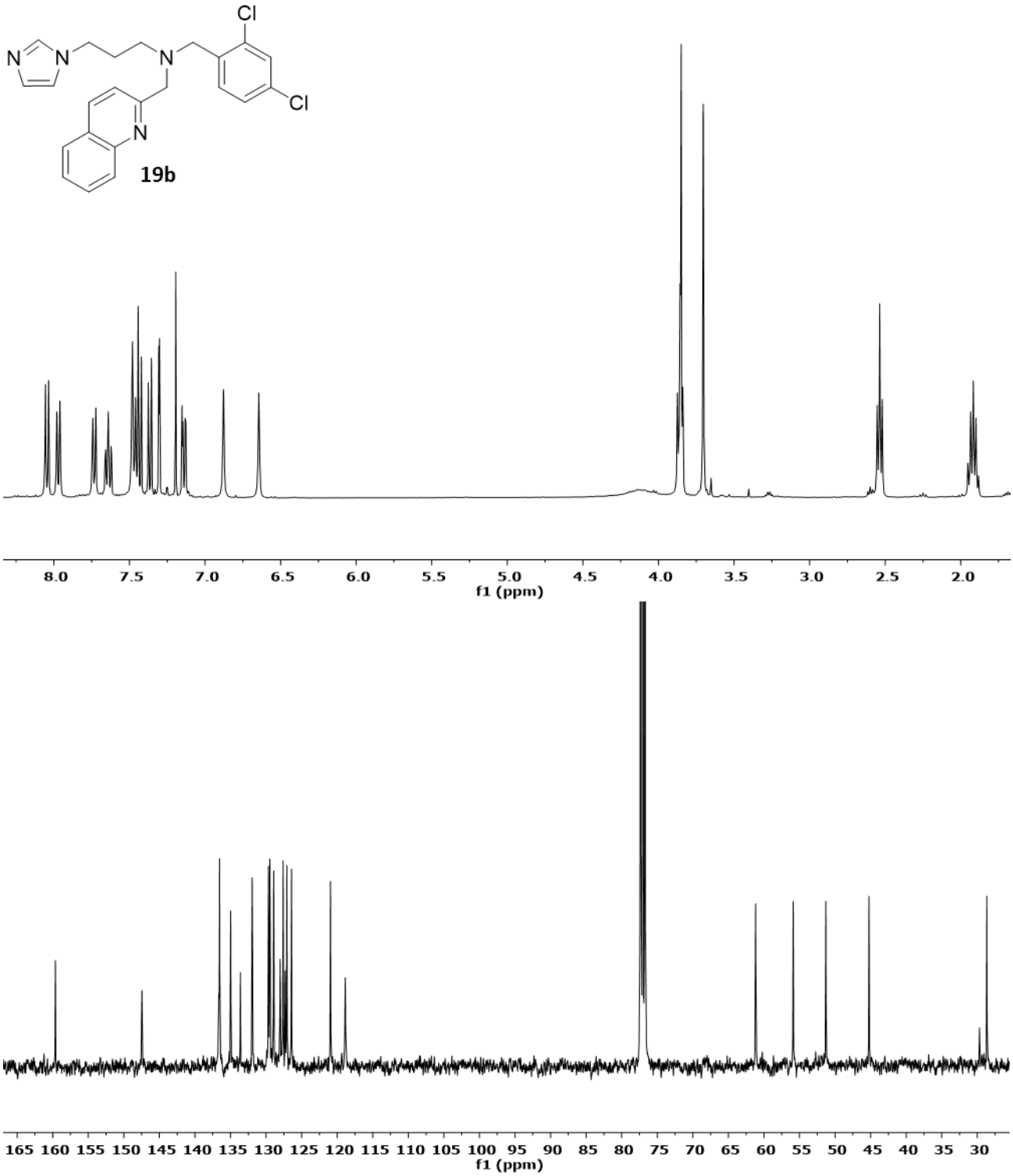

Figure 6.2 – ^{1}H (top) and ^{13}C (bottom) NMR of compound **19b**.

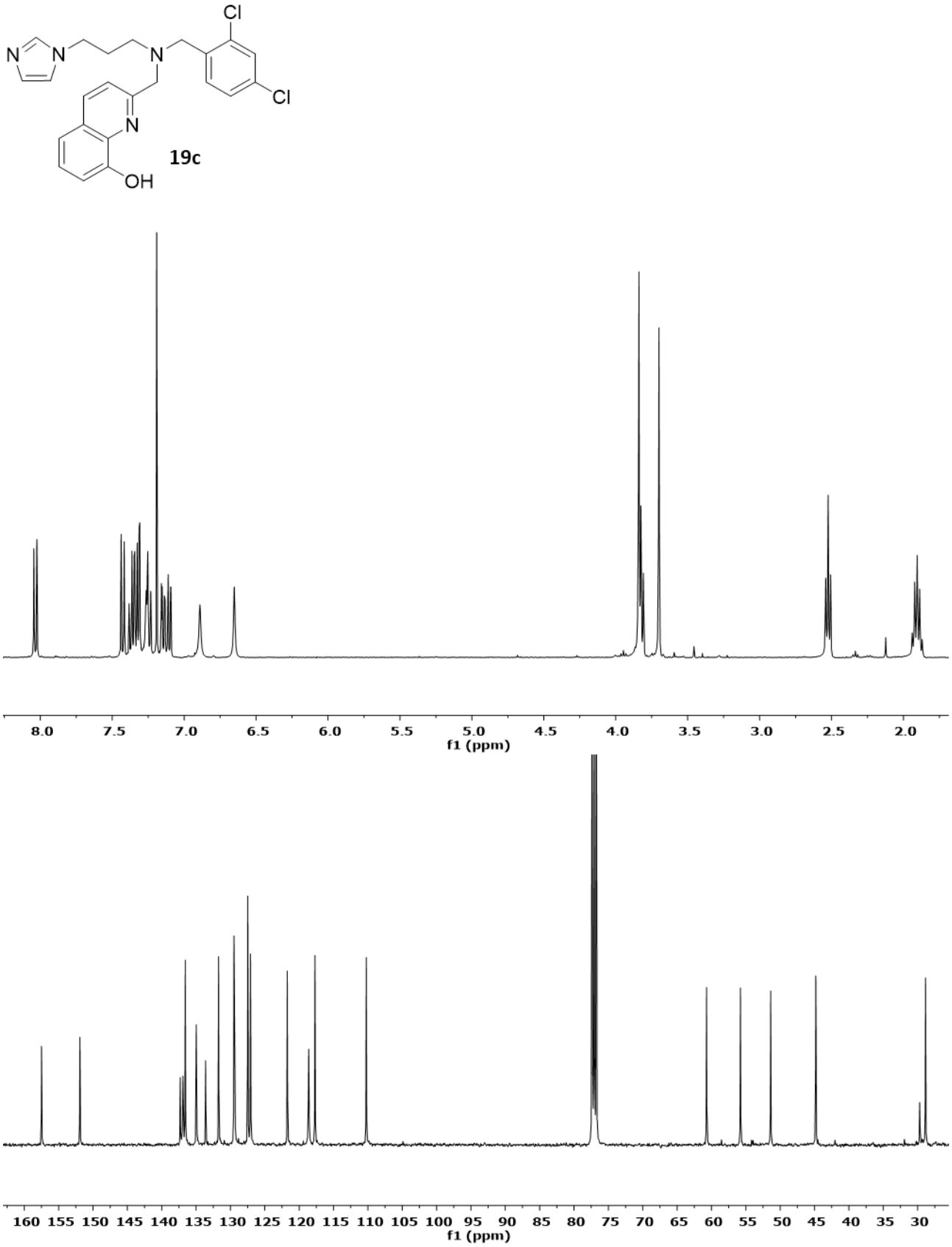

Figure 6.3 – ^{1}H (top) and ^{13}C (bottom) NMR of compound **19c**.

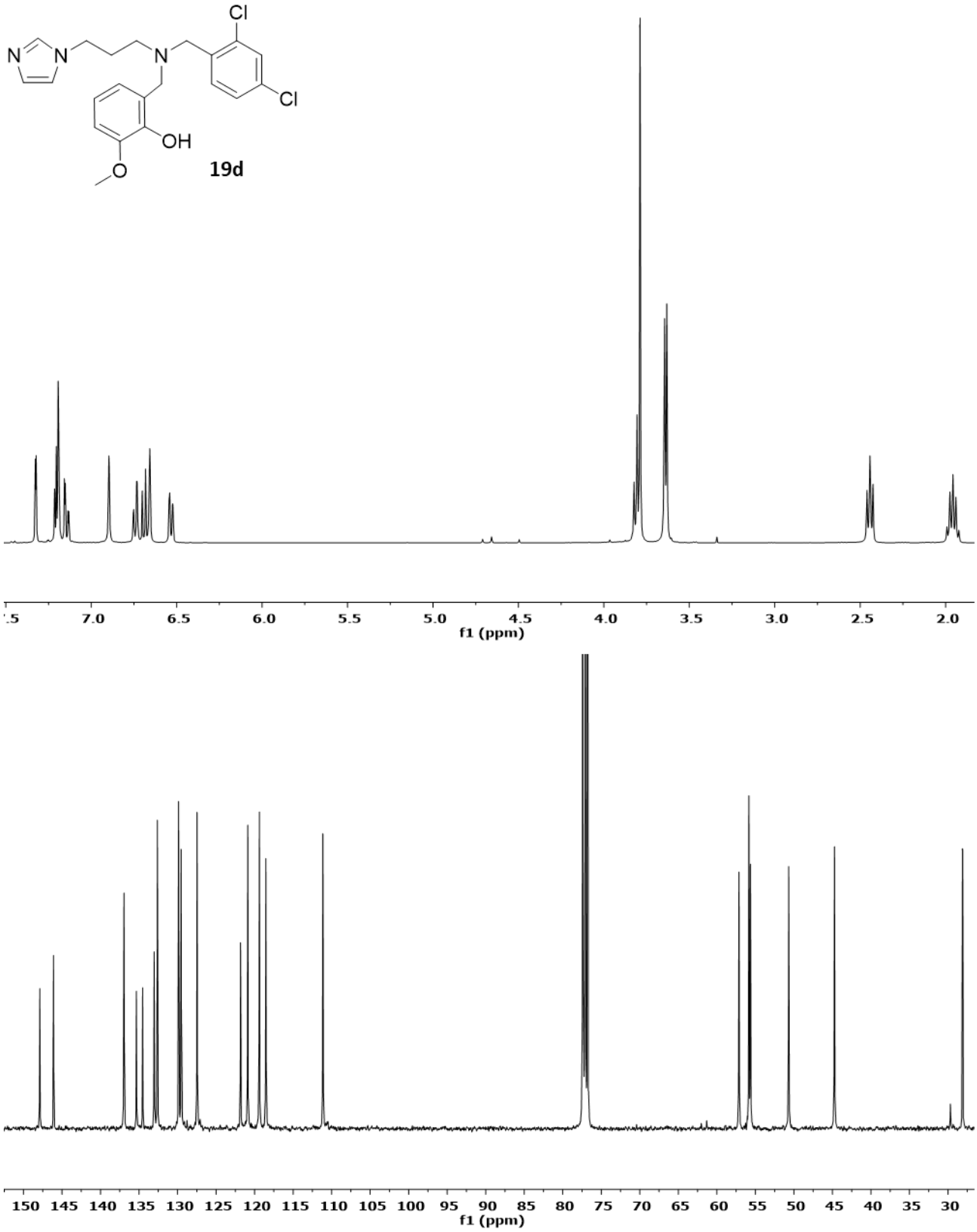

Figure 6.4 – ^{1}H (top) and ^{13}C (bottom) NMR of compound **19d**.

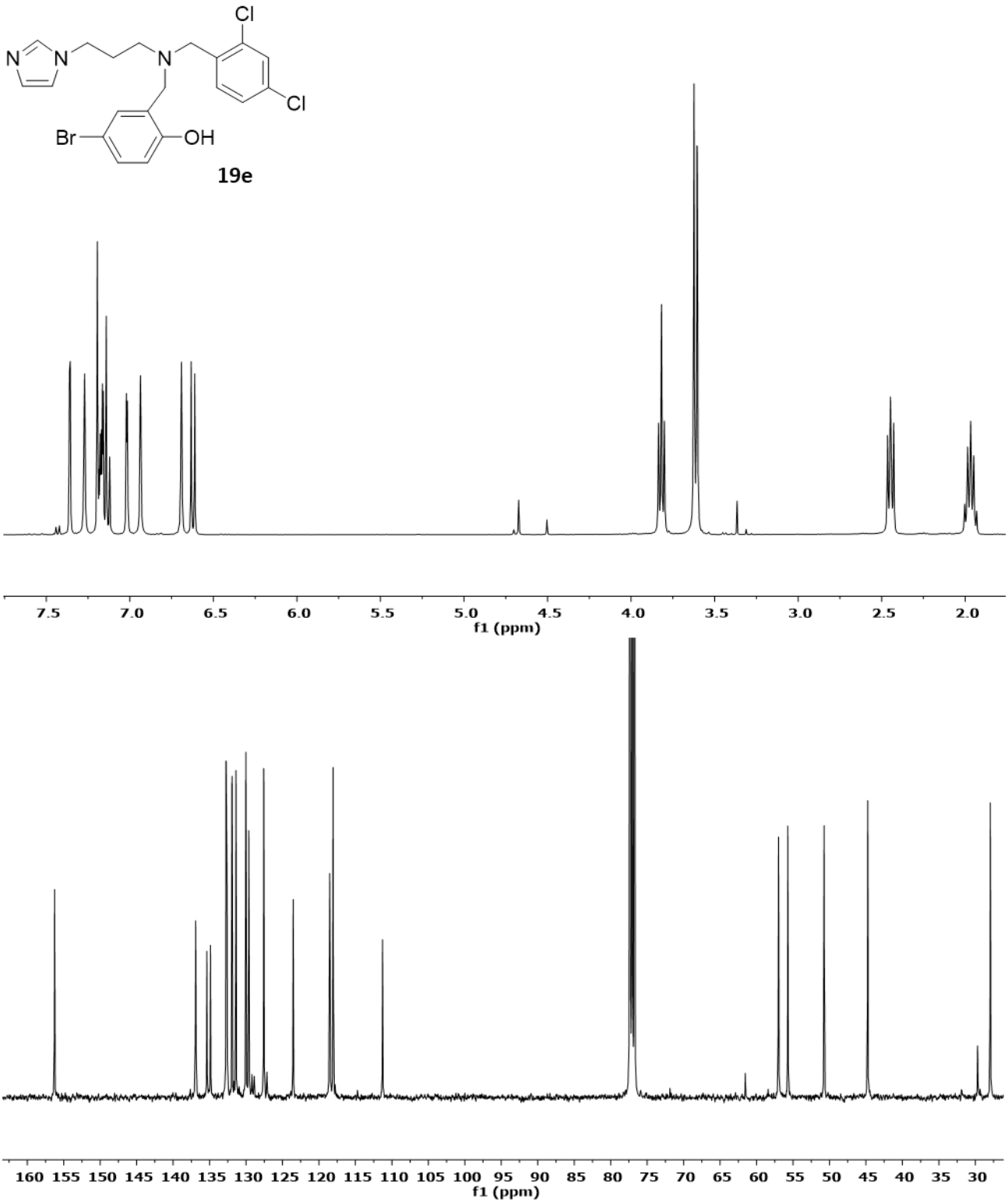

Figure 6.5 – ^{1}H (top) and ^{13}C (bottom) NMR of compound **19e**.

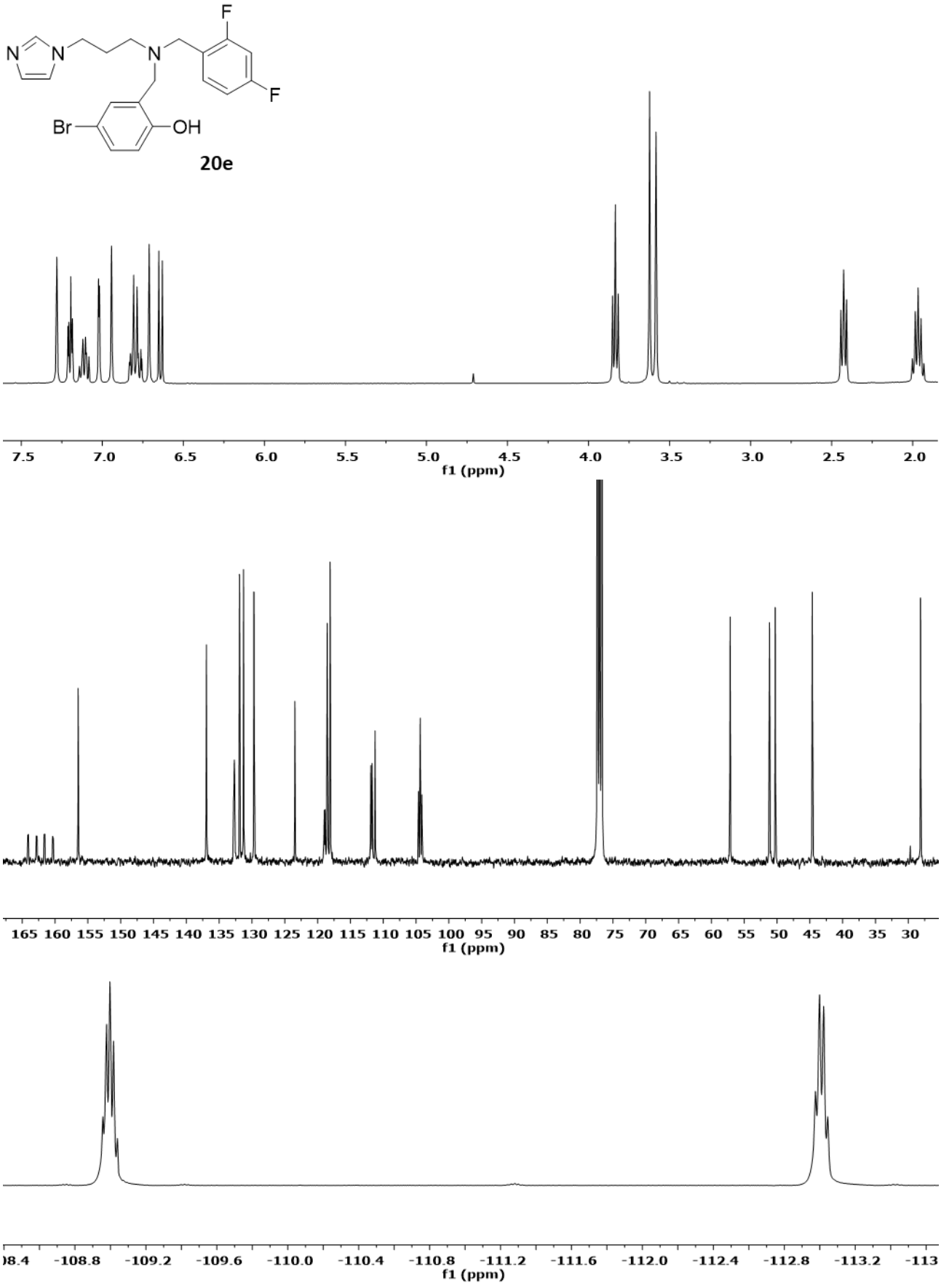

Figure 6.6 – ^{1}H (top), ^{13}C (middle) and ^{19}F (bottom) NMR of compound **20e**.

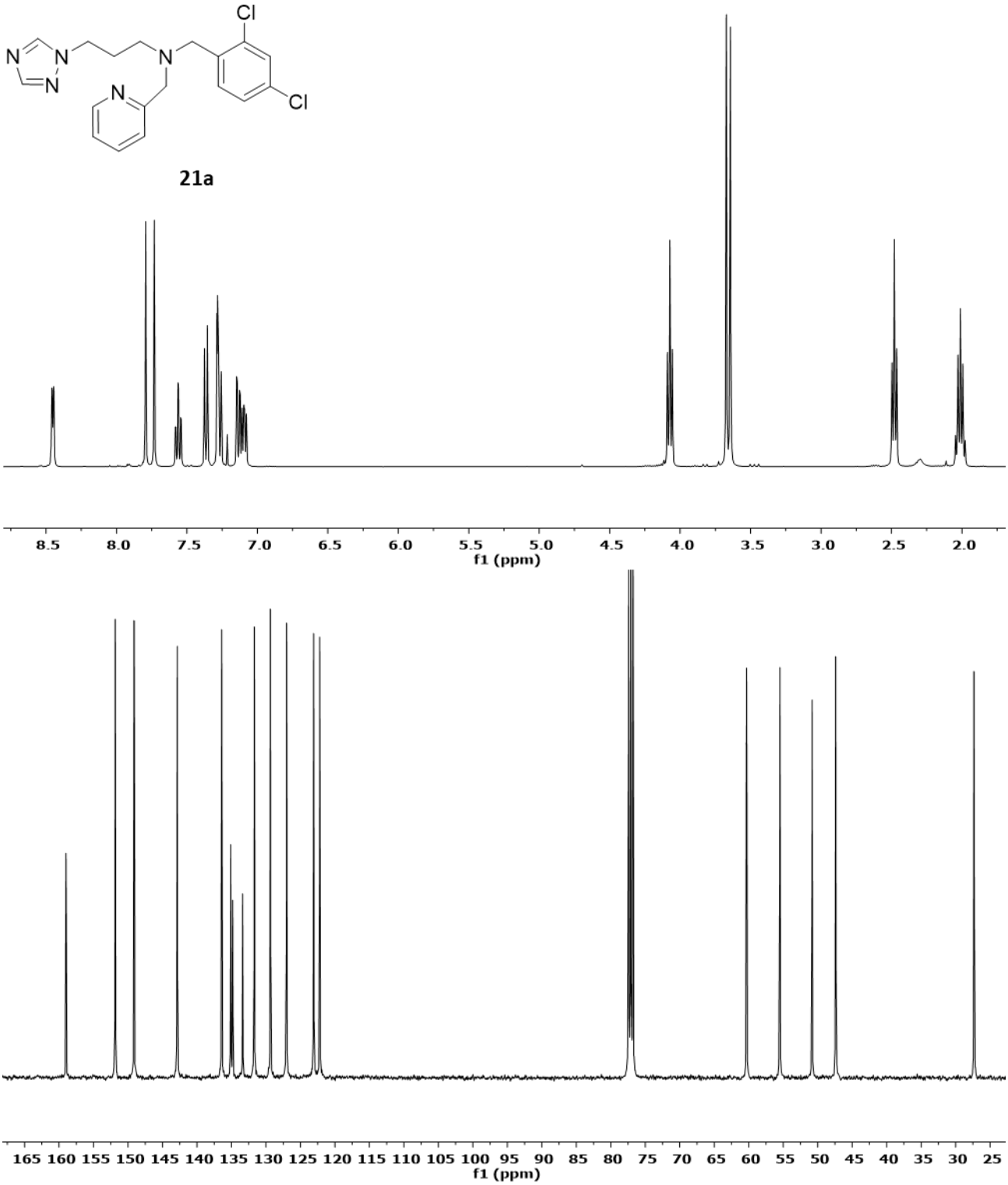

Figure 6.7 – ^{1}H (top) and ^{13}C (bottom) NMR of compound **21a**.

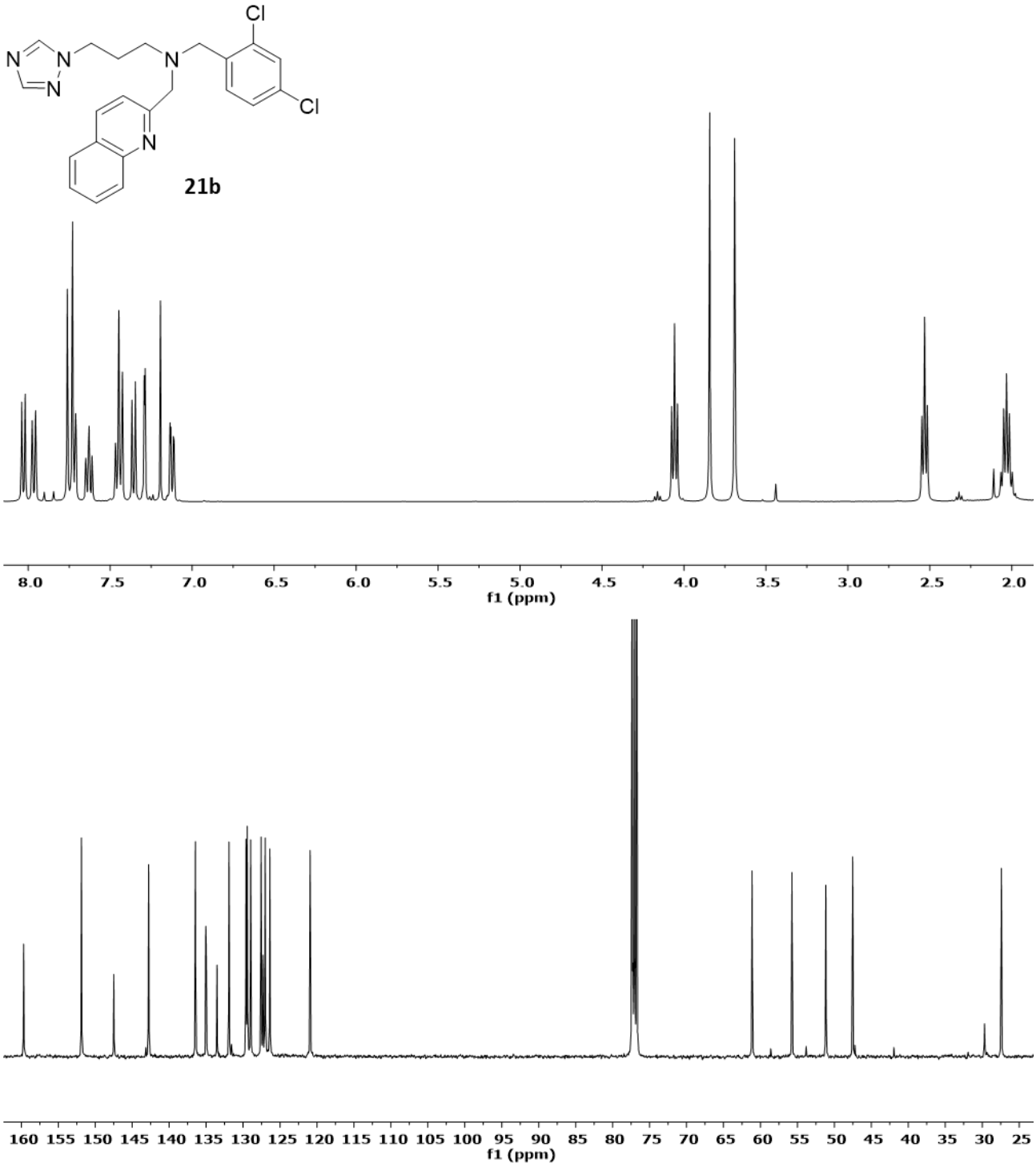

Figure 6.8 – ^{1}H (top) and ^{13}C (bottom) NMR of compound **21b**.

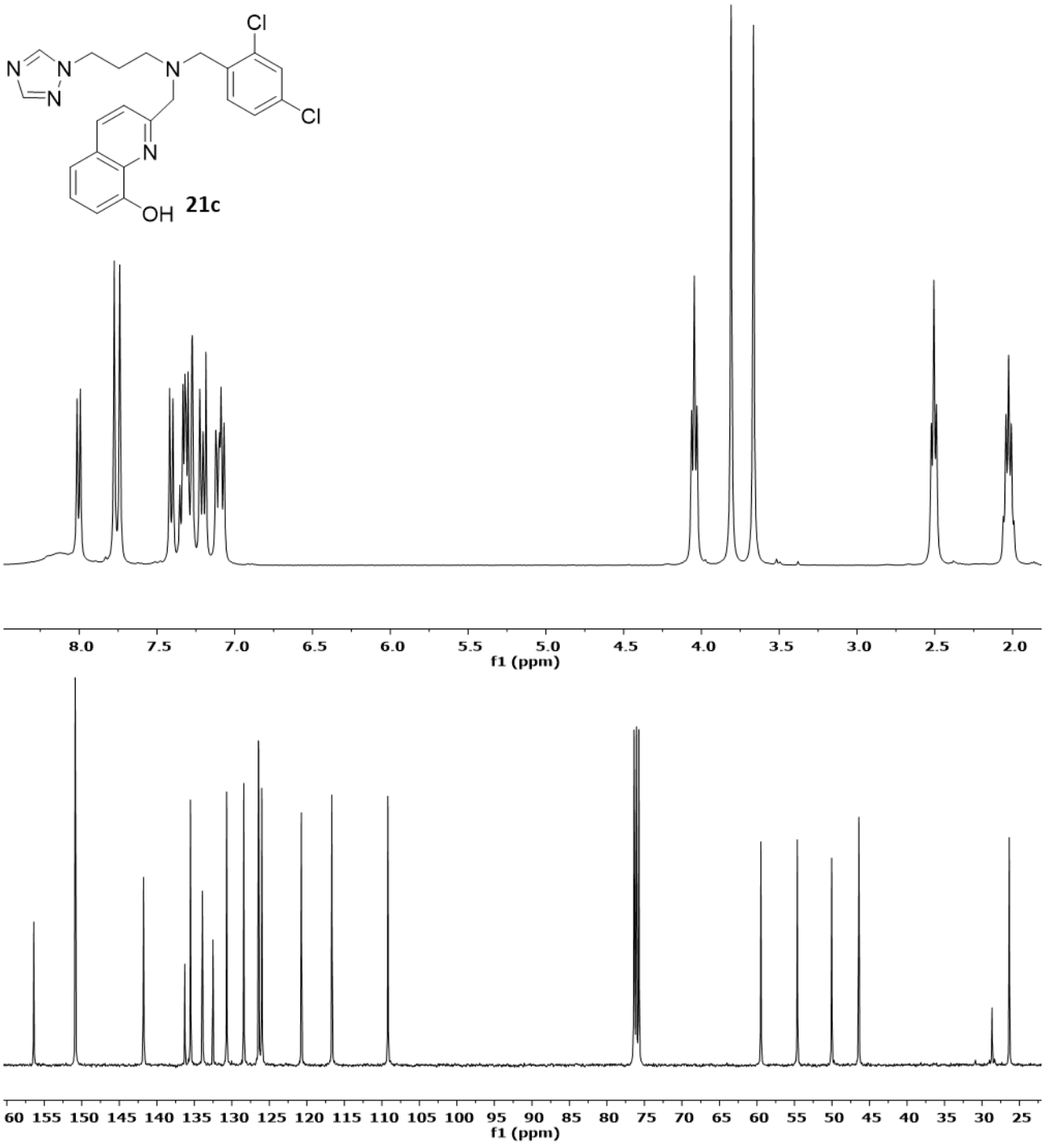

Figure 6.9 – ^{1}H (top) and ^{13}C (bottom) NMR of compound **21c**.

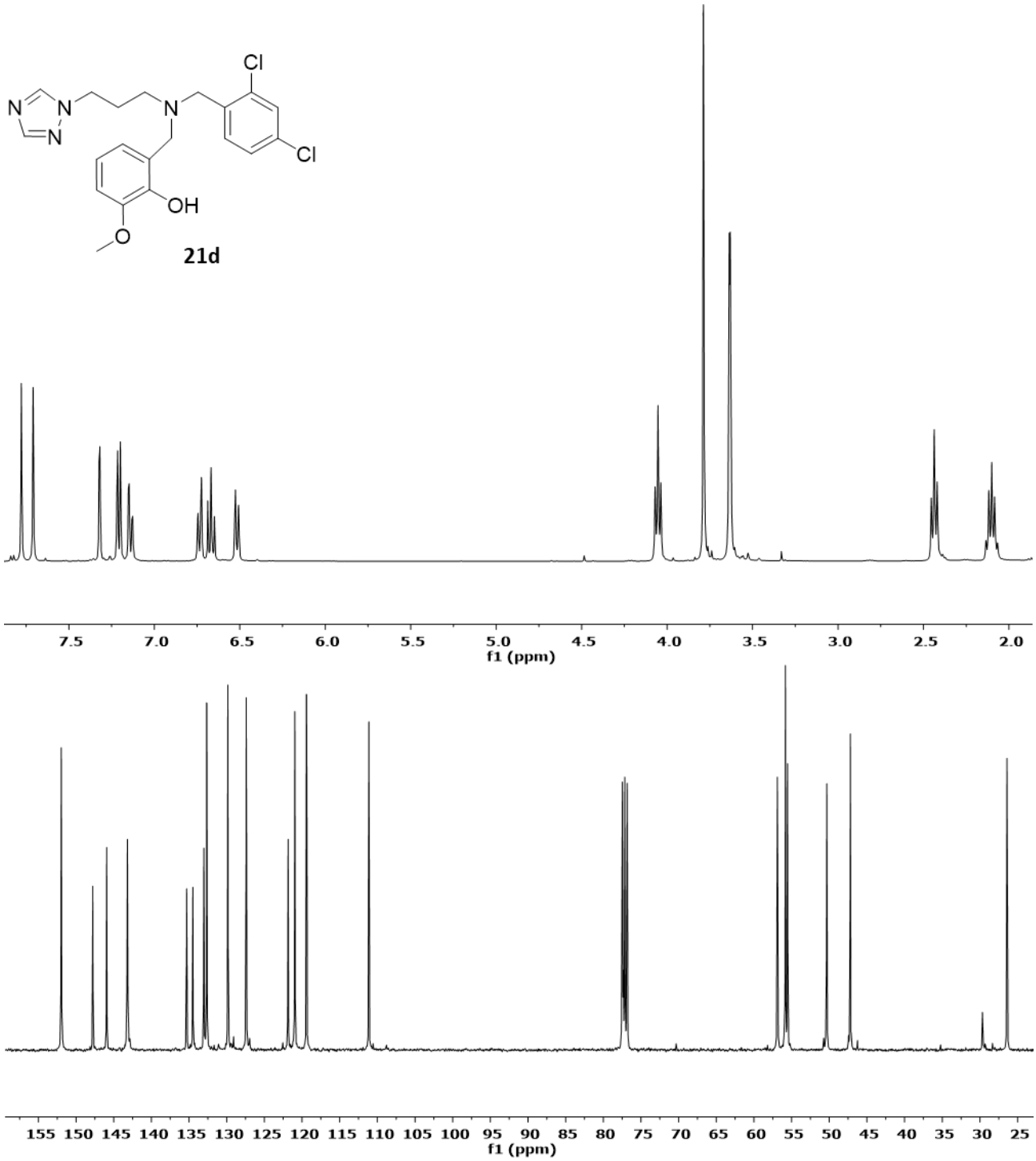

Figure 6.10 – ^{1}H (top) and ^{13}C (bottom) NMR of compound **21d**.

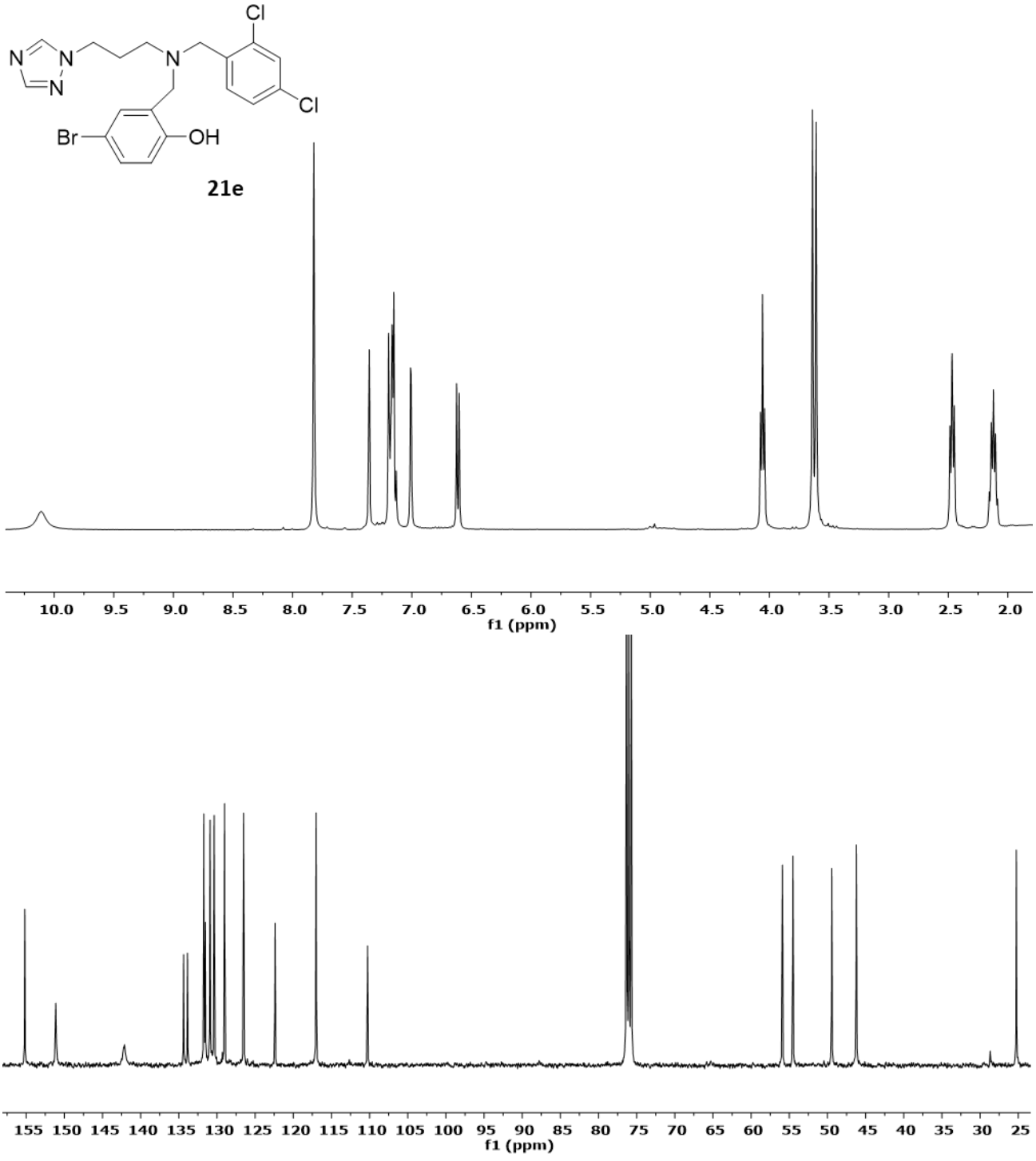

Figure 6.11 – ^{1}H (top) and ^{13}C (bottom) NMR of compound **21e**.

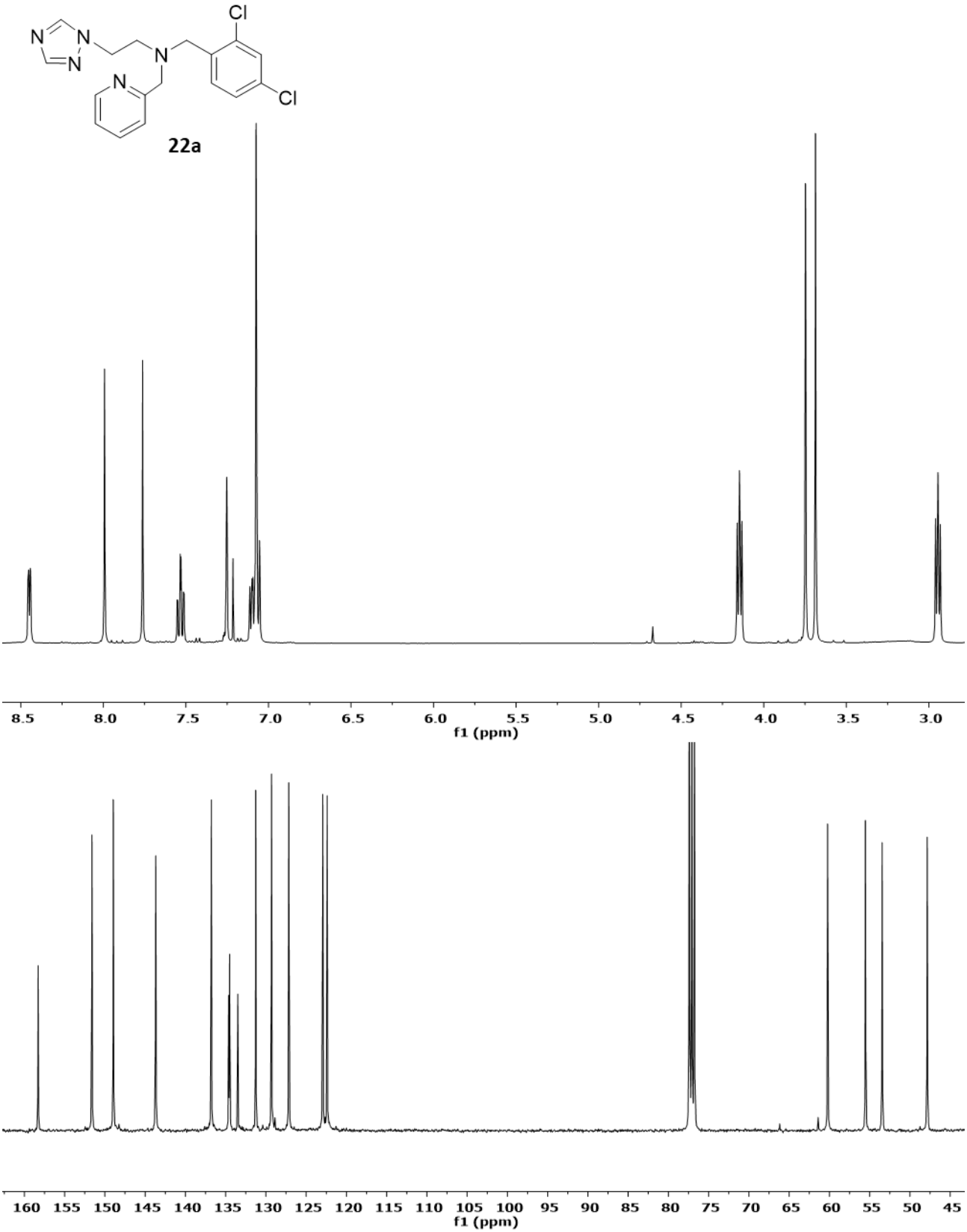

Figure 6.12 – ^{1}H (top) and ^{13}C (bottom) NMR of compound **22a**.

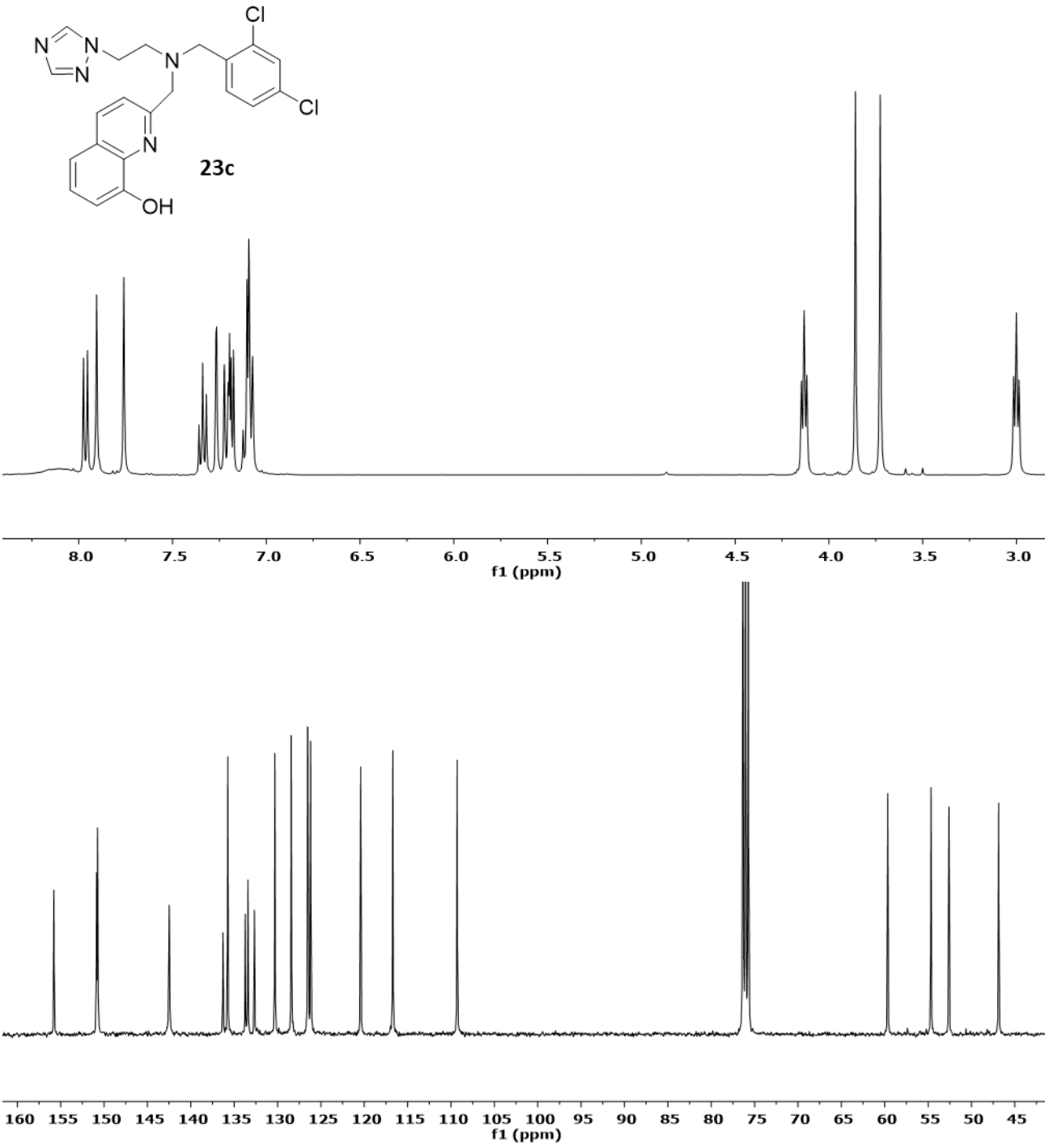

Figure 6.13 – ^{1}H (top) and ^{13}C (bottom) NMR of compound **23c**.

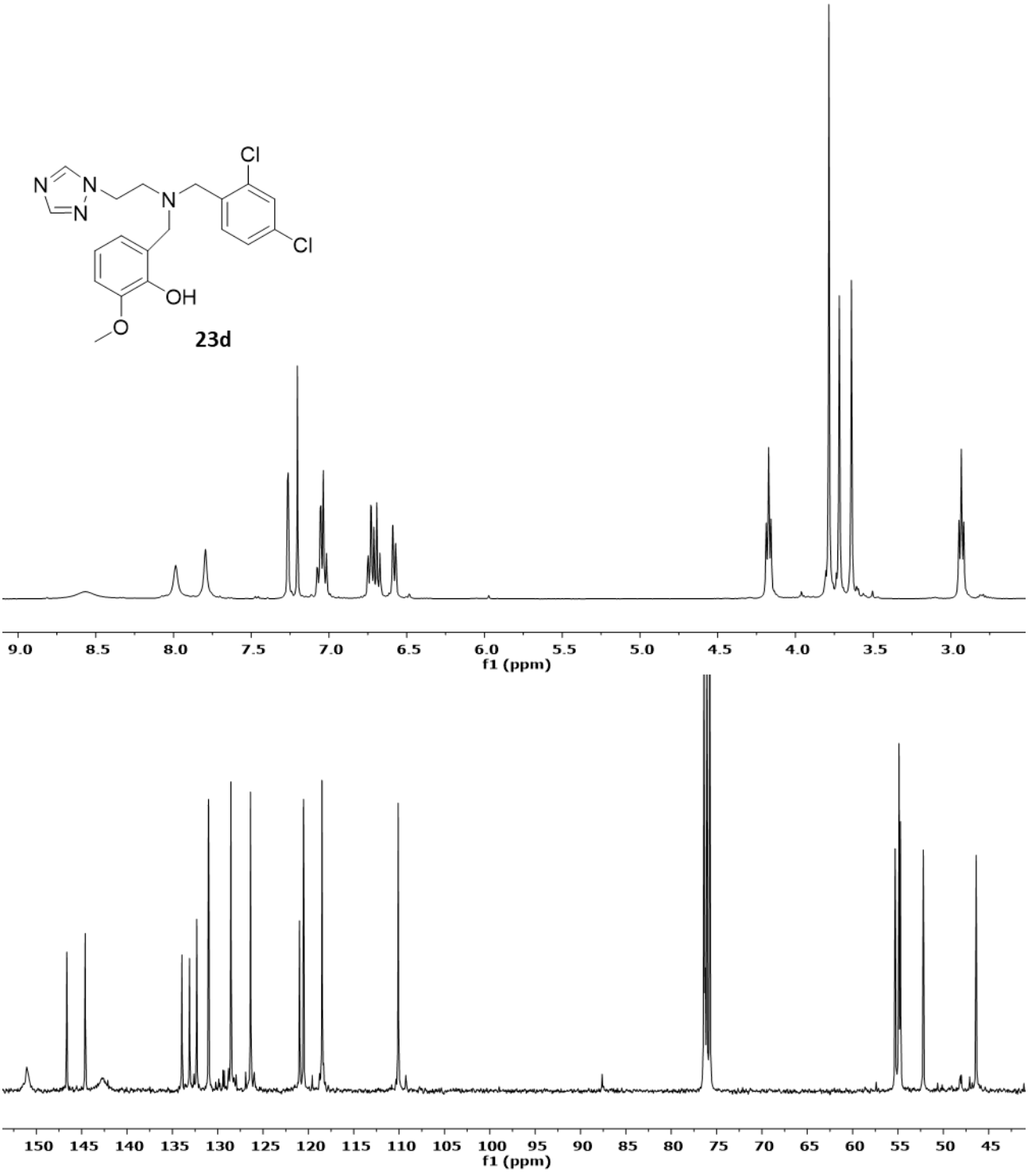

Figure 6.14 – ^{1}H (top) and ^{13}C (bottom) NMR of compound **23d**.

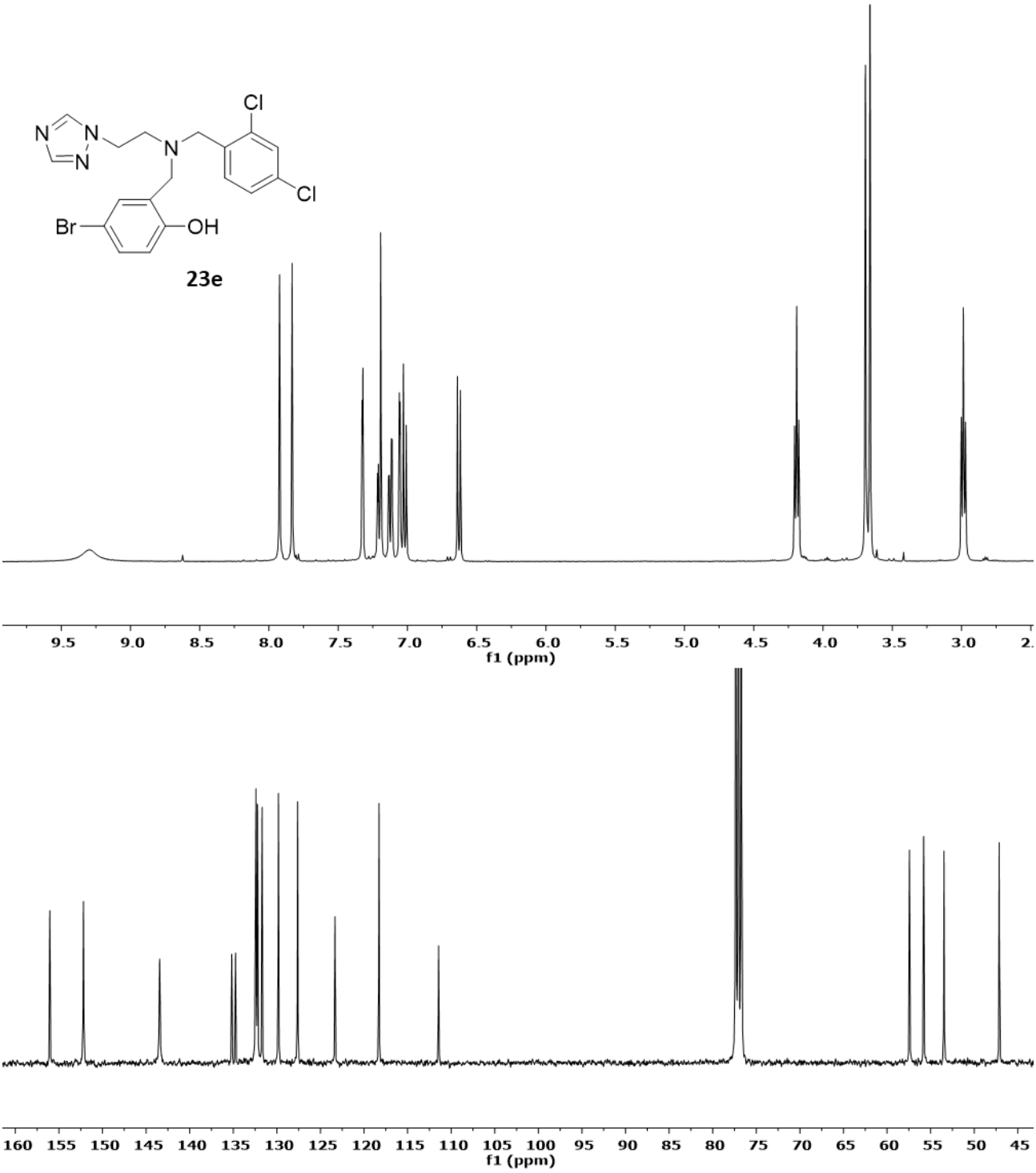

Figure 6.15 – ^{1}H (top) and ^{13}C (bottom) NMR of compound **23e**.